UNIVERSITÀ
DI SIENA
1240

Department of Molecular and Developmental Medicine

PhD course in Molecular Medicine

XXXVIII° Cycle

Coordinator: Prof. Vincenzo Sorrentino, PhD

New insights into retinal physiology and cerebral microcirculation in the 5xFAD murine model of Alzheimer's disease

Scientific disciplinary sector: Physiology (BIO/09)

PhD CANDIDATE

Dr. Lorenzo Guidotti

Department of Biology, Physiology Unit

SUPERVISOR

Prof. Massimo Dal Monte, PhD

Department of Biology, Physiology

CO-SUPERVISOR

Dr. Rosario Amato, PhD

Department of Biology, Physiology

Academic year 2024/2025

University of Siena

PhD course in Molecular Medicine

XXXVIII° Cycle

FINAL EXAMINATION DATA

25/02/2026

EXAMINATION COMMITTEE

Prof. Enrico Pierantozzi

Prof.ssa Elena Rapizzi

Dr. Roberto Silvestri

ALTERNATIVE COMMITTEE MEMBER

Prof.ssa Luisa Campagnolo

INDEX

LIST OF ABBREVIATIONS

Abbreviation	Full Name
AD	Alzheimer's disease
FAD	Familial Alzheimer's disease
Aβ	Amyloid beta
RPE	Retinal Pigment Epithelium
NR	Neural Retina
BRB	Blood-Retinal Barrier
ONL	Outer Nuclear Layer
INL	Inner Nuclear Layer
GCL	Ganglion Cell Layer
OPL	Outer Plexiform Layer
IPL	Inner Plexiform Layer
RGC	Retinal Ganglion Cell
RNFL	Retinal Nerve Fiber Layer
OS	Outer Segment
CC	Collecting Cilium
IS	Inner Segment
STR	Synaptic Terminal Region
cGMP	Cyclic Guanosine Monophosphate
ipRGC	Intrinsically Photosensitive Retinal Ganglion Cell
ROS	Reactive Oxygen Species
CNS	Central Nervous System
BBB	Blood-Brain Barrier
ZO-1	Zonula Occludens of type 1
SH3	Src Homology-3
VEGF	Vascular Endothelial Growth Factor
LOAD	Late-onset Alzheimer's disease
EOAD	Early-onset Alzheimer's disease
SAD	Sporadic Alzheimer's disease
APOE	Apolipoprotein E
FAD	Familial Alzheimer's disease
APP	Amyloid Precursor Protein
PSEN	Presenilin
ACh	Acetylcholine
sAPP	Soluble Ectodomain of APP
CTF	C-Terminal Fragment
BACE	β-site Amyloid Precursor Protein Cleaving Enzyme
AICD	Amyloid Precursor Protein Intracellular Domain
IDE	Insulin-Degrading Enzyme
Fe65	Adaptor Protein Fetal Embryonic 65
BACE2	β-site Amyloid Precursor Protein Cleaving Enzyme of type 2
RAGE	Receptor for Advanced Glycation End-Products

LRP1	Low-Density Lipoprotein Receptor-Related Protein 1
pTau	Phosphorylated Tau
MAP	Microtubule-Associated Protein
PRR	Proline-Rich Region
MTBD	Microtubule Binding Domain
DNA	Deoxyribonucleic Acid
RNA	Ribonucleic Acid
miRNA	Micro-Ribonucleic Acid
GSK3	Glycogen Synthase Kinase 3
PP	Protein Phosphatase
NFT	Neurofibrillary Tangles
NEP	Neprilysin
CD10	Cluster of Differentiation 10
CD40	Cluster of Differentiation 40
Iba1	Ionized Calcium-Binding Adapter Molecule 1
GFAP	Glial Fibrillary Acidic Protein
IL6	Interleukin-6
TNFα	Tumor Necrosis Factor Alpha
NF-κB	Nuclear Factor-κB
IκB	Inhibitor-κB
IKK	IκB-Kinase
NIK	Nuclear Factor-κB Inducing Kinase
NRF2	Nuclear Factor Erythroid 2-Related Factor 2
Keap1	Kelch-Like ECH-Associated Protein 1
Cul	Cullin
RBX1	RING Box Protein-1
β-TrCP	Beta-Transducin Repeat-Containing Protein
NQO1	NAD(P)H Quinone Dehydrogenase 1
FASL	Fetal Alcohol Syndrome Ligand
DD	Death Domain
FADD	Fetal Alcohol Syndrome Ligand-Associated Death Domain
TRADD	Tumor Necrosis Factor Receptor-Associated Death Domain
DISC	Death-Inducing Signalling Complex
CYT-c	Cytochrome-c
HtrA2/Omi	High Temperature Requirement Protein A2 Omi Stress-Regulated
DIABLO	Direct IAP Binding Mitochondrial Protein
Bcl-2	B-Cell Lymphoma 2
Bax	B-Cell Lymphoma 2-Associated X Protein
BID	BH3 Interacting-Domain Death Agonist
PET	Positron Emission Tomography
ERG	Electroretinographic
OCT	Optical Coherence Tomography
PERG	Pattern-ERG
ASO	Antisense Oligonucleotides
CRISPR	Clustered Regularly Interspaced Short Palindromic Repeats
DASH	Dietary Approaches to Stop Hypertension

EVOO	Extra-Virgin Olive Oil
ACE	Acebuche
WT	Wild-Type
Pde6brd1	Phosphodiesterase-6b Retinal Degeneration-1
PCR	Polymerase Chain Reaction
scERG	Scotopic-ERG
phERG	Photopic-ERG
PBS	Phosphate-Buffered Saline
RBPMS	RNA-Binding Protein with Multiple Splicing
GS	Glutamine Synthetase
RIPA	Radioimmunoprecipitation
OD	Optical Density
AEBSF	4-(2-aminoethyl) benzenesulfonyl fluoride hydrochloride
RIN	RNA Integrity Number
ORA	Over-Representation Analysis
qRT-PCR	Quantitative Real Time-PCR
SEM	Standard Error of the Mean
LDL	Low-Density Lipoprotein
HDL	High-Density Lipoprotein
ALP	Alkaline Phosphatase
GGT	Gamma-Glutamyl Transferase
GPT	Glutamate Pyruvate Alanine Aminotransferase
FITC	Fluorescein Isothiocyanate
NGL	Normalized Gray Levels
ThS	Thioflavin-S
HIF-1α	Hypoxia Inducible Factor 1α

ABSTRACT OF THIS THESIS

This PhD thesis comprises two complementary research projects concerning early pathological mechanisms and potential intervention strategies in Alzheimer's disease (AD), employing the 5xFamilial AD (FAD) murine model. The first project investigates the retina as a non-invasive window into early AD-related pathological changes. A detailed morpho-functional and molecular characterization reveals significant alterations in retinal function and structure starting from 6 months of age, including retinal ganglion cell loss, visual acuity deficits, and widespread deposition of amyloid beta (Aβ) and hyperphosphorylated Tau. These changes are accompanied by pronounced microglial activation, neuroinflammation, oxidative stress, and apoptosis. Notably, the downregulation of miR-3968 and miR-124-5p in the retina is strongly associated with enhanced neuroinflammatory and apoptotic signaling, underscoring the role of miRNAs in AD-related retinal pathology. These findings place the retina as a promising biomarker for early AD diagnosis and molecular monitoring. The second project focuses on cerebral microcirculation, highlighting early vascular impairments in 5xFAD mice as early as two months of age. Observed abnormalities include reduced arteriolar density, capillary rarefaction, increased permeability, and early downregulation of claudin-5, indicating disruption of the blood-brain barrier. These cerebrovascular abnormalities are also associated with hypoxic conditions, reduced expression of Aβ-degrading enzymes, increased Aβ burden, and activation of neuroinflammatory pathways. Importantly, dietary administration of Acebuche olive oil demonstrated protective effects by preserving vascular integrity, reducing hypoxia and inflammation, and improving cognitive performance. However, its long-term efficacy was lost at 6 months, likely due to systemic metabolic disturbances, including hepatic steatosis, highlighting the importance of dosing strategies for sustained benefits. Together, these studies emphasize the retina and cerebral vasculature as early and vulnerable targets in AD, driven by shared mechanisms of Aβ accumulation, glial reactivity, and inflammation. Furthermore, these studies advance the investigation of minimally invasive diagnostic tools and dietary interventions with translational applicability. Taken together, the findings provide new perspectives on the systemic pathophysiology of AD and inform the design of integrated, multi-modal strategies for early diagnosis, longitudinal monitoring, and preventive intervention.

1. INTRODUCTION

1.1 An in-depth overview of the retinal morpho-functional features

The retina represents the innermost layer of the eye and is formed by a highly organized and stratified structure characterized by different cell types that form morphologically and functionally distinct circuits working in parallel, and in combination, to convert the light into neurochemical signals in order to produce a complex visual image (Masland, 2012). The retina is structurally divided into the retinal pigment epithelium (RPE) and the neural retina (NR). The RPE represents the outermost part of the retina and is formed by a single layer of regular polygonal epithelial cells that play a key role in maintaining normal cell renewal, as well as protecting the retinal cells from photo-oxidation damage and forming a highly selective blood-retinal barrier (BRB) between the choroid vessels and NR components (Yang et al., 2021). On the other hand, NR is the innermost part of the retina and plays a crucial role in converting light signals into visual information. The NR is typically characterized by a multi-layered structure composed of three nuclear layers, namely the outer nuclear layer (ONL), inner nuclear layer (INL), and ganglion cell layer (GCL), as well as two plexiform layers, namely the outer plexiform layer (OPL) and inner plexiform layer (IPL). Within these layers are found numerous types of cells having specific functions, including six neuronal cell types such as photoreceptors (rods and cones), bipolar cells, interneurons (horizontal and amacrine cells), and retinal ganglion cells (RGCs), as well as sustaining cells such as macroglia (Müller cells and astrocytes), and immune cells such as microglia (resident tissue-specific macrophages) (**Fig. 1**) (Grigoryan, 2022). Particularly, the ONL contains the photoreceptor nucleus, the OPL contains the synapse between photoreceptors and bipolar cells, the INL contains the cell bodies of bipolar and interneurons, the IPL contains the synapse between bipolar, interneurons, and RGCs, while the GCL primarily contains RGCs whose axons form the retinal nerve fiber layer (RNFL) (Hussey et al., 2022).

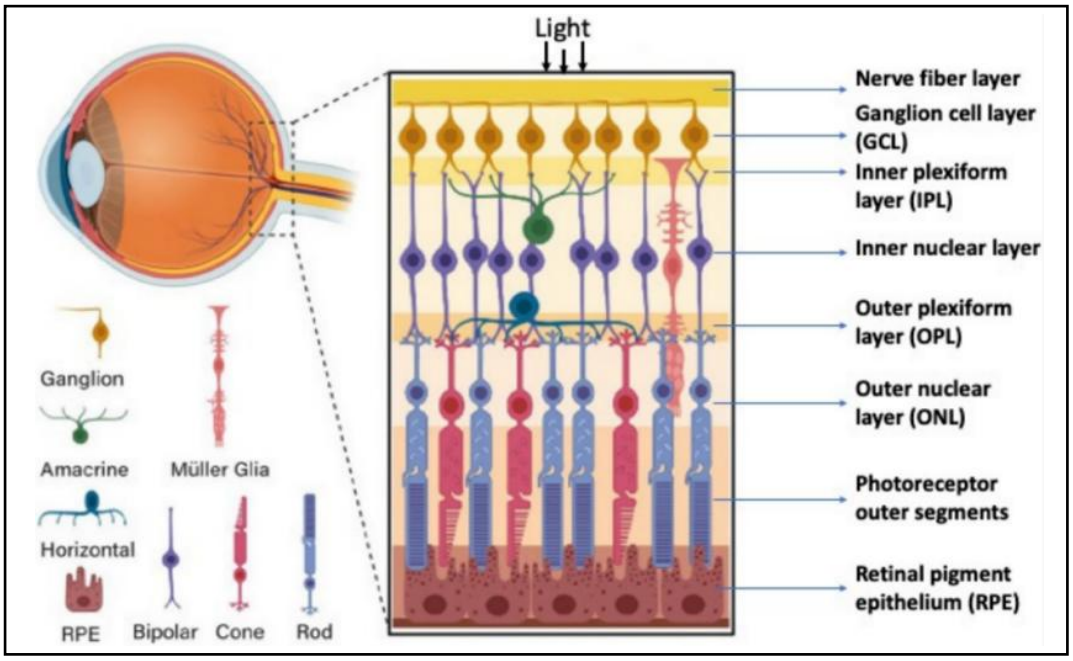

Figure 1. The structure of the retina and its main cell types (Grigoryan et al., 2022).

1.1.1 Photoreceptors and phototransduction process

Photoreceptors are specialized neurons able to convert a light stimulus into a neurochemical signal, ushering in the first steps of the phototransduction process. Both rods and cones have a highly compartmentalized structure characterized by an outer segment (OS), a collecting cilium (CC), an inner segment (IS), a nuclear region, and a synaptic terminal region (STR) (Molday and Moritz, 2015). The OS originates from the plasma membrane invaginations that overlap, forming a lamellar structure with a typical conical (in cones) or cylindrical (in rods) shape. The OS contains a large number of photopigment molecules, which are formed by a chromophore molecule (11-cis retinal) and a protein moiety (opsin) covalently linked through a Schiff base. The spectral sensitivity of each photoreceptor type is determined by the expression of different opsin proteins, which differ from one another due to their distinct amino acid compositions. The rods are involved in scotopic vision (low-light conditions) and express exclusively rhodopsin, a photopigment highly sensitive to light stimuli that shows maximal absorption efficiency at a wavelength of 498nm. The cones are implicated in photopic vision (light condition) and express S-, M-, or L-opsin, which have lower sensitivity to light stimuli but show maximal absorption efficiency at wavelengths of 420nm (blue), 534nm (green), and 564nm (red), respectively (Hussey et al., 2022; Inamoto and Shichida, 2014). The CC is an important microtubular structure that physically links OS and IS, also allowing the traffic of specific proteins between them. The IS contains the metabolic and biosynthetic machinery of the photoreceptor, including ion channels, membrane transport proteins, mitochondria, endoplasmic reticulum, Golgi complex, lysosomes, and other important subcellular organelles. In continuity with the IS, there is the nuclear region that houses the nucleus. The last part of the photoreceptors is represented by the STR, which consists of synaptic vesicles and a ribbon synapse for transmission of the neurotransmitter glutamate from photoreceptors to bipolar and other secondary neurons (Molday and Moritz, 2015). The phototransduction process begins when light reaches photoreceptors in the eye, causing a change in the chromophore from 11-cis-retinal to all-trans-retinal. This activates opsin, which triggers a cascade involving the G-protein transducin and the enzyme phosphodiesterase 6, leading to lower levels of cyclic guanosine monophosphate (cGMP), closure of cGMP-dependent sodium channels, hyperpolarization of the photoreceptor, and reduced glutamate release. In dark conditions, cGMP levels remain high with subsequent opening of cGMP-dependent sodium channels, depolarization of the photoreceptor, and release of glutamate (Hussey et al., 2022). Glutamate then acts on downstream bipolar cells: ON bipolar cells (with metabotropic receptors) hyperpolarize, while OFF bipolar cells (with ionotropic receptors) depolarize. In light conditions, reduced levels of glutamate cause the opposite responses. These signals are processed by bipolar and interneurons, eventually activating RGCs, which send action potentials along the optic nerve to the visual cortex of the brain (Nelson and Connaughton, 1995).

1.1.2 Retinal ganglion cells: morpho-functional and metabolic characteristics

RGCs play a key role in the transmission of the visual signals from the retina to the brain. These signals are involved in both the conscious visual perception and non-image-forming processes, such as the optokinetic,

vestibulo-ocular, and pupillary light reflexes, as well as circadian rhythm regulation and modulation of the sleep/wake cycle. RGCs can be divided into two main groups, namely intrinsically photosensitive RGCs (ipRGCs) and non-ipRGCs (Yang et al., 2024). The ipRGCs are non-image-forming retinal cells divided into M1–M6 subtypes. M1 cells express high levels of melanopsin and regulate circadian rhythms and reflexes, while M2–M6 are involved in the effects of light on mood and some visual processing, with lower melanopsin levels (Mure, 2021). On the other hand, the non-ipRGCs contribute to conscious visual perception by integrating signals from other retinal neurons. Nowadays, several non-ipRGCs types have been discovered, each of which is characterized by a variable number of dendrites having different shapes, sizes, stratification, and compactness. The cell body is generally larger than that of other retinal cells and is placed in the GCL. Their axons are projected from the cell body, enter the NFL, turn into the optic nerve head, cross the lamina cribrosa, and then emerge posterior to the ocular globe and become myelinated and organized in bundles, giving form to the optic nerve (Carelli et al., 2009). For the long intraocular length, these axons remain unmyelinated and thus very energy dependent to transmit the action potential. Once they achieve myelination posterior to the globe, their energy dependence drastically decreases due to the higher efficiency of saltatory action potential conduction. This physiological dichotomy is reflected in the need to distribute the mitochondria asymmetrically, such that they are very abundant in the intraocular unmyelinated portion, and remarkably fewer posterior to the lamina cribrosa, where they remain in clusters under the nodes of Ranvier or travel towards the synaptic terminal (Kim et al., 2021; Carelli et al., 2009). Due to the high energy demand of RGCs, mitochondrial activity is essential to sustain their function and guarantee their survival. Indeed, it is well-known that mitochondria ensure an optimal production of energy through oxidative phosphorylation processes and regulate the intracellular calcium levels to allow a proper synaptic transmission, neurotransmitter release, and RGC function. In addition, mitochondria maintain the redox homeostasis in RGCs by effectively controlling reactive oxygen species (ROS) levels and managing oxidative stress (Yang et al., 2024).

1.1.3 Glial cells support and modulate the retinal function

The term glial cell is derived from the ancient Greek word for “glue”, as initially these cells were thought to merely act as supporting structures for surrounding neurons. Nowadays, it is well-known that glial cells play several complex functions beyond the provision of structural support to retinal neurons, such as providing metabolic support to neurons, maintaining retinal homeostasis by regulating ion and glucose exchange, maintaining neuron functionality by regulating the levels of neurotransmitters as glutamate, protecting the neurons from oxidative stress and performing an immune activity against infections, damages as well as the accumulation of molecules with inflammatory properties (Garcia-Bermudez et al., 2021). Particularly, retinal glia is subdivided into macroglia and microglia. The macroglial component is characterized by two basic cell types: Müller cells and astrocytes. In addition, oligodendrocytes are occasionally seen in the retina, but only when myelinated RGC axons are present in the NFL. Müller cells represent the most common retinal glial cell, followed by astrocytes and microglial cells. They are a highly specialized cell type, radially oriented, which

spans the width of the NR from the outer limiting membrane (a network of junctions between photoreceptors and Müller cells), where their apical ends are located, to the GCL, where their basal feet terminate, forming the inner limiting membrane. The cell body of the Müller cells is generally located in the INL. Given their spatial arrangement, each Müller cell can be considered as the fulcrum of a columnar microunit of retinal neurons, by anatomically linking retinal neurons with retinal blood vessels, vitreous body, and subretinal space (Hoz et al., 2016). Among the numerous functions performed by Müller cells, one of the most important is based on controlling the retinal neuron functionality by regulating the extracellular concentration of neuroactive substances such as potassium ions, GABA, and glutamate. Müller cells are also involved in the warehousing and release of glucose, which represents the main energy source for the surrounding retinal neurons. Additionally, they play a key role in the removal of neuronal metabolic waste products, retinal repair processes, and neuroprotective processes through the secretion of neurotrophic factors, angiogenic molecules, and antioxidants. Moreover, their characteristic funnel shape, the radial alignment, and more suitable physical properties allow light to be optimally transmitted from the vitreous to the retinal photoreceptors (Kobat and Turgut, 2020). Astrocytes, also defined as astroglia, take their name due to their star shape. In contrast to Müller cells, astrocytes are not homogeneously distributed in all retinal layers but are almost entirely restricted to the NFL and the GCL. Similar to Müller cells, astrocytes are involved in maintaining retinal neuron homeostasis and play an essential part in the proper development and functioning of the retinal vascular system, including blood flow and the formation of the BRB (Garcia-Bermudez et al., 2021; Fernández-Sánchez et al., 2015). Not coincidentally, both macroglial cell types have a close relationship with neurons, endothelial cells, pericytes, and the major blood vessels that originate from the central retinal artery, giving life to a trilaminar vascular network comprising the superficial, intermediate, and deep vascular plexuses (**Fig. 2**). The presence of this complex vascular network is essential to support the activity of the various retinal regions by regulating local blood flow according to neuronal energy demand. In high-activity areas, blood flow is increased to deliver more oxygen and energy substrates, while in low-activity areas, blood flow is reduced (Grimes et al., 2024; Howarth, 2014). Microglial cells are resident immune cells spread in the central nervous system (CNS), including the retina. They are derived from progenitor cells of the yolk sac, and during CNS development, they infiltrate the retinal tissue where they regulate neurogenesis, promote neuronal survival, provide trophic support to the surrounding neurons, take part in myelination and the establishment of normal vascularization of the retina, and participate in synaptic pruning to ensure appropriate neuronal connections (Rathnasamy et al., 2019). In physiological conditions, these glial cells are generally confined to the inner retinal layers, where they are constantly engaged as the first line of defence against potentially pathogenic factors by monitoring the surrounding microenvironment with extremely motile processes and protrusions. When microglial cells recognize a damaging or pathogenic factor, they change from a highly ramified morphology to an ameboid form, shifting from a surveillant to an activated state. Once activated, microglial cells quickly migrate to the injury site and eliminate the pathogenic factor through phagocytosis (Wei et al., 2022). Particularly, microglial cells can be classified into two specific activated phenotypes: microglia of type 1 and type 2. Macroglial phenotype of type 1 was referred to as “classic activation”, where the cells release chemokines and pro-

inflammatory mediators, inducing neuroinflammation and neurotoxicity. Instead, the phenotype of type 2 was juxtaposed to an "alternative activation", and can be further subcategorized into 2a, 2b, and 2c types, all involved in wound healing and release of anti-inflammatory and neuroprotective factors (Guo et al., 2022; Wei et al., 2022).

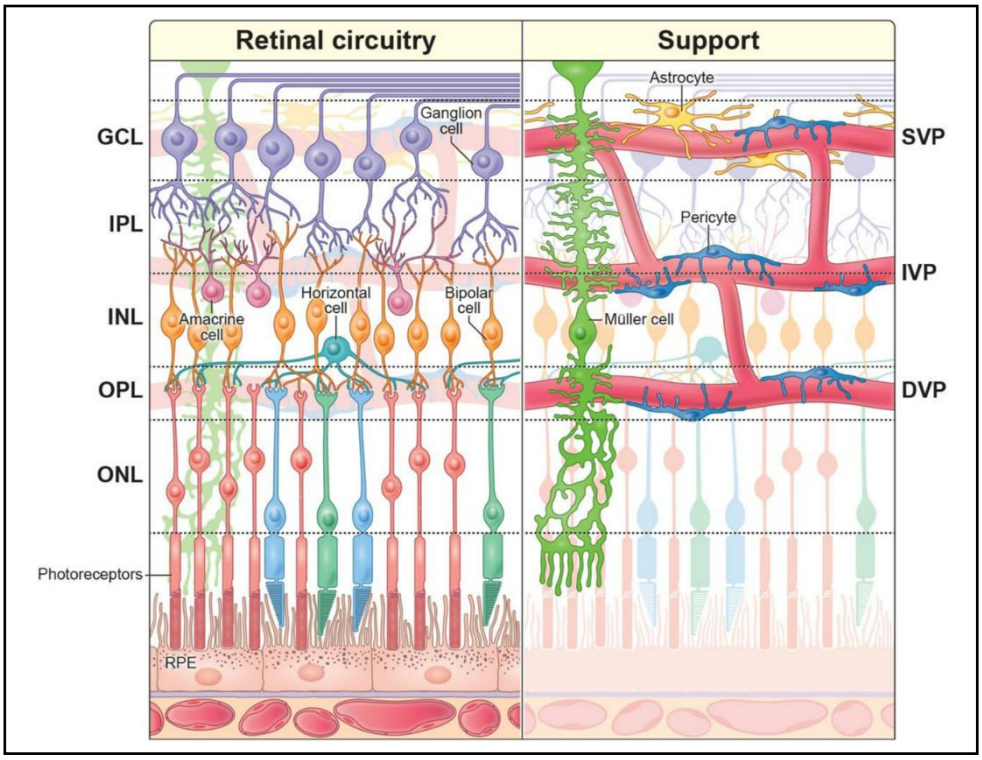

Figure 2. Schematic representation of retinal cell components (left) and retinal blood vessel network (right). GCL, ganglion cell layer; IPL, inner plexiform layer; INL, inner nuclear layer; OPL, outer plexiform layer; ONL, outer nuclear layer; SVP, superficial vascular plexus; IVP, intermediate vascular plexus; DVP, deep vascular plexus (Grimes et al., 2024).

1.2 An overview of the brain: anatomical and functional characteristics

The human brain represents one of the most complex biological systems, with over 100 billion neurons involved in developing and regulating numerous essential processes, such as movement, senses, emotions, language, communication, thinking, and memory. Brain development is a dynamic and highly regulated process that begins prenatally and continues in adulthood, involving several key phases such as neurogenesis, neural migration, neuronal differentiation, synaptogenesis, myelination, and synaptic pruning (Maldonado and Alsayouri, 2025; Stiles and Jernigan, 2010). Once formed, the brain can be structurally divided into 3 main parts: cerebrum, cerebellum, and brainstem. The cerebrum can be further classified based on the embryological origin or morphological features. From an embryonic point of view, the cerebrum is subdivided into prosencephalon (forebrain), mesencephalon (midbrain), and rhombencephalon (hindbrain). On the other hand, the cerebrum can be morphologically separated by a longitudinal fissure, defined as the corpus callosum, into the right and left hemispheres, both characterized by an outer layer of gray matter, known as the cerebral cortex, and a subcortical layer of white matter (Maldonado and Alsayouri, 2025). Each of the hemispheres consists of 4 different lobes (frontal, occipital, parietal, and temporal), each of which plays fundamental functions. The frontal lobe is responsible for motor function, as well as regulating behavioral processes such as attention, affect, mood, personality, self-awareness, and social reasoning. The occipital and parietal lobes are mainly involved in the processing of visual information and interpreting hearing, sensory, and motor functions, respectively. The temporal lobe is essential for the understanding of spoken and written language, as well as for processing spatial information, and the formation of short- and long-term memory (**Fig. 3**) (Maldonado and Alsayouri, 2025; Jawabri and Sharma, 2023). The cerebellum is located in the posterior cranial fossa, above the foramen magnum, and comprises the deep cerebellar nuclei surrounded by the cerebellar cortex, in turn characterized by the molecular, Purkinje, and granular layers (Carey, 2024). In particular, the cerebellar circuitry is defined by two anatomically and functionally distinct excitatory input pathways, mossy and climbing fibers. On the one hand, the mossy fibers synapse with the granular cells, whose axons ascend through the granule cell layer, past Purkinje cell bodies, and reach the molecular layer, where they bifurcate and become parallel fibers, which form numerous en-passant synapses with the dendrites of Purkinje cells and different inhibitory interneurons such as stellate, basket, and Golgi cells. On the other hand, the climbing fibers originate from the inferior olive, and their axons climb the Purkinje cell dendritic trees, making hundreds of synaptic contacts. Notably, Purkinje cells represent the sole output of the cerebellar cortex toward the cerebrum and brainstem (D'Angelo, 2018). From a functional point of view, the cerebellum plays a crucial role in coordinating voluntary muscle movements, maintaining posture and balance, as well as regulating motor learning, eye movement coordination, and some cognitive processes such as attention, language, and executive functions (Rudolph et al., 2023; D'Angelo, 2018). The brainstem is located anterior to the cerebellum, between the base of the cerebrum and the spinal cord, and contains the midbrain, pons, and medulla. It is responsible for many vital functions, including the regulation of breathing, consciousness, blood pressure, heart rate, and sleep (Basinger and Hogg, 2025).

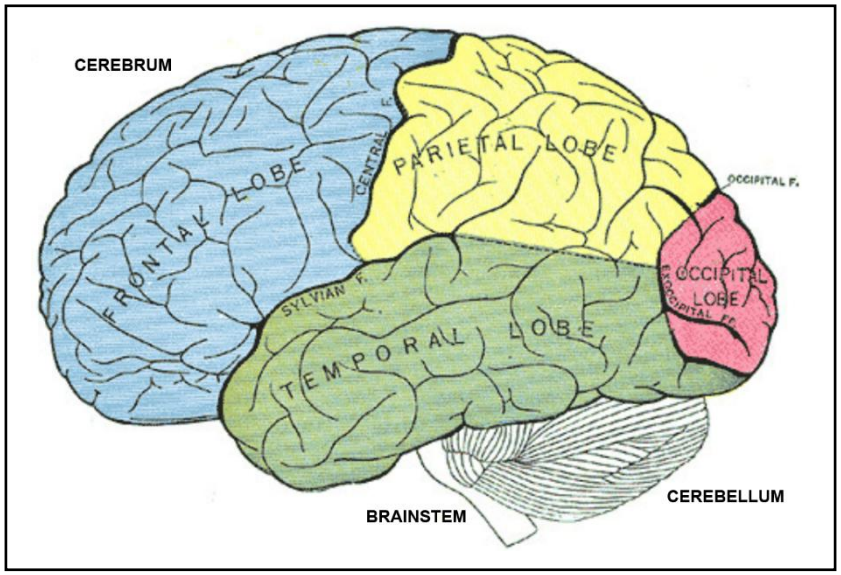

Figure 3. Principal parts of the brain include the cerebrum with its lobes and fissures, as well as the cerebellum and the brainstem. Different colours were used to visualize a specific brain lobe, including the frontal lobe (light blue), parietal lobe (yellow), temporal lobe (green), and the occipital lobe (dark pink) (Rehman and Khalili, 2023).

1.2.1 Cerebral microcirculation and biological role of the Blood-Brain Barrier

The cerebral circulation is characterized by a dense, ramified, and highly specialised vascular network that regulates the flow of oxygen and nutrients to the brain, as well as allows the removal of potentially toxic catabolites produced during the neuronal and glial cell metabolic activities (Kandel et al., 2014). This complex vascular network comprises several vessels having variable calibres and different morpho-functional features, including arteries, veins, arterioles, venules, and capillaries (Liu et al., 2025). In particular, the proper cerebral blood flow is guaranteed by the circle of Willis, an anastomotic vascular system located at the base of the brain that links the carotid and vertebral arteries. The carotid arteries originate from the common carotid arteries and carry oxygenated blood to the anterior parts of the brain. The vertebral arteries, which arise from the subclavian arteries, converge to form the basilar artery that carries oxygenated blood to the posterior parts of the brain, as well as to the cerebellum and the brainstem (Kandel et al., 2014). The major arteries ramify, leading to the formation of increasingly smaller vessels such as the pial arteriolar vessels, which play a crucial role in maintaining an appropriate perfusion of the surface cerebral structures. The pial arteriolar vessels give rise to the cortical penetrating arterioles, which pass through the cerebral parenchyma and extend into the deep capillaries, collectively forming the cerebral microcirculation. The latter is fundamental to ensure a correct and well-regulated blood flow to all single neurons and glial cells by providing oxygen, glucose, and other essential nutrients (Kandel et al., 2014; Bär, 1980). Besides the arterial system, the venous system also plays important functions, including that of collecting oxygen-poor blood from the arterial capillaries through a sort of venous reticulum devoid of valves. Particularly, the blood enters the post-capillary venules, and is quickly drained at the level of the dural venous sinuses and then converges in the internal jugular vein, thus completing the cerebral circulation circuit (Hufnagle and Tadi, 2025; Safadi and Tadi, 2023).

Each cerebral capillary is covered by a single layer of endothelial cells that interacts with different surrounding cell types, including astrocytes, microglial cells, pericytes, and neurons, giving rise to the neurovascular unit, which plays a key role in the formation and maintenance of the Blood-Brain Barrier (BBB) (Yu et al., 2020) (**Fig. 4**). The BBB consists of a complex and highly specialized structure, which plays an essential role in maintaining cerebral homeostasis, as well as in protecting against potentially neurotoxic substances, pathogen agents, and fluctuations in the extracellular microenvironment. A core element of the BBB is represented by endothelial cells, which have unique morpho-functional features such as high mitochondrial density, reduced pinocytotic activity, absence of fenestrations, and presence of numerous tight junctions, that make them phenotypically different from other endothelial cells located in different parts of the body (Kandry et al., 2020). Particularly, the tight junctions constitute the main physical barrier to the non-selective and paracellular diffusion of solutes and hydrophilic molecules, leading to a high transendothelial electric resistance, which is considered a key index of the BBB permeability level. The main proteins involved in the formation of the tight junctions include transmembrane protein complexes such as claudins, occludin, and junctional adhesion molecules, as well as cytoplasmic adapter proteins such as zonula occludens of type 1 (ZO-1), ZO-2, and ZO-3 (Obermeier et al., 2013). ZO-1, -2, and -3 have sequence similarity with each other and belong to a membrane-associated guanylate kinase-like protein. They contain three PDZ domains (PDZ-1, PDZ-2, and PDZ-3), one Src Homology-3 (SH3) domain, and one guanyl kinase-like domain. Claudins belong to a superfamily of highly conserved transmembrane proteins, with over 27 isoforms identified in mammals, while occludins are larger transmembrane phosphoproteins. Both claudins and occludins are characterized by four transmembrane domains, two extracellular loops, a long COOH-terminal cytoplasmic domain, and a short NH2-terminal cytoplasmic domain. Their extracellular loops can interact with other extracellular loops of adjacent claudins and occludins, forming homotypic and heterotypic cell-cell connections, while their cytoplasmic domains are directly anchored to the actin cytoskeleton by interacting with PDZ domains of ZO proteins (Kandry et al., 2020). Noteworthy, claudin-5 represents the most expressed isoform in the BBB, followed by occludin and other claudin isoforms such as claudin-1, -3, and -12. Claudin-5 is essential for the stability and ion selectivity of the BBB, while occludin contributes to the structural integrity and modulates the molecular traffic. Instead, claudin-1, -3, and -12 isoforms seem to be transiently expressed during embryonic development and some pathological conditions. Besides endothelial cells, pericytes and astrocytes also play a crucial role in maintaining BBB integrity, regulating blood flow, and supporting brain metabolism (Kandry et al., 2020; Krause et al., 2008). Pericytes are vascular mural cells that wrap around endothelial cells within the basement membrane of blood microvessels such as arterial capillaries and post-capillary venules. Their close association with endothelial cells allows the exchange of ions, metabolites, second messengers, and ribonucleic acids between the two cell types. Moreover, pericytes regulate the expression of several proteins in the BBB. In addition, they control the alignment of the tight junctions and regulate angiogenesis, microvascular stability, and angioarchitecture during vascular remodelling. Recent findings have reported that some pericytes may display phagocytosis functions by removing toxic metabolites, and present contractile features similar to smooth muscle cells, by taking part in the regulation of capillary diameter and the cerebral

blood flow (Kandry et al., 2020; Sweeney et al., 2016). Astrocytes represent the most abundant cells in the CNS and are involved in numerous physiological processes, such as compartmentalization of the neural parenchyma, pH regulation, maintenance of the ionic homeostasis of the extracellular space, mediation of signals from neurons to the vasculature, neurotransmitter clearance and recycling, controlling immune reactions, providing energy-rich substrates to the neuron cells, and regulation of the BBB morpho-functional activities. Particularly, perivascular astrocyte end-feet, which encircle the abluminal side of cerebral microvessels, are highly specialised and polarized structures with an orthogonal array of intramembranous particles, consisting of the most abundant water channel aquaporin-4, and ATP-sensitive inward rectifier potassium channels. The astrocytic end-feet processes wrap around the cerebral capillaries and release paracrine signals, such as vascular endothelial growth factor (VEGF), angiopoietin-1, and tumor growth factor-β, that promote endothelial differentiation and the formation of tight junctions (Kandry et al., 2020; Obermeier et al., 2014; Duffy et al., 2013).

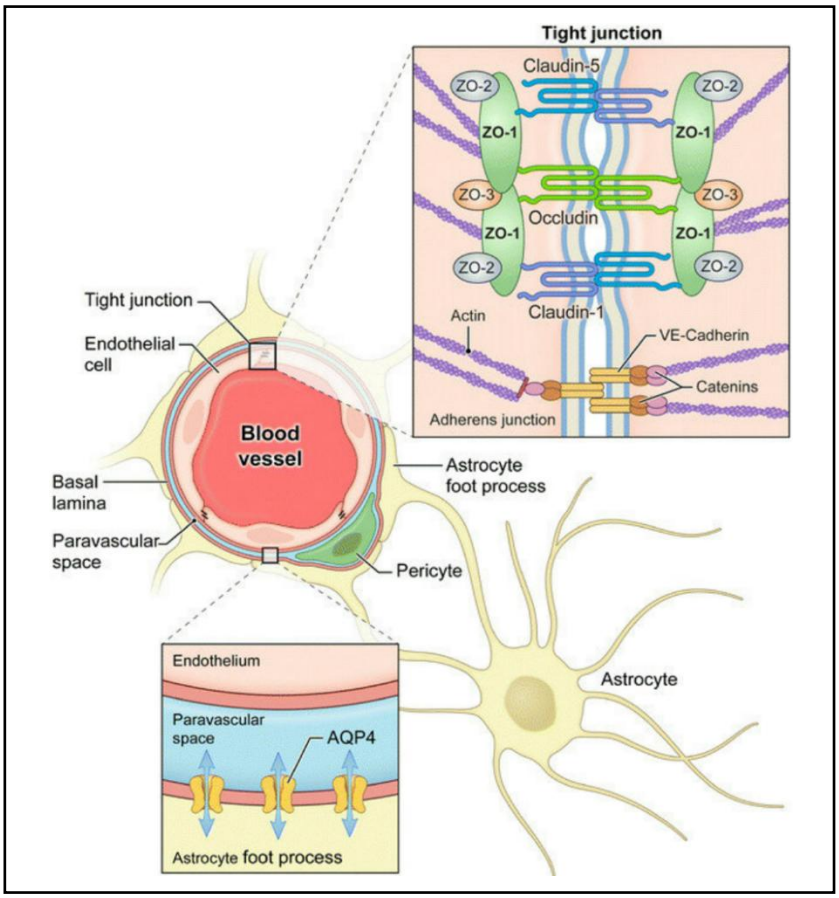

Figure 4. Blood-Brain Barrier composition and tight junction types. ZO-1, Zonula Occludens of type 1; ZO-2, Zonula Occludens of type 2; ZO-3, Zonula Occludens of type 3; VE-Cadherin, Vascular Endothelial-Cadherin; AQP4, Aquaporin-4 (Murayi and Chittiboina, 2016).

1.3 Alzheimer's Disease: main clinical, genetic, and molecular aspects

Alzheimer's Disease (AD) represents one of the most common forms of dementia, with over 40 million people affected worldwide (Shi et al., 2021). AD is a neurodegenerative disorder with an insidious onset followed by a gradual and irreversible impairment of behavioral and cognitive functions, including memory, comprehension, language, attention, reasoning, and judgment (Williams et al., 2021; Deardoff and Grossberg, 2019; Jahn, 2013). The AD symptoms can depend on the stage of the disease, passing through a pre-symptomatic stage to a mild cognitive impairment, and severe stages. Particularly, episodic short-term memory loss is the initial and most common AD-related symptom. Over time, people may manifest increasingly evident symptoms, up to showing language disorder, impaired visuospatial abilities, dyspraxia, dystonia, akathisia, olfactory dysfunction, and neuropsychiatric signs like apathy, social withdrawal, disinhibition, agitation, psychosis, and wandering. In the end-stage disease, AD patients display reduced primitive reflexes, incontinence, and total loss of their independence (Kumar et al., 2024). Depending on the age of onset, two different AD forms were identified: late-onset AD (LOAD) and early-onset AD (EOAD). The LOAD, also called Sporadic AD (SAD), represents the most common AD form, comprising almost the entirety of patients (about 95%), and is defined by a multifactorial etiology with an age of onset over 65 years (Rabinovici, 2019). Given its multifactorial nature, it is complicated to identify the mechanisms underlying the SAD progression, even if a strong association with aging, as well as the development of neuroinflammatory processes, and oxidative stress arising from environmental stimuli (air pollutant), mitochondrial dysfunction, metal exposure (aluminium, lead, and cadmium), concomitant diseases (cardiovascular complications, obesity, diabetes, insulin-resistance, chronic infections), lifestyle, and diet has been observed (Kotredes et al., 2025; Wang et al., 2023; Dhana et al., 2020; Claassen, 2015). The SAD form seems to be associated also with the presence of over 20 common genetic variants that take part in different biological pathways, such as lipid metabolism, innate immunity, and endocytosis. Among them, the strongest genetic risk factor is represented by the apolipoprotein E (APOE) gene, which encodes for three common allelic variants, of which two seem to be protective (APOE-ε2 and APOE-ε3), and one harmful (APOE-ε4) (Armstrong, 2019). On the other hand, the EOAD, also known as Familial AD (FAD), is considerably less frequent (about 5%) than SAD and is characterized by an age of onset less than 65 years. The FAD presents a strictly genetic etiology having an autosomal dominant inheritance with a high degree of penetrance. In particular, the FAD patients carry one or more-point mutations in one of the three main genes involved in amyloid beta (Aβ) processing, including amyloid precursor protein (APP), presenilin 1 (PSEN1), and PSEN2. In addition, FAD patients show a more aggressive clinical course, more frequent delay in diagnosis, higher prevalence of traumatic brain injury, less memory impairment, greater psychosocial difficulties, and atypical clinical features such as headaches, myoclonus, seizures, gait abnormalities, pseudobulbar palsy, or hyperreflexia (Pradeepkiran et al., 2024; Mendez, 2019).

1.3.1 Aβ and Tau: the pillars of AD pathogenesis

Nowadays, based on the current understanding of AD, two main pathophysiological hypotheses have been proposed: cholinergic and amyloid. The cholinergic hypothesis proposes that the reduced cerebral acetylcholine (ACh) levels, resulting from neuronal loss in the nucleus basalis of Meynert, play a key role in AD development. On the other hand, the amyloid hypothesis suggests that the progressive Aβ cerebral accumulation, caused by an abnormal enzymatic processing of APP, leads to neuronal loss and AD development. Among these, the amyloid hypothesis is currently the most widely accepted pathophysiological mechanism for AD, especially in cases of FAD (Kumar et al., 2024).

The APP is an evolutionarily conserved transmembrane glycoprotein implicated in different biological processes, including neurogenesis, neuronal maturation, synaptogenesis, neurotrophic support, and cell proliferation. In particular, APP is encoded by the APP gene located on the 21st chromosome. Following the alternative splicing, three different APP isoforms are formed, of which two are ubiquitously expressed in the whole body (APP751 and APP770), and one is mainly expressed in the CNS (APP695). All three isoforms share a common structure characterized by a large N-terminal extracellular domain, a short C-terminal intracellular domain, a transmembrane domain, and an Aβ domain that partially extends into both the extracellular and transmembrane domains. During its lifetime, APP is processed by different proteolytic cleavage pathways, including the η-secretase, non-amyloidogenic, and amyloidogenic pathways (Coronel et al., 2018) (**Fig. 5**). In the η-secretase pathway, the C-terminal extracellular domain of APP is initially cleaved at position 505 by the η-secretase enzyme, releasing a soluble ectodomain of APP (sAPP-η). The remaining C-terminal fragment (CTF-η) is further processed by β-site amyloid precursor protein cleaving enzyme (BACE), also known as β-secretase, or α-secretase enzyme, thereby liberating the Aη-β and Aη-α peptides into the extracellular medium, respectively (Coronel et al., 2018). On the one hand, the remaining CTF-β and CTF-α fragments can be further processed by the γ-secretase enzymatic complex, in turn characterized by structural subunits (presenilin enhancer 2, nicastrin, and anterior pharynx-defective 1), and catalytic subunits (PSEN1 or PSEN2), giving rise to the APP intracellular domain (AICD), which is degraded into smaller cytosolic fragments by the proteasome, or some proteins having a proteolytic activity, such as insulin-degrading enzyme (IDE), and cathepsin B (Wolfe, 2019). On the other hand, the potential biological functions carried out by the Aη-β and Aη-α peptides are still not well understood, although it has been reported that they can inhibit hippocampal neuronal activity under physiological conditions (Willem et al., 2015). In the non-amyloidogenic pathway, the APP is processed by the α-secretase enzyme at position 16 within the Aβ domain, thus preventing the generation of Aβ peptides and promoting the release of the soluble ectodomain of APP (sAPP-α). The remaining C-terminal fragment (CTF-α) is quickly processed by the γ-secretase enzymatic complex by generating the soluble and non-toxic peptide 3, as well as the AICD (Coronel et al., 2018; Bandyopadhyay et al., 2007). The amyloidogenic pathway has a similar dynamic to the non-amyloidogenic pathway, except that it involves the BACE in place of the α-secretase. The extracellular domain of APP is initially cleaved at position 671 by the BACE, liberating the soluble ectodomain of APP (sAPP-β). The remaining C-terminal fragment (CTF-β) is further processed by the γ-secretase enzymatic complex by generating the AICD and

different isoforms of Aβ peptides. In contrast to the non-amyloidogenic pathway, the AICD is quickly stabilized in the cytoplasm by the interaction with the adaptor protein fetal embryonic 65 (Fe65), forming the AICD-Fe65 complex, which is able to translocate into the nucleus, where it forms a transcriptionally active complex with Tat-interacting protein 60, thus regulating the expression of numerous target genes (Hampel et al., 2021; Coronel et al., 2018). Noteworthy, the FAD-related mutations determine a higher affinity of BACE to the mutated APP sequence, as well as a greater activity of γ-secretase enzymatic complex, leading to an increased amyloidogenic flow, and subsequent increment in the Aβ production (Schilling et al., 2023; Thordardottir et al., 2017; Chen et al., 2017). Besides the conventional pathways, other alternative APP processing pathways were found, which seem to play protective functions. The BACE can also cleave the APP at a secondary site called β', located between Tyr10 and Glu11 of the Aβ domain, generating the C89 fragment. C89 is subsequently processed by the γ-secretase enzymatic complex, releasing different smaller and less-toxic isoforms of Aβ peptides. In addition, it also exists BACE of type 2 (BACE2), which shares 64% amino acid homology and a similar structural organization with BACE. BACE2 effectively cleaves the APP at the θ-site located within the Aβ domain, thus noticeably reducing the Aβ production (Tan and Gleeson, 2019).

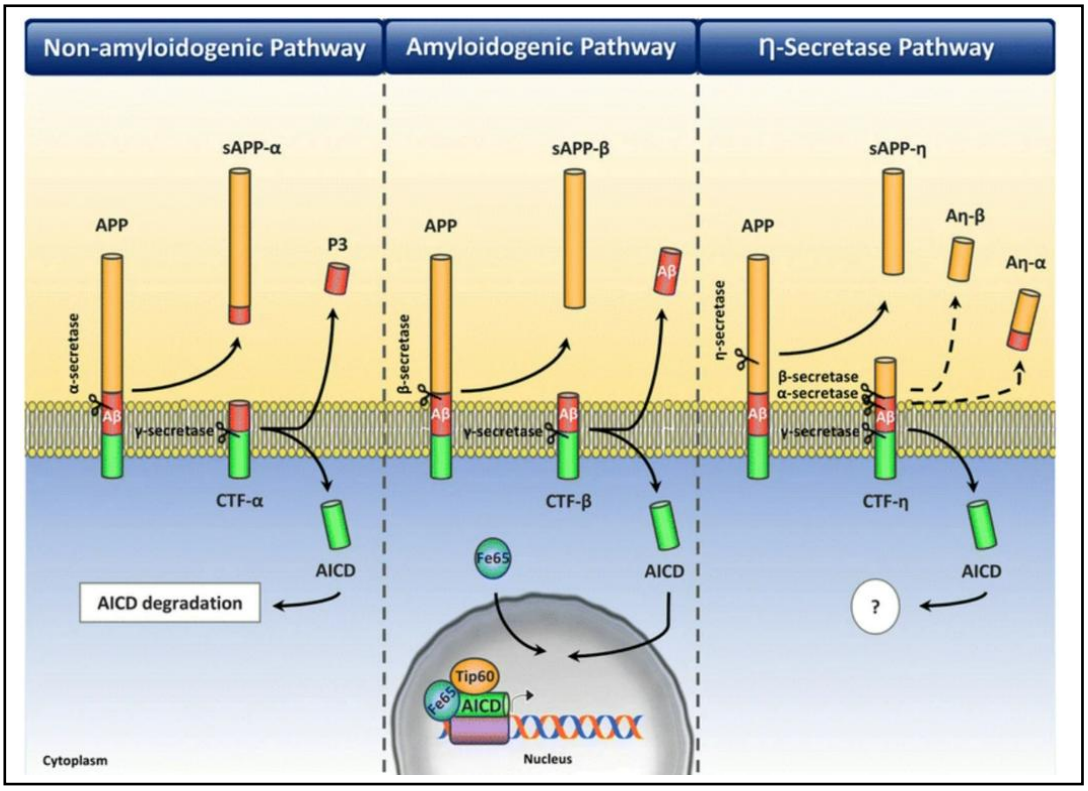

Figure 5. The main processing pathways of APP. On the left-hand side is depicted the non-amyloidogenic pathway, while the middle and right-hand sides show the amyloidogenic and η-secretase pathways, respectively. APP, amyloid precursor protein; sAPP-α, soluble APP-α; P3, Peptide 3; sAPP-β, soluble APP-β; Aβ, amyloid beta; sAPP-η, soluble APP-η; Aη-β, amyloid-η-β; Aη-α, amyloid-η-α; CTF-α, C-terminal fragment-α; CTF-β, C-terminal fragment-β; CTF-η, C-terminal fragment-η; AICD, APP intracellular domain; Fe65, Fetal embryonic 65; Tip60, Tat-interacting protein 60 (Coronel et al., 2018).

The Aβ sequence is remarkably ancient and well-preserved, to the extent that almost all vertebrates produce Aβ peptides with high amino acid homology (approximately 95%) compared to human Aβ peptides. Not surprisingly, numerous studies highlighted that low concentrations (in the order of picomolar) of Aβ peptides play an important role in many biological and evolutionary activities, including synaptic plasticity, memory consolidation, neuronal growth and survival, and protection against oxidative stress, neuroactive compounds, toxins, and pathogens (Bishop and Robinson, 2004). In contrast, higher concentrations (in the order of nanomolar or more) promote the Aβ aggregation, giving rise to heterogeneous oligomers of approximately 2-100 Aβ monomers. These Aβ oligomers may be subjected to primary nucleation, fragmentation, secondary nucleation, and elongation processes, generating ordered, insoluble, and non-crystalline structures, well-known as Aβ fibrils, which are progressively deposited, forming Aβ plaques (Alijanvand et al., 2021; Chen et al., 2017). The most expressed Aβ isoforms are represented by Aβ at 40 amino acids (Aβ40) and Aβ42, which structurally differ by two additional C-terminal residues (isoleucine and alanine) on Aβ42. While the Aβ40 presents a high solubility and reduced toxicity, the Aβ42 is characterized by a higher hydrophobicity rate, which is at the core of its lower solubility and higher propensity to form cytotoxic aggregates. Among the different types of aggregates, the Aβ oligomers seem to be most toxic, thanks to their capacity to bind several receptors expressed by neurons and glial cells, including the receptor for advanced glycation end-products (RAGE), N-methyl-D-aspartate receptor, low-density lipoprotein receptor-related protein 1 (LRP1), α7 nicotinic ACh receptor, the metabotropic glutamate receptor 5 and many other, triggering damaging phenomena such as neuroinflammation, oxidative stress, excitotoxicity, Ca^{2+} dyshomeostasis, damaged mitochondrion, synaptic damage, inhibition of axonal transport, glial reactivity, neuronal apoptosis, and Tau hyperphosphorylation (Chen et al., 2017; Gu and Guo, 2013).

Tau protein belongs to the microtubule-associated protein (MAP) family and is encoded by the MAP-Tau gene, located on the 17th chromosome. Following the alternative splicing, six different Tau isoforms are produced, having variable sizes from 352 to 441 amino acids. All these isoforms share a common structure composed of the N-terminal domain, a proline-rich region (PRR), a microtubule binding domain (MTBD), and a C-terminal domain (Penke et al., 2020). In particular, the N-terminal domain is involved in regulating microtubule dynamics by influencing the attachment and/or spacing between microtubules and other cell components. The PRR is involved in the regulation of microtubule assembly and actin binding and has been identified as a deoxyribonucleic acid (DNA) and ribonucleic acid (RNA)-interacting site, indicating its importance in neuronal cell signalling, nuclear function, and maintenance of the neuronal cytoskeleton (Penke et al., 2020). Moreover, PRR harbours seven Pro-XX-Pro motifs, providing potential recognition sites for SH3-containing proteins such as the Src family, lymphocyte cell-specific protein-tyrosine kinase, bridging integrator 1, phosphatidylinositol 3-kinase, and phospholipase C (Guo et al., 2017). The MTBD consists of three- or four-repeat groups containing 18 amino acid sequences separated by 13- or 14-amino acid-long flanking regions and is mainly involved in the binding and stabilization of microtubules (Goode and Feinstein, 1994). The C-terminal domain contains several interaction sites with numerous kinase and phosphatase proteins, such as glycogen synthase kinase 3 (GSK3), dual specificity tyrosine phosphorylation regulated

kinase 1A, protein phosphatase (PP) of type 1, serine/threonine PP2A, and PP2B (also called calcineurin) (Guo et al., 2017; Anderton et al., 2001). The main physiological function of Tau consists of assembly, spatial organization, and dynamic behaviour of the microtubules, although recent advances have revealed that Tau can also play an important role in cell signalling, synaptic plasticity, and genomic stability (Penke et al., 2020). During its life, Tau shows a large number of post-translational modifications, including glycation, sumoylation, glycosylation, acetylation, methylation, and phosphorylation. In particular, the Tau phosphorylation state has been extensively studied as it changes the biological activity of the protein. Indeed, following the hyperphosphorylation, phosphorylated Tau (pTau) changes its conformation by separating from the microtubule filaments, and then forms pathological intracellular aggregates such as oligomers, fibrils, and neurofibrillary tangles (NFT) (Guo et al., 2017). It has been widely accepted that the big Tau assemblies, like NFT, are less toxic than the smaller Tau oligomers, which are able to spread into the intracellular environment, resulting in a disaggregation of microtubules, impaired signal transmission, increased excitability of neurons, synaptic loss, disturbing neuronal circuits, altered intracellular transport, energy metabolism impairment, abnormalities of protein degradation, glial reactivity, neuroinflammation, and harmful effects on the genome (Niewiadomska et al., 2021) (**Fig. 6**).

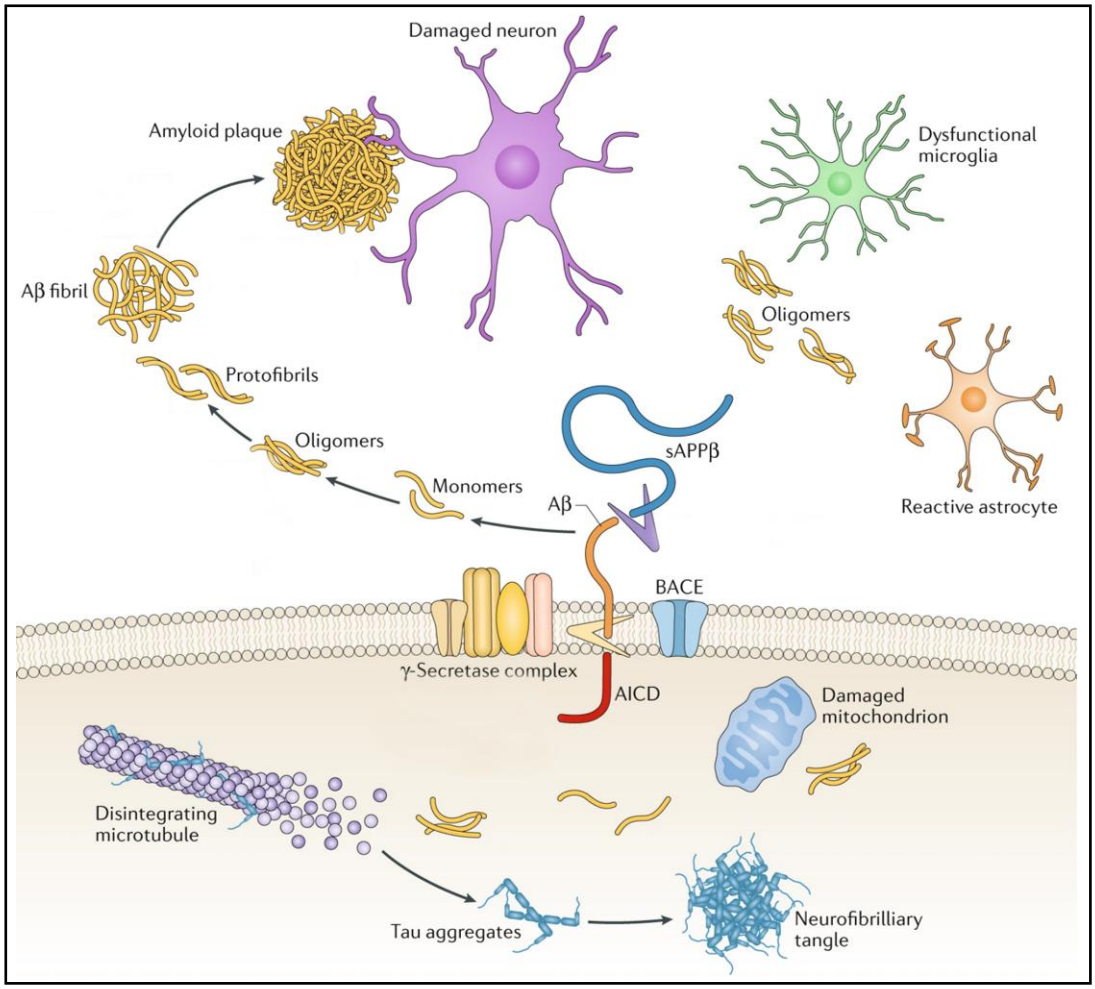

Figure 6. Aβ and Tau in AD. Aβ, amyloid beta; sAPP-β, soluble APP-β; BACE, β-site amyloid precursor protein cleaving enzyme; AICD, APP intracellular domain (Panza et al., 2019).

1.3.2 Aβ homeostasis: degradation and transport systems

The production of Aβ is normally counterbalanced by the presence of numerous biological processes, including proteolytic degradation mainly mediated by a large number of peptidases and proteinases, cell-mediated clearance, active and passive transports out of the brain, and deposition into insoluble aggregates, thus maintaining a homeostatic condition over time (Saido and Leissring, 2012). Proteolytic degradation is a catalytic and irreversible process, meaning that each peptidase or proteinase can permanently eliminate many Aβ peptides, while itself remaining unchanged, although some environmental factors and aging seem to affect the proteolytic activity. The mean proteases involved in Aβ degradation include several zinc-metalloproteases, such as neprilysin (NEP, also known as cluster of differentiation 10 (CD10)), NEP-like peptidases, endothelin-converting enzymes, angiotensin-converting enzymes, matrix-metalloproteinases, IDE, as well as some serine-proteases, like plasmin, and other cysteine-aspartyl-proteases, such as cathepsin B and cathepsin D (Saido and Leissring, 2012). Among these, the most important proteases are represented by NEP and IDE. On the one hand, NEP is almost exclusively expressed in the subcellular compartments of the neuron cells and consists of a type II membrane-associated peptidase, the active site of which faces the intraluminal or extracellular side of membranes, a topology that is ideally suited for the degradation of largely extracytoplasmic peptides such as Aβ. On the other hand, IDE belongs to a superfamily having distinct evolutionary origins, referred to as inverzincins because they feature a HxxEH zinc-binding motif that is inverted compared to the canonical one, HExxH, present in most known zinc-metalloproteases. IDE is mainly localised in the cytosol as well as in the mitochondria, and its structure is similar to a shell characterized by a large internal chamber formed from two bowl-shaped halves connected by a flexible linker. Since the oligomeric or fibrillar forms of Aβ are too large to fit completely into its internal chamber, IDE can degrade only the monomeric Aβ isoforms (Chen et al., 2017; Saido and Leissring, 2012). Besides the proteolytic degradation, the excess of Aβ peptides released into the extracellular space can be reduced and kept under control through receptor-mediated transport systems such as RAGE and LRP1, as well as some chaperones like APOE. Interestingly, astrocytes and microglial cells secrete into the interstitial fluid of the brain variable amounts of APOE. The latter interacts with some lipid molecules, forming lipoproteins, which can bind the Aβ peptides, thus generating complexes that can be recognized by LRP1, internalized, and degraded through the endo-lysosomal pathway (Chen et al., 2017; Liu et al., 2013).

1.3.3 Neuroinflammation and glial reactivity as key drivers in AD pathogenesis

The extracellular Aβ aggregates and intracellular pTau accumulation lead to increasingly high levels of neuroinflammation, which play a key role in AD pathogenesis (Heneka et al., 2025). Generally, neuroinflammatory processes have a dual function, playing a neuroprotective role during the acute-phase response against infections, toxic agents, or lesions, and a detrimental activity when a chronic response is mounted, as observed in AD as well as in other neurodegenerative disorders (Kinney et al., 2018). This chronic neuroinflammation is mainly attributed to the microglia activation, during which they change their phenotype,

passing from an inactivated state to an active state. Once activated, the microglial cells can migrate towards the Aβ plaques, removing them through phagocytosis, as well as release a large number of proinflammatory cytokines that recruit additional microglial cells, resulting in a characteristic halo of activated microglia surrounding Aβ plaques (Merighi et al., 2022; Kinney et al., 2018). In the early stages of AD pathogenesis, the microglia activation determines protective effects, promoting Aβ clearance, but in the advanced stages of the disease, the prolonged activation leads to a microgliosis condition, resulting in sustained pro-inflammatory cytokine signaling, increased ionized calcium-binding adapter molecule 1 (Iba1) levels, and decreased phagocytic efficiency, becoming a source of damage for surrounding neurons (Kinney et al., 2018; Akiyama et al., 2000). Besides microglial cells, the astrocytes also play a central role in AD. During the AD progression, astrocytes undergo noticeable phenotypic changes, giving rise to astrogliosis, belatedly followed by astropathy. In astrogliosis conditions, the astrocytes show deep transcriptional, biochemical, metabolic, and physiological changes, which manifest as increased phagocytic activity, cell hypertrophy, elevated levels of glial fibrillary acidic protein (GFAP), along with heightened production of chemokines, and different pro-inflammatory cytokines, such as interleukin-6 (IL6), IL1β, and tumor necrosis factor α (TNFα). Over time, astrocytes can also be subjected to astrodegeneration, involving functional loss, dysfunctional energy metabolism, reduced intake of glutamate, altered regulation of cerebral blood flow, and atrophy (Lucena and Heneka, 2024). The nuclear factor-κB (NF-κB) is one of the main pro-inflammatory transcription factors involved in AD progression, so much so that its activated forms are particularly present in neurons and glial cells surrounding Aβ plaques (Sun et al., 2022). The NF-κB family is composed of five structurally related members, including NF-κB1 (p50), NF-κB2 (p52), RelA (also known as p65), RelB, and c-Rel (Guo et al., 2024). In physiological conditions, NF-κB is sequestered in the cytoplasm by the inhibitor-κB (IκB) proteins. The activation of NF-κB involves two distinct signaling pathways: canonical and non-canonical (also called alternative) (Lawrence., 2009). The canonical pathway is promoted by diverse stimuli, including pro-inflammatory cytokines, growth factors, mitogens, microbial products, stress agents, and Aβ peptides, which can bind different receptors, triggering the activation of the multi-subunit IκB-Kinase (IKK) complex, in turn formed by two catalytic subunits (IKKα and IKKβ), as well as a regulatory subunit named NF-κB essential modulator. Upon activation, IKK quickly phosphorylates IκB at two N-terminal serine residues, triggering the ubiquitin-dependent IκB degradation in the proteasome, resulting in rapid and transient nuclear translocation of canonical NF-κB members, by way of the p50/p65 and p50/c-Rel dimers (Trares et al., 2022; Liu et al., 2017). On the other hand, the non-canonical pathway selectively responds to specific stimuli, including a subset of TNF receptors, such as B-cell activating factor receptor, CD40, lymphotoxin-β receptor, and receptor activator of NF-κB, which are able to induce the activation of the NF-κB-inducing kinase (NIK). Subsequently, NIK activates and functionally cooperates with IKK to mediate p100 phosphorylation, which is quickly ubiquitinated and processed, resulting in the generation of mature p52 that translocates into the nucleus as a non-canonical p52/RelB dimer (Rodriguez et al., 2024; Liu et al., 2017; Sun, 2011). Numerous studies highlighted that both NF-κB canonical and non-canonical pathways are particularly involved in AD pathogenesis by promoting

increased BACE expression, amyloidogenesis, Tau hyperphosphorylation, gliosis, neuroinflammation, and apoptosis (Sivamaruthi et al., 2023; Sun et al., 2022) (**Fig. 7**).

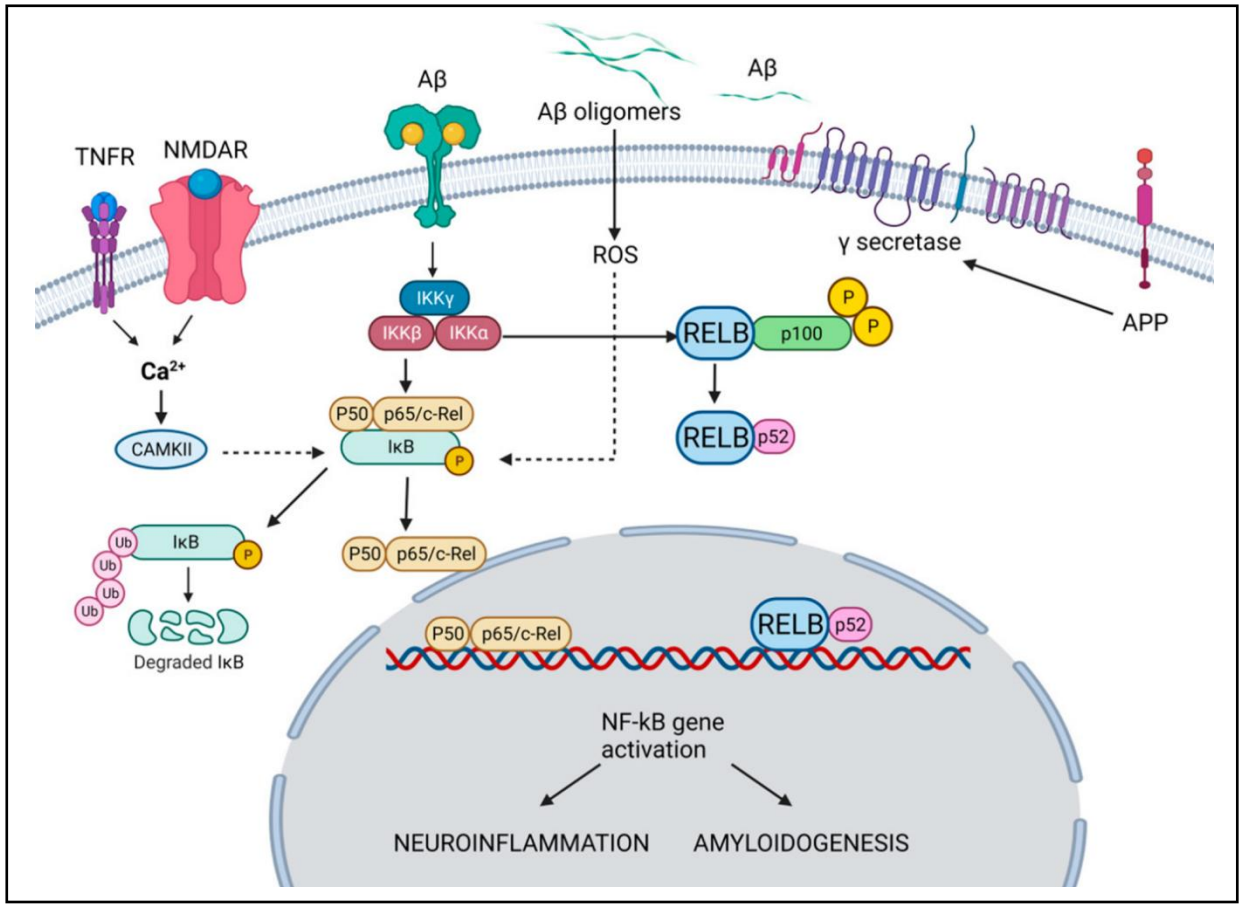

Figure 7. NF-κB pathways and their role in AD pathogenesis. TNFR, tumor necrosis factor receptor; NMDAR, N-methyl-D-aspartate receptor; Aβ, amyloid beta; APP, amyloid precursor protein; CAMKII, calcium/calmodulin-dependent protein kinase II; IκB, inhibitor-κB; Ub, ubiquitin; IKK, IκB-Kinase; NF-κB, nuclear factor-κB (Sivamaruthi et al., 2023).

1.3.4 Oxidative stress: another core element in AD pathogenesis

Oxidative stress is generally induced by a large number of free radicals derived from oxygen. These free radicals, also known as ROS, are highly oxidizing molecules that carry one unpaired electron in their outer shell, making them particularly unstable and prone to react with surrounding molecules (Jakubczyk et al., 2020). The precursor of most ROS and mediators in oxidative stress chain reactions is the superoxide anion, which can be partially reduced to a hydroxyl radical, one of the strongest oxidants in nature. ROS are normally produced by numerous metabolic reactions and regulate several physiological processes, including cell signaling, gene expression, enzymatic reactions, mitochondrial function, and antimicrobial activity (Bayir, 2005). Despite its physiological relevance, some organs like the brain are particularly susceptible to oxidative damage due to their high oxygen consumption, abundant lipid content, and relatively low levels of antioxidant molecules (Fanlo-Ucar et al., 2024; Cobley et al., 2018). Not surprisingly, an excessive production of ROS has been found in AD patients, which is deleterious as well as an important mediator of damage to DNA, proteins,

and lipids, leading to synaptotoxicity and neuronal death. It is well-known that Aβ may trigger ROS production mainly through the reduction of metal ions as iron and copper, while ROS contributes to Aβ formation and aggregation by promoting the BACE activity and amyloidogenic pathway, thus creating a detrimental vicious cycle (Fanlo-Ucar et al., 2024; Huang et al., 2016). The high ROS production may also impair Aβ clearance by affecting the activity of proteolytic enzymes, transmembrane receptors, and the ubiquitin-proteasome system (Cheignon et al., 2017). In addition, Aβ may alter the biological function of some proteins through oxidative modifications and trigger lipid peroxidation, neuroinflammation, and apoptosis phenomena (Kumari et al., 2023; LaRocca et al., 2021; Butterfield and Lauderback, 2002). One of the most important proteins involved in the antioxidant response is nuclear factor erythroid 2-related factor 2 (NRF2), which is also considered a key regulator of AD pathogenesis (Osama et al., 2020). Under homeostatic conditions, NRF2 is sequestered in the cytosol by interaction with its inhibitor Kelch-like ECH-associated protein 1 (Keap1), leading to ubiquitination through the formation of the Keap1-Cullin (Cul) 3-RING box protein-1 (RBX1) complex, which induces the NRF2 proteasomal degradation. NRF2 may also be conducted to degradation by the activity of GSK3, which specifically phosphorylates some serine residues located in the NRF2-ECH homology domain 6, creating a binding site for the E3 ligase adaptor beta-transducin repeat-containing protein (β-TrCP). In turn, β-TrCP recruits the Cul1/RBX1 complex, leading to ubiquitination and subsequent proteasomal degradation of NRF2 (De Plano et al., 2023). In the AD patients, the presence of Aβ aggregates induces an increasing ROS production, which modifies the cysteine sulfhydryl groups of Keap1, resulting in a detachment of Keap1 from NRF2, which is free to translocate into the nucleus, where it heterodimerizes with small MAF protreins and then bind the antioxidant response element gene sequences (De Plano et al., 2023; George et al., 2022), thus promoting the transcription of several antioxidant genes, including those encoding for heme oxygenase 1, NAD(P)H quinone dehydrogenase 1 (NQO1), glutamate cysteine ligase, phenol sulfotransferase, glutamate-cysteine ligase catalytic subunit, glutathione reductase, gamma-glutamyl cysteine synthetase, thioredoxin reductase, peroxiredoxin, and some heat shock proteins (Tejo and Quintanilla, 2021; Moreira et al., 2010).

1.3.5 Apoptosis and AD: exploring the mechanisms behind neuronal loss

Apoptosis, also known as programmed cell death, is a highly regulated form of cell death that normally occurs during development and aging, serving as both a homeostatic mechanism to maintain the cell population and a defence mechanism for damaged cells due to diseases or noxious agents (Elmore, 2007; Afford and Randhawa, 2000). It is a process distinct from uncontrolled cell death (necrosis) and is typically characterized by deep phenotypical modifications that lead to cell shrinkage, chromatin condensation (pycnosis), DNA fragmentation (karyorrhexis), and formation of extroflexions of the cell membrane (blebbing), followed by separation of cell fragments into apoptotic bodies (budding). Apoptotic bodies consist of small vesicles containing cytoplasm with tightly packed organelles and some nuclear fragments, enclosed within an intact plasma membrane. These apoptotic bodies are quickly phagocytosed by macrophages or parenchymal cells

and then degraded within the phagolysosomal pathway. In contrast to necrosis, the phagocytizing cells do not release pro-inflammatory cytokines, and the apoptotic cells do not release their cellular constituents, thereby preventing damage to the surrounding interstitial tissue (Elmore, 2007). Nowadays, two apoptotic mechanisms have been identified: extrinsic and intrinsic (Yanumula and Cusick, 2023). The extrinsic pathway starts when some specific ligands, such as the fetal alcohol syndrome ligand (FASL) and TNFα, interact with their receptors, FASR and TNFR, both characterized by cysteine-rich extracellular domains, and an intracellular domain of about 80 amino acids called death domain (DD), which play a key role in transmitting death signals from the cell surface to the intracellular environment. Upon ligand binding, FASR is activated and recruits some cytosolic adapter proteins like FAS-associated DD (FADD), while TNFR recruits TNFR-associated DD (TRADD). These receptor-ligand complexes then serve as a recognition site for an enzymatic precursor called procaspase-8, leading to the formation of the death-inducing signaling complex (DISC). This results in the auto-catalytic activation of procaspase-8, followed by the conversion of procaspase-8 into initiator caspase-8, which promotes the cleavage and activation of effector caspase-3. The latter degrades the structural and regulatory components of the cell, leading to pycnosis, karyorrhexis, blebbing, and budding (Pistritto et al., 2016; Nair et al., 2014; Elmore, 2007). On the other hand, the intrinsic pathway is triggered by a diverse array of non-receptor-mediated stimuli, such as hypoxia, viral infections, toxins, radiation, and oxidative stress. Each of these stimuli cause changes in the inner mitochondrial membrane, resulting in the opening of the mitochondrial permeability transition pore, loss of the mitochondrial transmembrane potential, and the release of pro-apoptotic proteins from the intermembrane space into the cytosol, including cytochrome-c (CYT-c), second mitochondrial activator of caspase (Smac), direct IAP binding mitochondrial protein (DIABLO), and the serine protease high temperature requirement protein A2 Omi stress-regulated (HtrA2/Omi), which are able to promote the caspase-dependent mitochondrial pathway (Krasovec et al., 2023). Specifically, CYT-c interacts with the apoptotic peptidase-activating factor 1 and procaspase-9, forming the apoptosome complex, which promotes the cleavage and activation of caspase-3, while the Smac/DIABLO and HtrA2/Omi induce apoptosis by inhibiting the inhibitors of apoptosis proteins (Schafer and Kornbluth, 2006). Besides these proteins, other pro-apoptotic proteins are released by mitochondria during the late stages of apoptosis, including the apoptosis-inducing factor, endonuclease G, and the carbamoyl-phosphate synthetase 2-aspartate transcarboxylase enzyme, which induce DNA fragmentation and cell death (Li et al., 2001). The control and regulation of these mitochondrial events occur through members of the B-cell lymphoma 2 (Bcl-2) family, which include some anti-apoptotic proteins like Bcl-2, Bcl-x, Bcl-XL, Bcl-XS, Bcl-w, Bcl-2-associated athanogene, and pro-apoptotic proteins, such as Bcl-10, Bcl-2-associated X protein (Bax), Bcl-2 homologues antagonist/killer, BH3 interacting-domain death agonist (BID), Bcl-2-associated agonist of cell death, Bcl-2 interacting mediator of cell death, Bcl-2 interacting killer, and B lymphocyte kinase (Krasovec et al., 2023; Nair et al., 2014; Elmore, 2007). It is well-known that Aβ and pTau accumulation can directly or indirectly trigger both the intrinsic and extrinsic apoptotic pathways, by promoting mitochondrial dysfunction, energy depletion, cholinergic insufficiency, hormonal imbalance, endoplasmic reticulum stress, oxidative stress, and neuroinflammation, which stimulate various signalling molecules responsible for activation of a series of

caspases, leading to neuronal death in the cerebral areas like the hippocampus and cerebral cortex, which are essential for learning, memory, and cognitive ability (Kumari et al., 2023). Moreover, in different AD individuals, the expression of anti-apoptotic proteins such as Bcl-2 is suppressed, while some pro-apoptotic proteins like Bax result upregulated. AD patients also display high levels of FASL and TNFα, which interact with their receptors, promoting the extrinsic pathway of apoptosis. In the extrinsic pathway, caspase-8 may also cleave the pro-apoptotic protein BID, inducing the release of mitochondrial pro-apoptotic factors like CYT-c, and the subsequent formation of the apoptosome (Kumari et al., 2023; Nilsen et al., 2006; Chong et al., 2005) (**Fig. 8**).

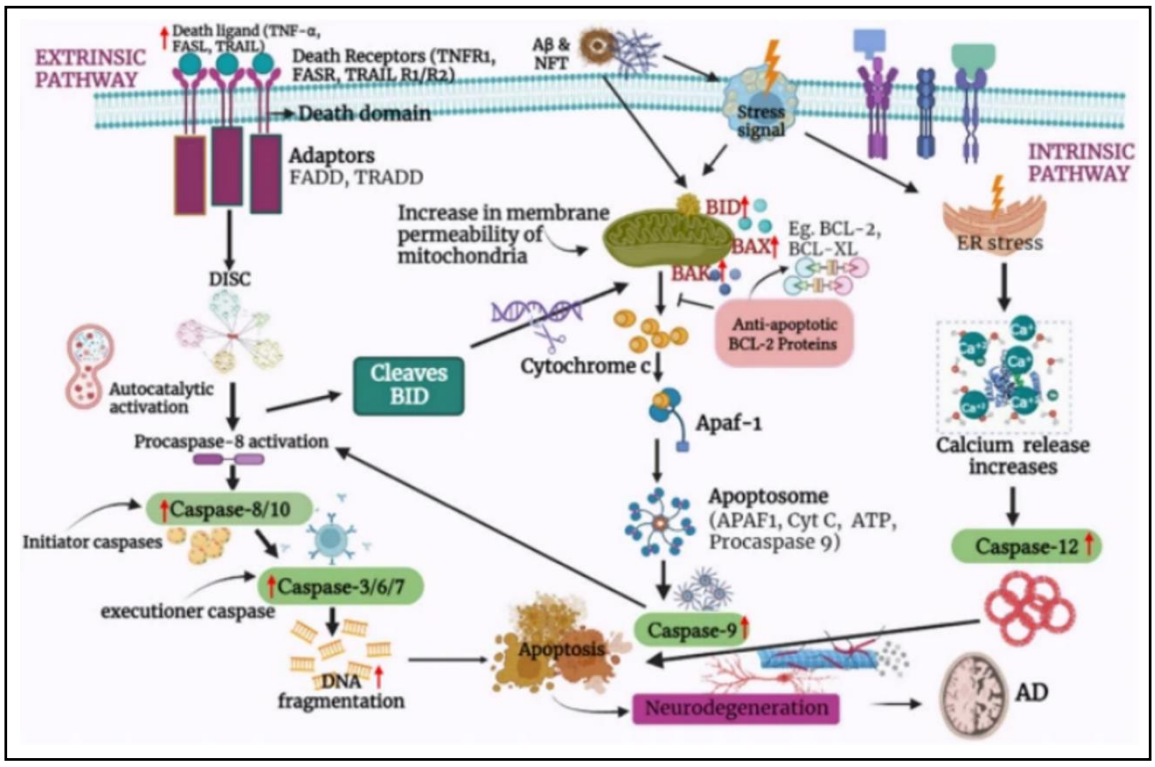

Figure 8. The extrinsic and intrinsic apoptotic pathways in AD. TNFα, tumor necrosis factor α; FASL, fetal alcohol syndrome ligand; TRAIL, TNF-related apoptosis-inducing ligand; FADD, FAS-associated death domain; TRADD, TNFR-associated death domain; DISC, death-inducing signaling complex; BID, BH3 interacting-domain death agonist; Bcl-2, B-cell lymphoma 2; BAX, Bcl-2-associated X protein; BAK, Bcl-2 homologues antagonist/killer; Apaf-1, apoptotic peptidase-activating factor 1; Aβ, amyloid beta; NFT, neurofibrillary tangles; ER stress, endoplasmic reticulum stress; AD, Alzheimer's disease (Kumari et al., 2023).

1.3.6 The retina as a non-invasive biomarker for early diagnosis of AD

Nowadays, different AD diagnostic biomarkers have been validated in AD clinical trials and healthcare management, including brain imaging of Aβ and pTau burden using positron emission tomography (PET), the observation of cerebral atrophy or brain shrinkage using structural magnetic resonance imaging, the use of fluorodeoxyglucose PET to evaluate the metabolic activity, typically reduced in the parietal or temporal areas of the brain, and search for some blood or cerebrospinal fluid bioproducts. However, the widespread adoption of these biomarkers in AD clinical practice is hindered by numerous limitations, including invasiveness, high

costs, reduced accessibility, health risks associated with exposure to radioactive isotopes, and resource demands. Moreover, the use of blood-based biomarkers is currently under validation for advanced clinical stages since they do not allow a direct visualization of CNS pathology at the site of injury, and their stability is affected by different brain-derived molecules. Therefore, despite major advances in AD biomarkers, it is necessary to find new applicable techniques for the diagnosis and monitoring of the disease (Gupta et al., 2021; Masters et al., 2015). Unlike the brain, which is shielded by the skullcap, the retina is an optically accessible space that can be easily studied in vivo from a functional point of view through different electroretinographic (ERG) analyses, as well as visualized in vivo using different noninvasive and high-resolution optical imaging methods, such as fundus photography, optical coherence tomography (OCT), OCT-angiography, fluorescence lifetime imaging ophthalmoscopy, and hyperspectral imaging, which provide important information on the vascular, cellular, and molecular features of the retina (Gaire et al., 2024; Ashraf et al., 2023). Moreover, the latter represents an anatomical extension of the CNS, characterized by a multi-layered structure, functions, and immune response processes similar to the brain, with which it shares a common embryological origin (Ptito et al., 2021). In addition, the characteristics of the retina described in chapter 1.1 (i.e., the different neuron types as well as the presence of glial cells and of BRB) make the retina one of the most intriguing potential biomarkers for AD (Gaire et al., 2024). Not surprisingly, emerging evidence from histopathological, molecular, and in vivo imaging analyses has revealed that AD affects both the brain and some parts of the visual system, including the retina. In particular, the main pathological traits identified in the retina of AD patients and those of AD animal models include Aβ and pTau accumulation, extensive vascular abnormalities, inflammation, glial activation, mitochondrial dysfunction, degenerative changes in the optic nerve, and retinal cell degeneration, which lead to a progressive and irreversible visual impairment (Gaire et al., 2024; Ashraf et al., 2023; Koronyo et al., 2023; Grimaldi et al., 2019). Among retinal cells, the most affected appear to be RGCs, resulting in RGC loss followed by a significant thinning of the RNFL and GCL layers, as well as a reduced amplitude and increased latency in the pattern-ERG (PERG). The higher predisposition and sensitivity to neurodegenerative damage of RGCs are mainly due to defective mitochondrial dynamics and axonal transport, as well as oxidative stress and energy depletion, given the high metabolic demand and performance typical of these cells, mostly determined by the asymmetric myelination (Liao et al., 2021; Mavillo et al., 2020; La Morgia et al., 2015; Krasodomska et al., 2010). Preliminary studies also highlight that Aβ is not only deposited in the inner retinal layers but also in the RPE and around the photoreceptoral cells, including rods and cones. The presence of Aβ in the outer retinal layers seems to trigger senescence and necroptosis phenomena in the photoreceptor, mainly rods, followed by loss of function, altered morphology, and lower expression of phototransduction proteins, even if no alteration in the thickening of outer retinal layers was observed (Liao et al., 2021; Zhang et al., 2021).

1.3.7 Vascular dysfunction and microcirculatory impairment in the pathogenesis of AD

Due to the high metabolic demand, the brain is particularly sensitive to reduced blood flow and hypoxic conditions. Indeed, the brain is extremely well perfused through an extensive network of blood vessels having different sizes, thicknesses, and contractile abilities, which ensure a constant delivery of oxygen and nutrients, as well as a proper removal of carbon dioxide and other waste metabolites produced by the numerous metabolic reactions (Wilson and Matscinsky, 2020). One of the earliest inciting events in AD pathogenesis is based on vascular dysregulation, which then initiates a cascade of molecular and neuropathological changes leading to neuronal dysfunction and the onset of typical AD symptoms. Not surprisingly, different vascular pathologies such as cerebral atherosclerosis, cerebral silent infarcts or microinfarcts, chronic cerebral hypoperfusion, cerebral vasculopathy, cerebral amyloid angiopathy, cerebral small vessel disease, hypertension, heart failure, as well as the presence of concomitant metabolic disorders like hyperlipidaemia, diabetes mellitus, dyslipidaemia, obesity, metabolic syndrome, and hyperhomocysteinemia were associated with a higher risk of AD onset (Korte et al., 2020). AD patients exhibit altered glucose metabolism, increased cerebral vascular resistance, and reduced cerebral blood flow, which is attributed to both the loss of blood vessels and their narrowing (Tarawneh, 2023). Although the mechanism by which the thickness of smaller blood vessels is restricted has not yet been definitively explained, some potential theories have been made based on the recent findings. The most promising approach consists of a "long-term pericyte-mediated constriction", in which oxidative stress and neuroinflammation caused by the gradual accumulation of Aβ and pTau induce a significant increase in extracellular levels of endothelin-1, which interacts with its receptors expressed on all classes of pericytes (Korte et al., 2020; Palmer et al., 2012; Barnham et al., 2004). This induces the subsequent activation and contraction of pericytes, which determines a quick narrowing of the vascular lumen, decreasing blood flow up to 50% or more in some cerebral areas. Besides this, two other mechanisms involved in the occlusion of blood vessels were reported, including blockage by neutrophils and clot formation. In particular, neutrophils are larger and less distensible than other blood cells, resulting in a greater tendency to become lodged at the smallest diameter parts of capillaries. At the same time, in the narrow blood vessels, the reduced blood flow can facilitate coagulation processes and clot formation, which contributes to the further reduction of blood flow (Korte et al., 2020; Farkas and Luiten, 2001; Mehta et al., 1988). The constriction of blood vessels observed in the AD brain leads to an increasingly hypoxic condition, which contributes to the reduction in metabolic activity of specific brain regions such as the amygdala, entorhinal cortex, and hippocampus (Park et al., 2019), as well as decreasing the level of proteins involved in Aβ degradation and upregulating the expression of the BACE, which promotes the production of toxic Aβ isoforms (Liu and Le, 2014; Zhang et al., 2007; Sun et al., 2006). Over time, Aβ levels exceed the clearance mechanisms, leading to the formation of a positive feedback loop that induces a growing Aβ perivascular accumulation, pericyte activation, and reduced blood flow (Korte et al., 2020) (**Fig. 9**). The concomitant presence of high Aβ levels, hypoxia, and the destruction of tight junctions and adherent junctions may ultimately lead to pericyte and endothelial cell degeneration with subsequent loss of BBB integrity, which is essential for the tight control of the chemical composition of brain interstitial fluid, in turn, fundamental for proper synaptic functionality, information

processing, and neuronal connectivity. A dysfunctional BBB may lead to altered hemodynamic responses and an increase in vascular permeability, which enables toxic blood-derived molecules, cells such as lymphocytes, neutrophils, or peripheral macrophages, and microbial agents to enter the brain, resulting in inflammatory and immune processes at the basis of neurodegenerative phenomena (Sweeney et al., 2018; Kisler et al., 2017; Zlokovic, 2011; Iadecola, 2004). BBB breakdown can also hinder the delivery of some drugs based on the use of antibodies, proteins, peptides, and small molecules like nucleic acids, which could likely get trapped in pathologically altered brain tissue within the enlarged perivascular spaces along with other blood-derived debris, preventing them from reaching their neuronal targets (Sweeney et al., 2018). A prolonged hypoxic condition also induces a reduction in the phosphatidylinositol 3-kinase/protein kinase B pathway activity, which promotes GSK3 activation with subsequent Tau hyperphosphorylation and impairs synaptic function (Korte et al., 2020).

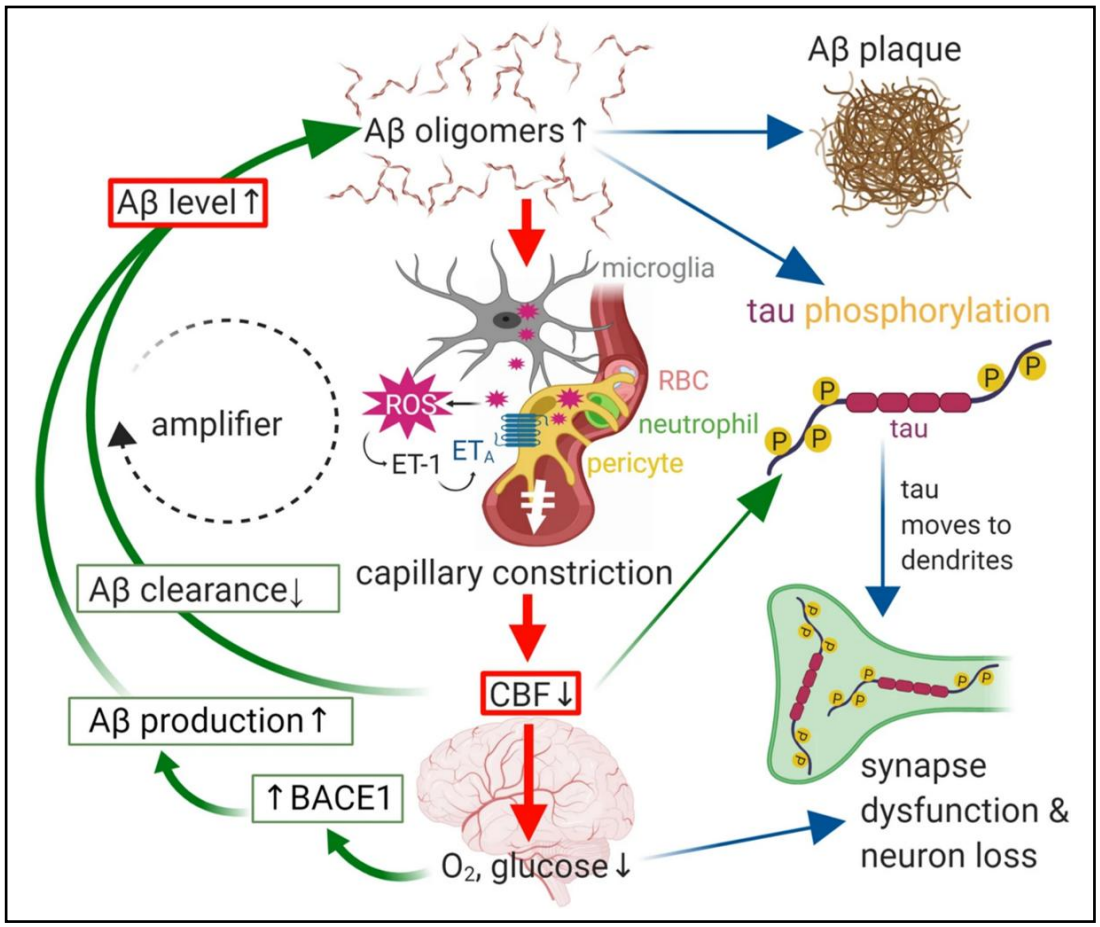

Figure 9. The microvascular abnormalities exacerbate the molecular alterations, resulting in progressive synapse dysfunction and neuronal loss. Aβ, amyloid beta; BACE, β-site Amyloid Precursor Protein Cleaving Enzyme; ROS, reactive oxygen species; ET-1, endothelin-1; ET_A, endothelin receptor type A; RBC, red blood cell; CBF, cerebral blood flow (Korte et al., 2020).

1.3.8 An overview of therapeutic approaches and nutritional strategies for AD prevention

Nowadays, numerous drugs have been approved by the Food and Drug Administration for clinical use, including tetrahydroaminoacridine, donepezil, carbalatine, galantamine, metrifonate, memantine, and lecanemab. The first five types of drugs are quickly absorbed and work by blocking the acetylcholinesterase activity, which is normally responsible for the degradation of ACh in the synaptic gap. By inhibiting this enzyme, these drugs increase the availability of ACh, potentially improving the cholinergic effects, neuronal activity, memory, and learning abilities (Peng et al., 2023; McGleenon et al., 1999). Memantine is an antagonist of the glutamate receptors, especially the N-methyl-D-aspartate receptor, thus reducing the neurotoxicity due to the excessive neuronal stimulation caused by some excitatory neurotransmitters like glutamate (Peng et al., 2023). Lecanemab, also known as leqembi, is a humanized monoclonal antibody specifically designed to bind with high affinity to soluble Aβ protofibrils, thereby slowing cerebral Aβ accumulation and AD progression (Van Dyck et al., 2022). Besides these conventional drugs, many other molecules were and/or are still the object of study in different clinical trials, including those anti-Tau, anti-Aβ (Peng et al., 2023), inhibitors for BACE (verubecestat, lanabecestat, and atabecestat) (Patel et al., 2022), inhibitors for γ-secretase (semagacestat and avagacestat) (Willis et al., 2012), enhancers of Aβ clearance based on passive (bapineuzumab, gantenerumab, crenezumab, ponezumab, donanemab, and aducanumab) and active (AN1792, ACC-001, and CAD106) immunotherapy (Ostrowitzki et al., 2022; Nicoli et al., 2019; Klein et al., 2019; Salloway et al., 2018), inhibitors for GSK3 (tideglusib) (Lovestone et al., 2015), inhibitors for Tau aggregation (methylthioninium chloride, hydromethanesulfonate, and TRx-0014) (Gauthier et al., 2016; Wischik et al., 2015), stabilizers for microtubules (davunetide and epothilone D) (Gozes et al., 2011; Brunden et al., 2010), enhancer for mitochondrial activity (idebenone and methylene blue) and mitochondrial biogenesis (bezafibrate) (Dumont et al., 2012), inhibitors for mitochondrial permeability transition (alisporivir, N-methyl-4-isoleucine-cyclosporin, imidazole, thiadiazole, isoxazoles, N-phenylbenzamides, and dimebon) (Shevtsova et al., 2021; Schiavone and Trabace, 2018), and usage of different multi-target ligands named as polypharmacophore (dimebon, phenothiazine, carbazoles, idalopirdine, and masitinib), that are hybrid molecules characterized by two or more pharmacophores linked together with spacers able to simultaneously affect multiple biological targets, such as Aβ, metal ions, and ROS (Dubois et al., 2023; Makhaeva et al., 2020; Dao et al., 2017; Wilkinson et al., 2014; Doody et al., 2008). Despite the clinical advances, the major part of these drugs has not yielded encouraging results, showing limited effectiveness, poor tolerability, toxicity, and the development of several side effects, such as brain shrinkage, altered cognitive functions, agitation, weight loss, infections, microbleeds, diabetes, and in some cases cancer (Tartaglia and Ingelsson, 2024; Peng et al., 2023). In recent years, another potentially more efficient approach was found, which is based on genetic interventions, such as RNA interference and gene editing. RNA interference is a natural process involved in regulating protein synthesis, based on the ability of small fragments of RNA to inhibit protein translation by binding to specific regions of mRNA (Tartaglia and Ingelsson, 2024). It has been recognized for some time that this system may be mimicked by applying synthesized RNA, often referred to as antisense oligonucleotides (ASO). ASO is a single-stranded RNA molecule of about 15-22 nucleotides designed to bind

complementary RNA targets. Nowadays, there are at least 15 therapies at the clinical stage based on the use of ASO, mainly aimed at suppressing the translation of genes encoding for APP/Aβ and Tau, in order to reduce their accumulation in the brain (Lauffer et al., 2024; Zamecnik and Stephenson, 1978). Despite promising results, a primary challenge associated with this type of treatment lies in the necessity to prevent excessive protein expression, but at the same time, maintain a basal physiological activity of the protein (Tartaglia and Ingelsson, 2024). On the other hand, gene editing refers to a group of technologies that can insert, delete, modify, or replace single nucleotides in the DNA molecule. Among the conventional gene editing approaches, there are the oldest methods based on the use of meganucleases, zinc finger nucleases, and transcription activator-like effector-based nucleases, as well as the latest clustered regularly interspaced short palindromic repeats (CRISPR) (Rhaman et al., 2024; Tartaglia and Ingelsson, 2024). The latter is based on the action of the CRISPR-associated protein of type 9 endonuclease and a guide RNA, which are projected to bind a specific site on the DNA molecule, inducing a double-stranded break, followed by the subsequent reduction of target-protein expression involved in the detrimental mechanisms at the base of AD onset and progression. Currently, this therapeutic approach seems to be more suitable for modifying monogenic variants associated with an increased generation of both total Aβ (as for several APP mutations) and the more aggregation-prone Aβ42 (as for a majority of the PSEN1/PSEN2 mutations) (Tartaglia and Ingelsson, 2024; Konstantinidis et al., 2022; Duan et al., 2022; György et al., 2018). Besides drug therapies and genetic approaches, growing evidences suggest that a proper balanced diet containing high levels of anti-inflammatory compounds, antioxidant molecules, B-group vitamins, and polyunsaturated fatty acids, such as the Mediterranean diet, the dietary approaches to stop hypertension (DASH) diet, and the Mediterranean-DASH intervention for neurodegenerative delay diet, may have beneficial effects on the AD onset and progression. On the other hand, a diet enriched in processed and poor-quality foods, hydrogenated fats, and foods contaminated with pollution, heavy metals, or toxins may accelerate AD pathogenesis (Stefaniak et al., 2022; Ogawa., 2014). One of the most important components of the Mediterranean diet is represented by extra-virgin olive oil (EVOO), which contains several active biomolecules, including polyphenols, phytosterols, monounsaturated fatty acids, and vitamin E, as well as high levels of phenolic compounds, such as tyrosol, hydroxytyrosol, oleuropein, oleuropein aglycone, luteolin, and oleocanthal that have well-known anti-inflammatory, antioxidant, and neuroprotective properties (Alkhalifa et al., 2024). In particular, EVOO and its phenolic compounds emerge as multifaceted players in AD (Angeloni et al., 2017; Rigacci, 2015) (**Fig. 10**), by attenuating Aβ accumulation through the enhancement of clearance mechanisms and autophagic activity, as well as reducing Tau hyperphosphorylation and subsequent NFT formation (Batarseh and Kaddoumi, 2018; Qosa et al., 2015). Moreover, the EVOO's role extends to maintaining the BBB integrity, potentially fortifying its selective permeability, and limiting the infiltration of neurotoxic substances (Kaddoumi et al., 2022; Rihani et al., 2019; Qosa et al., 2015). The presence of phenolic compounds has been observed to reduce glial reactivity, as well as to attenuate the production of pro-inflammatory cytokines, such as IL-6 and IL-1β, by inhibiting the NF-κB and nucleotide-binding domain and leucine-rich repeat family, pyrin domain-containing 3 inflammasome pathways. In addition, the current literature reported that these phenolic compounds can affect different

signaling pathways, leading to the production of antioxidants, mitochondrial biogenesis, the increase in adenosine triphosphate levels, the improvement of synaptic activity, spatial working memory, short-term neuronal plasticity, and the extension of lifespan (Alkhalifa et al., 2024; Leri et al., 2021; Lauretti et al., 2020; Richard et al., 2011). Despite its neuroprotective effects, an inordinate and unbalanced consumption of olive EVOO can lead to adverse effects on health, mainly due to the excess caloric intake caused by the high content of fatty acids, including weight gain, obesity, metabolic alterations, and the onset of hepatic, gastrointestinal, and cardiovascular complications, exacerbating AD pathogenesis (Komiya et al., 2023). Not surprisingly, the liver plays a crucial role in Aβ clearance, metabolizing and degrading approximately 60% of total circulating Aβ through hepatocyte-mediated degradation or indirectly by modulating plasma carrier protein levels (Cheng et al., 2023; Wu et al., 2023; Estrada et al., 2019). On the other hand, alterations of the gastrointestinal tract can lead to an altered composition of the bacteria populating the gut microbiota, which can secrete large amounts of noxious substances, contributing to the alteration of signaling pathways, to increased permeability of the intestinal epithelial barrier, and the production of pro-inflammatory and neurotoxic molecules associated with AD pathogenesis (Chandra et al., 2023; Chen et al., 2023; Jiang et al., 2017).

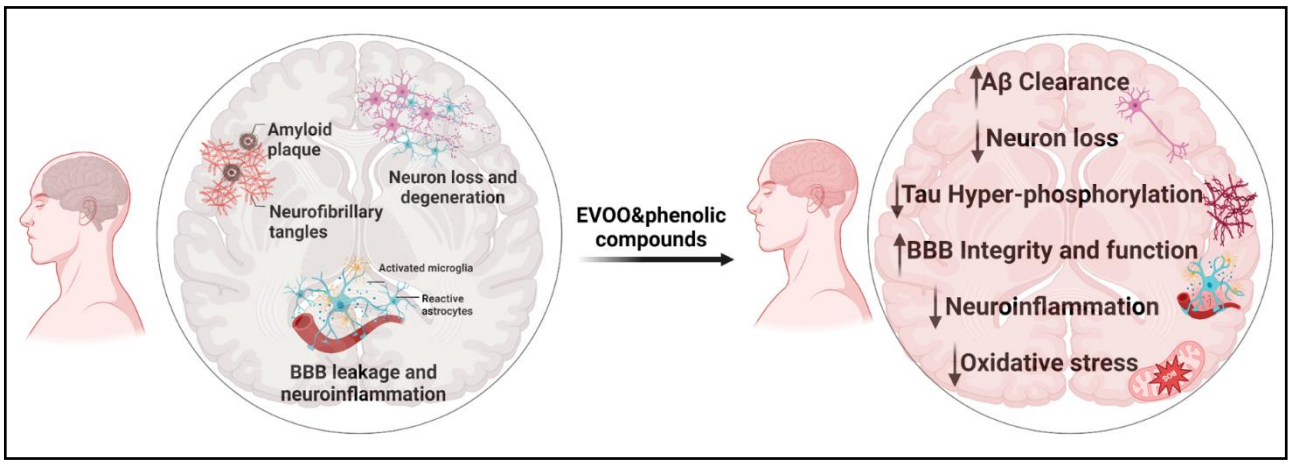

Figure 10. Neuropathological features of AD (left) contrasted with the neuroprotective effects of EVOO and phenolic compounds (right). BBB, blood-brain barrier; EVOO, extra-virgin olive oil; Aβ, amyloid beta (Alkhalifa et al., 2024).

1.3.9 The 5xFAD murine model of AD

Nowadays, many transgenic murine models have been developed to reproduce the neuropathological features associated with AD, ranging from Aβ deposition, cerebrovascular abnormalities, gliosis, neuroinflammation, oxidative stress, synaptic disorganization, neurotransmission defects, axonal dystrophy, and neuronal loss to cognitive decline (Zhong et al., 2024; Sanchez-Varo et al., 2022). In this regard, the heterologous 5xFAD mouse represents one of the most accurate murine models of AD, as it quite faithfully recapitulates the progression of AD in patients, which involves an initial asymptomatic phase, followed by a prodromal, symptomatic, and severe phase. 5xFAD mice express five familial AD mutations under the control of the cerebral neuron-specific thymus cell antigen 1 promoter, of which three are specifically on the human APP695 gene (London V717I, Swedish K670N/M671L, and Florida I716V), and two on the human PSEN1 gene

(M146L and L286V). These mutational variants promote an increased amyloidogenic flow by enhancing BACE and γ-secretase activity, leading to early and intense amyloid pathology and subsequent neurodegeneration. No human Tau transgene is expressed in this mouse line, even if signs of Tau hyperphosphorylation and NFT formation were observed (Oblak et al., 2021; Claeysen et al., 2020). Besides the cerebral deficits and behavioral abnormalities, 5xFAD mice also display a progressive retinal Aβ accumulation, mainly associated with morphological changes, functional alterations, microglial activation, neuroinflammatory processes, oxidative stress, and RGC loss (McCool et al., 2025; Zhang et al., 2021; Lim et al., 2020).

1.4 Aims of the thesis

AD is a neurodegenerative disorder characterized by cognitive decline due to progressive Aβ and pTau accumulation, widespread neurovascular alterations, and neuronal death. Although the cerebral damage remains the primary target of AD research, increasing attention has recently been directed toward the identification of other reliable biomarkers that may reflect pathological changes in the CNS. In this context, the retina, being an embryological extension of the brain, represents a more accessible and promising interface to study AD pathogenesis. Simultaneously, scientific interest in nutraceutical-based approaches has highlighted the therapeutic potential of certain plant-derived compounds, including EVOO, which is well-known for its antioxidant, anti-inflammatory, and vasoprotective properties. Based on these premises, the present thesis pursues a dual objective. In the first instance, a detailed characterization of the retinal morpho-functional and molecular features was performed on 3-, 6-, and 9-month-old 5xFAD and wild-type (WT) mice, in order to provide additional information on the prospective role of the retina as a biomarker for studying AD progression, as well as identify new dysregulated miRNAs potentially involved in AD-retinal pathology. Secondly, an in-depth analysis of the morpho-functional and molecular brain microcirculation features was carried out on 2-, 4-, and 6-month-old 5xFAD and WT mice, and the potential beneficial effect of a diet enriched with Acebuche (ACE), an olive oil containing remarkable levels of bioactive molecules having anti-inflammatory, antioxidant, and neuroprotective effects, was tested. Overall, this multidisciplinary thesis intends to contribute to a deeper understanding of the interaction between neurodegeneration, vascular dysfunction, and nutraceutical interventions, offering new insights for early diagnosis and the development of innovative preventive and therapeutic strategies for AD.

2. MATERIALS AND METHODS

2.1 Materials and methods for retinal assessments

2.1.1 Animals

The 5xFAD murine model expresses five familial AD mutations, three associated with the human APP gene (Florida I716V, Swedish K670N/M671L, and London V717I) and two associated with the human PSEN1 gene (L286V and M146L), each driven by the mouse thymus cell antigen 1 promoter, a neuron-selective promoter widely used for *in vivo* neuronal transduction to generate transgenic animals with neuron-specific expression of target genes (Forner et al., 2021; Oakley et al., 2006). Due to these mutations, 5xFAD mice quickly develop severe and progressive amyloid pathology, with plaques appearing in the brain starting at 2 months of age, triggering microgliosis and inflammation as well as synaptic and neuronal loss (Oblak et al., 2021; Canter et al., 2019; Elmer and Vassar, 2013; Jawhar et al., 2012; Kimura and Ohno, 2009; Oakley et al., 2006). Deficits in spatial learning start at 4 months of age, generally followed by synaptic impairment in the hippocampus at about 6 months of age (Eimer and Vassar, 2013; Oakley et al., 2006; Kimura and Ohno, 2009). Male 5xFAD mice (B6.Cg-Tg(APPSwFlLon, PSEN1*M146L*L286V)6799Vas/Mmjax) were purchased from Jackson Labs (Bar Harbor, Mainer, ME, USA; stock # 008730). In origin, both transgenes were co-injected in the cells of C57BL/6XSJL hybrid embryos, and founders were bred with B6SJL mice. Since SJL mice express the retinal degeneration allele phosphodiesterase-6b retinal degeneration-1 (Pde6brd1) that does not allow the use of transgenic mice for retinal studies, transgenic mice were then backcrossed to C57BL/6J mice to breed out of the strain the retinal degeneration allele. Male 5xFAD mice were bred in our animal facilities with female C57BL/6J mice (Jackson Labs). The mice were genotyped for APP and PSEN1 transgenes. In addition, the absence of the Pde6brd1 allele was verified using polymerase chain reaction (PCR) with specific primers (**Table 1**). Non-carrier mice obtained from mating male 5xFAD mice with female C57BL/6J mice were used as WT controls. In the present study, we used 3-, 6-, and 9-month-old 5xFAD mice. A total number of 102 mice (51 WT and 51 5xFAD) was used. The present study was performed in accordance with the Guide for the Care and Use of Laboratory Animals of the National Institutes of Health, the ARVO Statement for the Use of Animals in Ophthalmic and Vision Research, the Italian guidelines for animal care (DL 6/14, permission n. 864/2024-PR), and the European Communities Council Directive (2010/63/UE), and the principles of the 3Rs. Animals were housed under standard conditions of 12 h cycles of light and dark, 23 ± 1°C, with food and water ad libitum.

Table 1. List of primers used for genotyping experiments.

Primer	Sequence (5'→ 3')	Catalogue
Mutant Reverse	CGG GCC TCT TCG CTA TTA C	27367
WT Reverse	TAT ACA ACC TTG GGG GAT GG	37599

Common Forward	ACC CCC ATG TCA GAG TTC CT	37598
Mutant Pde6b^{rd1}	AAG CTA GCT GCA GTA ACG CCA TTT	oIMR2093
WT Pde6b^{rd1}	ACC TGC ATG TGA ACC CAG TAT TCT ATC	oIMR2094
Common Forward	CTA CAG CCC CTC TCC AAG GTT TAT AG	oIMR2095

2.1.2 Electroretinography

The mice were subjected to different types of electroretinography, including an analysis of the rod pathway with scotopic-ERG (scERG), an analysis of the cone pathway with photopic-ERG (phERG), and an analysis of RGC activity with PERG. After overnight dark adaptation, the mice were anesthetized with an intraperitoneal injection of avertin (1.2% avertin, 0.02 mL/g body weight; Sigma-Aldrich) and placed in a custom-made stereotaxic apparatus allowing for an unobstructed visual field. The body temperature was maintained at 37°C with a feedback-controlled heating pad, while corneal moisture was maintained with a saline solution. Recording silver-silver chloride electrodes (0.2 mm loop-shaped) were laid on the corneal surface of each eye using micromanipulators, while stainless-steel needles were inserted subcutaneously in the frontal region and used as reference electrodes (one for each eye). Another stainless-steel needle was subcutaneously inserted at the base of the tail and used as the ground electrode. Flash stimuli were delivered with a Ganzfeld stimulator (CSO, Firenze, Italy), and the ERG recordings were acquired through a commercially available data acquisition device (Retimax Advanced, CSO). Scotopic responses were elicited using 10 cd-s/m^2 stimuli. Five consecutive signals recorded simultaneously from each eye were averaged to reduce noise after amplification (5000-fold) and subsequently band-pass filtered (0.1-100 Hz). In the deriving waveform, the amplitude of the a-wave (baseline to trough) and that of the b-wave (trough to peak) were measured. Immediately after the acquisition of the scotopic responses, the animals were light-adapted for 60 s before recording photopic cone-mediated responses using 10 cd-s/m2 stimuli on a 30 cd-s/m2 rod-saturating green background light. The phERG responses simultaneously recorded from both eyes were amplified (10,000-fold) and band-pass filtered (1-30 Hz). The waveform deriving from the average of 50 consecutive responses was analyzed for the b-wave (baseline to peak) and the photopic negative response (phNR; baseline to first negative deflection after the b-wave). Following the phERG session, PERG responses were recorded. They were evoked by a visual stimulus consisting of 0.05 cycles/deg black and white (98% contrast) bars contrast-reversing at 1 Hz temporal frequency. The pattern stimuli were generated by a 19'' light-emitting diode display (area: 74° x 62°) with a mean luminance of 50 cd/m2 aligned at about 30 cm from the corneal surface. Each pattern reversal-deriving signal was amplified (10,000-fold) and band-pass filtered (1-30 Hz). A total of 300 consecutive pattern reversals was averaged to reduce noise contamination by a factor of $\sqrt{300}$ = 17.32. The PERG response was evaluated by measuring the amplitude of the N35–P50 and P50–N95 waves (from the trough of the negative peak, N35, to the peak of the positive peak, P50, and from the peak of the

positive peak, P50, to the trough of the negative peak, N95, respectively). The implicit time was determined by measuring the time from the onset of the stimulus to the P50 and N95 peaks. Recordings were taken from the left eye.

2.1.3 Prusky water maze test

The Prusky water maze test is a behavioral test used for the quantitative measurement of visual discrimination in mice. It has been validated as a cognitive-independent assay of visual acuity since, unlike spatial navigation tasks such as the Morris Water Maze, this task requires no long-term memory (Prusky et al., 2000). This test relies on the animal's ability to discriminate high-contrast visual stimuli in real time. It is based on a binary forced-choice task in which the animal must swim to a monitor presenting a vertical grating pattern (target stimulus, associated with the presence of a hidden rescue platform), while avoiding another monitor presenting a uniform gray screen (neutral stimulus). The visual stimuli had a constant luminance of 39.95 cd/m², with spatial frequencies ranging from 0.087 to 0.645 cycles/deg. The mice were initially trained at 2 months of age following a published protocol (Corsi et al., 2025). The spatial frequency was systematically increased or decreased to determine the limits of the animal's ability to find the platform. The value of visual acuity was assessed as the highest spatial frequency at which at least 75 % of the correct responses were recorded.

2.1.4 Optical coherence tomography

The in vivo assessment of retinal morphology was performed by image-guided optical coherence tomography (OCT) in WT and 5xFAD mice at 3, 6, and 9 months of age using the Micron IV system (Phoenix Research Laboratories, Pleasanton, CA, USA). The mice were anesthetized with an intraperitoneal injection of avertin (1.2% avertin, 0.02 mL/g body weight; Sigma-Aldrich). Mydriasis was induced by 1% tropicamide, and 2% hydroxypropyl-methylcellulose drops were used to avoid eye drying. Bidimensional OCT images were acquired by image-guided circular scans (550 µm diameter) around the optic nerve head. The segmentation of retinal layers and the quantification of layer thickness were performed using Insight software (Phoenix Research Laboratories). Data from both eyes were averaged.

2.1.5 Immunofluorescence

Mice were sacrificed by cervical dislocation. Both eyes were immediately enucleated and immersion-fixed in 4% paraformaldehyde in 0.1 M phosphate-buffered saline (PBS) 1x for 2 h at room temperature. The fixed eyes were transferred to 0.1 M PBS 1x containing 25% sucrose and stored at 4°C until usage. Subsequently, the eyes were embedded in cryo-gel, frozen using liquid nitrogen, cut into 10 µm-thick coronal sections with a cryostat, and mounted onto gelatin-covered glass slides. The sections were then incubated with primary antibodies (**Table 2**) diluted in 0.1 M PBS 1x containing 0.1% Triton X-100 overnight at 4°C, followed by incubation with appropriate secondary antibodies conjugated with Alexa-Fluor 488 (ab150077, Abcam, Cambridge, UK) or Alexa-Fluor 555 (ab150078, Abcam) at 1:200 dilution in 0.1 M PBS 1x containing 0.1%

Triton X-100 for 2 h at room temperature in the dark. After rinsing, the slides were coverslipped with Fluoroshield mounting medium containing 4′,6-diamidino-2-phenylindole (DAPI, Abcam). Images were viewed with an epifluorescence microscope (Ni-E; Nikon-Europe, Amsterdam, The Netherlands) and acquired with a DS-Fi1c digital camera (Nikon-Europe). To evaluate the RGC number, 3 retinal sections adjacent to the optic nerve head (central retina) were chosen from each retina (six retinas per group). The RGC number was calculated as the average number of RNA-binding protein with multiple splicing (RBPMS) immunopositive somata.

Table 2. List of antibodies used for immunofluorescence.

Antibody	Source	Catalogue	Dilution
Rabbit monoclonal antibody anti-β-Amyloid	Cell Signaling	8243	1:800
Rabbit polyclonal antibody anti-RBPMS	Novus Biologicals	NBP2-20112	1:500
Rabbit polyclonal antibody anti-glutamine synthetase	Abcam	ab228590	1:400
Rabbit monoclonal antibody anti-GFAP	Abcam	ab207165	1:400
Rabbit monoclonal antibody anti-Iba1	Abcam	ab178846	1:200
Rabbit monoclonal antibody anti-active caspase 3	Cell Signaling	9664S	1:100

2.1.6 Western blotting

The eyes were enucleated, and the retinas (2 retinas from the same mouse for each sample) were dissected and stored at -80°C. For Western blotting, the retinas were lysed by sonication in radioimmunoprecipitation (RIPA) lysis buffer (Santa Cruz Biotechnology, Dallas, TX, USA) supplemented with phosphatase and protease inhibitor cocktails. Protein concentration was measured with the Micro BCA Protein Assay (Thermo Fisher Scientific, Waltham, MA, USA). For each sample, 30 μg of proteins were run on SDS-PAGE gels (4-20%; Bio-Rad Laboratories, Inc) and transferred onto nitrocellulose membranes (Bio-Rad Laboratories, Inc). Blots were blocked for 1 h at room temperature with 3% or 5% skimmed milk, depending on the primary antibody used (**Table 3**). The blots were incubated with primary antibodies overnight at 4°C. β-actin was used as an endogenous control. The blots were then incubated for 2 h with appropriate HRP-conjugated secondary antibodies (goat anti-rabbit, 170-6515, Bio-Rad Laboratories, Inc; rabbit anti-mouse, A9044, Sigma-Aldrich) at a 1:5000 dilution and developed by the Clarity Western enhanced chemiluminescence substrate (Bio-Rad Laboratories, Inc). Images were acquired with the ChemiDoc XRS+ instrument (Bio-Rad Laboratories, Inc.), and the optical density (OD) of the target bands was evaluated with Image Lab 6.0.1 software (Bio-Rad

Laboratories, Inc.). The data were normalized to the relative OD of β-actin or total non-phosphorylated protein, as appropriate.

Table 3. List of antibodies used for Western Blotting.

Antibody	Source	Catalogue	Blocking	Dilution
Mouse monoclonal antibody (AT8) anti-pTau	Thermo Fisher	MN1020	3% skimmed milk	1:500
Mouse monoclonal antibody (BT2) anti-Tau	Thermo Fisher	MN1010	3% skimmed milk	1:500
Rabbit monoclonal antibody anti-Nrf2	Abcam	ab92946	5% skimmed milk	1:1000
Rabbit monoclonal antibody anti-NQO1	Abcam	ab80588	5% skimmed milk	1:1000
Rabbit monoclonal antibody anti-pNFκB (p65)	Abcam	ab76302	5% skimmed milk	1:1000
Rabbit polyclonal antibody anti-NFκB (p65)	Abcam	ab16502	5% skimmed milk	1:1000
Mouse monoclonal antibody anti-IL6	Santa Cruz	sc57315	5% skimmed milk	1:200
Rabbit monoclonal antibody anti-Bax	Abcam	ab18273	5% skimmed milk	1:500
Rabbit polyclonal antibody anti-Bcl2	Abcam	ab194583	5% skimmed milk	1:500
Mouse monoclonal antibody anti-β-actin	Sigma-Aldrich	A2228	5% skimmed milk	1:2500

2.1.7 ELISA

The eyes were enucleated, and the retinas were dissected and stored at -80°C. One retina for each sample was homogenized through sonication in homogenization buffer (5 M guanidine-HCl in 50 mM Tris, pH 8.0) with a 1x protease inhibitor cocktail containing 4-(2-aminoethyl) benzenesulfonyl fluoride hydrochloride (AEBSF) (Cat. P2714, Sigma, USA. The homogenates were mixed 6 times for 10 s every 5 minutes and centrifuged at 16000x *g* for 20 minutes at 4°C. The supernatants were collected, and the protein concentration was measured with the Micro BCA Protein Assay (Thermo Fisher). The proteins were diluted 1:1000 with standard diluent buffer, and an ELISA kit (Thermo Fisher, cat. N. KMB3441) was used according to the manufacturer's protocol to measure the levels of Aβ (1-42). The absorbance was determined at 450 nm within 10 min using a microplate reader (FLUOstar Omega, BMG Labtech, Ortenberg, Germany). The levels of the target protein in the retinal tissues were calculated using the standard curves and expressed as pg/mg protein.

2.1.8 Retinal miRNome and bioinformatic analysis

Following the manufacturer's instructions, an enriched fraction of miRNAs was extracted from dissected retinas using the miRNeasy Mini Kit (Qiagen, Hilden, Germany). Briefly, the retinas (5 samples for each time point for each strain, each containing 2 retinas from the same mouse) were homogenized in QIAzol Lysis Reagent using the Tissue Lyser instrument (Qiagen) and spun. The supernatants were added with chloroform and centrifuged again. The transparent supernatants were recovered and added with pure ethanol, transferred to the miRNeasy spin columns, and washed with the supplied buffers. The fraction of enriched miRNAs was then eluted in 30 µL RNase-free water. The quantity and purity of miRNAs were evaluated using Biophotometer D30 (Eppendorf, Hamburg, Germany). The integrity of the samples was determined by RNA integrity number (RIN) evaluation using an Agilent 2100 Bioanalyzer (Agilent Technologies, Mountain View, California). Only samples with a RIN > 7 were selected for library preparation and sequencing. Libraries were prepared using the QIASeq miRNA library kit with an input of 100 ng/sample, a cycle of library amplification consisting of 16 PCR cycles. Libraries were sequenced single-end with an Illumina Sequencing NextSeq500 with a depth of 13M fragments/samples on average. The fragment size was 75 bp. After adapter sequences' removal with cutadapt (Martin, 2011), reads were aligned to miRBase (Kozomara et al., 2019), with the SHRiMP aligner (Rumble et al., 2009). **Table 4** summarizes the sample sequencing statistics. After read count with UMI and count normalization, an analysis of differentially expressed miRNAs was performed using DEseq2 (Love et al., 2014), applying the Apeglm shrinkage for LFC. Differentially expressed miRNAs were filtered using a cutoff of $p < 0.05$ (statistically significant results). The analysis of miRNA target genes was performed using MultiMiR (1.26.0) (Ru et al., 2014). Entrez IDs of target genes were used to perform gene ontology through an over-representation analysis (ORA) by using the enrichGO function of the ClusterProfiler R package (4.10.1) (Yu et al., 2012). The ORA results were graphically represented using the cnetplot function of the ClusterProfiler R package.

Table 4. Sample sequencing statistics.

Sample	Seq	Passing filter	Passing filter (%)	Passing filter mapped (%)	Sequenced mapped (%)	Mapped duplicate (%)	miRNA	miRNA reads
5xFAD_3M_1	10700155	7818248	73,07	86,67	63,33	4,05	1335	733
5xFAD_3M_2	12052942	8159492	67,7	84,41	57,14	4,4	1383	741
5xFAD_3M_3	10838343	7258811	66,97	83,48	55,91	4,02	1393	725
5xFAD_3M_4	10413492	6689310	64,24	82,34	52,89	3,67	1382	716

5xFAD_3M_5	11124231	8782416	78,95	90,56	71,5	4,31	1229	730
5xFAD_6M_10	12174698	8349967	68,58	78,73	54	3,86	1573	825
5xFAD_6M_6	12546322	8773768	69,93	83,62	58,48	4,24	1414	759
5xFAD_6M_7	13377299	9117591	68,16	81,05	55,24	4,07	1549	784
5xFAD_6M_8	9458050	6229640	65,87	79,06	52,07	3,34	1457	725
5xFAD_6M_9	12472120	8470775	67,92	78,56	53,35	3,87	1557	812
5xFAD_9M_11	13752822	10228841	74,38	85,93	63,91	4,84	1408	779
5xFAD_9M_12	12860992	9597325	74,62	87,29	65,14	4,72	1391	750
5xFAD_9M_13	10576602	7316868	69,18	83,01	57,42	3,85	1420	728
5xFAD_9M_14	13213051	9725513	73,61	87,58	64,46	4,52	1321	741
5xFAD_9M_15	10526415	8485167	80,61	90,97	73,33	4,45	1179	720
WT_3M_1	15529045	11207580	72,17	86,54	62,46	4,69	1421	801
WT_3M_2	12780361	9462311	74,04	89,02	65,91	4,52	1276	737
WT_3M_3	10778916	7751793	71,92	87,82	63,16	4,15	1217	706
WT_3M_5	14360657	10801280	75,21	88,85	66,82	4,97	1311	778
WT_6M_10	11767610	8908025	75,7	89,77	67,96	4,38	1198	714
WT_6M_6	12745887	9813618	76,99	89,2	68,68	4,6	1268	750
WT_6M_7	11223757	8869390	79,02	90,24	71,31	4,48	1223	707
WT_6M_8	10395678	7869802	75,7	89,3	67,6	4,36	1162	677
WT_6M_9	14295802	10925006	76,42	89,73	68,57	5,08	1244	759
WT_9M_11	12075893	9290009	76,93	90,25	69,43	4,63	1195	729
WT_9M_12	10860239	7941205	73,12	88,69	64,85	4,4	1240	696

WT_9M_13	12573685	8831200	70,24	84,34	59,23	4,42	1399	771
WT_9M_14	10617639	6761805	63,68	79,21	50,44	3,53	1441	719
WT_9M_15	13418682	10199780	76,01	88,17	67,02	4,79	1338	774

2.1.9 Validation of miRNA expression

On the retinal samples from 9-month-old mice, both WT and 5xFAD, used for miRNA profiling, miRNA expression was validated by quantitative RT-PCR (qRT-PCR) using a commercially available master mix (SsoAdvanced Universal SYBR Green Supermix, Bio-Rad Laboratories, Inc.) with a reverse universal primer (Mir-XTM miRNA First-Strand Synthesis Kit, Takara, CA, USA) and miRNA-specific forward primers on a detection system (CFX Connect Real-Time PCR Detection System provided with the software CFX manager version 3.1; Bio-Rad Laboratories, Inc.). The miRNA specific forward primer sequences were: miR-124-5p, 5'-CGTGTTCACAGCGGACCTTGAT-3'; miR-3968, 5'-CGAATCCCACTCCAGACACCA-3'; miR-3963, 5'-TGTATCCCACTTCTGACAC-3'; miR-3473f, 5'-CAAATAGGACTGGAGAGATG-3'; miR-12191-3p, 5'-CCCATGGAGCTGTAGGAGCCG-3'. Small nuclear RNA U1 was used as an endogenous control for miRNA expression. All reactions were run in triplicate for each sample.

2.1.10 Statistical Analysis

Data were expressed as the mean ± standard error of the mean (SEM). Statistical significance was evaluated using the two-way ANOVA followed by the post-hoc Bonferroni comparisons test. GraphPad Prism 9.0 software was used to analyze the data. $p < 0.05$ values were considered statistically significant.

2.2 Materials and methods for cerebral microcirculation assessments

2.2.1 Animals

In this study, the 2-, 4-, and 6-month-old 5xFAD mice and age-matched WT controls were genotyped and used as previously described in section 2.1.1 of this thesis.

2.2.2 Dietary supplementation

In the present study, both the 5xFAD mice and WT littermates were fed with an ACE oil-enriched diet or a standard diet immediately after weaning until 2, 4, and 6 months of age. To prepare the ACE oil-enriched diet, a commercial rodent chow (Teklad 2018, Envigo, San Giorgio al Natisone, Italy) was crushed in powder form and then homogeneously mixed with ACE oil to reach a final concentration of 12% (w/w) of this oil, following previous literature (Lucchesi et al., 2024; Santana-Garrido et al., 2024; Santana-Garrido et al., 2021; Santana-Garrido et al., 2020). The so-prepared oil-powder pellets were maintained at 4°C in the dark until daily usage.

2.2.3 Measurement of body Weight, water, and food intake

The body weight was monitored monthly by placing the animals on a common laboratory balance. The water consumption was monitored weekly by measuring the given and remaining volumes in the water bottles of each cage, and the food intake was measured daily by weighing the given and remaining food in each cage.

2.2.4 Measurement of blood glucose and body fat mass

The blood glucose concentrations were measured monthly using a OneTouch Ultra glucometer (LifeScan Inc., Milpitas, CA, USA). The amount of body fat mass was quantified in both WT and 5xFAD mice receiving the standard or the ACE oil-enriched diet at 2, 4, and 6 months of age by dissecting and weighing the adipose tissue from each animal.

2.2.5 Serum biochemical analysis

The mice were anesthetized by an intraperitoneal injection of avertin (1.25% avertin/g body weight). Subsequently, the blood was collected and centrifuged at 16000x *g* for 5 minutes at 4°C. The serum was collected and promptly stored at -80°C until use. On the experimental day, the serum was used to detect low-density lipoprotein (LDL), high-density lipoprotein (HDL), total cholesterol, alkaline phosphatase (ALP), gamma-glutamyl transferase (GGT), and glutamate pyruvate alanine aminotransferase (GPT). Particularly, the LDL, HDL, and total cholesterol serum levels were evaluated using direct colorimetric methods (ASKIT2104, ASKIT1904, ASKIT0802, Assel, Guidonia, Rome), while the serum levels of ALP, GGT, and GPT were quantified using kinetic methods (ASKIT1203, ASKIT1402, ASKIT1702, Assel, Guidonia, Rome).

2.2.6 Surgical animal preparation

The mice were anesthetized by intraperitoneal injection of Avertin (1.25% solution/g body weight), tracheotomized, and mechanically ventilated with room air and supplemental oxygen after being paralyzed with tubocurarine chloride (1mg/kg · h, i.v.). The ventilator settings were adjusted to keep blood gas levels within the physiological range, with continuous monitoring of end-tidal CO_2. Periodic arterial blood samples (100 µL) were collected through a catheter inserted into the femoral artery for blood gas analysis. Body temperature was measured and maintained at 37.0 ± 0.5°C using a heating stereotaxic frame (Lapi et al. 2016). The lateral tail vein, located on either side of the tail was used to intravenous injection of the fluorescent tracer [fluorescein isothiocyanate, FITC bound to dextran, molecular weight 70 kDa (FD 70), 50 mg/100 g b.w., as 5% wt/vol solution in 3 min just once at the start of experiment after 10 min of the preparation stabilization] through a small-gauge needle (e.g., 27-30 G). Successively, to visualize the pial microvasculature, a closed cranial window (3 mm × 4 mm) was implanted above the left parietal cortex (stereotactic coordinates: posterior 2 mm to bregma; lateral, 3 mm to midline) (Mayhan and Heistad., 1986). During the drilling of the cerebral cortex, a cold saline solution was superfused on the skull to avoid overheating. The skull and the dura mater

were removed, and the brain parenchyma was continuously superfused with artificial cerebrospinal fluid (Lapi et al. 2020).

2.2.7 Fluorescence microscopy and assessment of microvascular parameters

A fluorescence microscopic technique was utilized in vivo to observe the pial microcirculation. The microscope (Leitz Orthoplan Wetzlar, Germany) was equipped with long-distance objectives [5x, numerical aperture (NA) 0.08; 10x, NA 0.20; 32x, NA 0.40], a 10x eyepiece, and a filter block (Ploemopak, Leitz). A mercury lamp (100-Watt) provided the epi-illumination, and a heat filter prevented the overheating of the preparations (Leitz KG1). The pial microvascular networks were televised by a Dage MTI 300 low-light-level camera, and the real-time recordings were stored through a computer-based frame grabber (Pinnacle DC10 plus, Avid Technology, Burlington, MA, USA). For each microvascular network, vessel diameter and length were measured using a frame-by-frame computerized method (MIP Image; Institute of Clinical Physiology, CNR, Pisa, Italy), and pial arterioles were classified according to Strahler's scheme (Lapi et al., 2019; Kassab et al., 1994; Jiang et al., 1994; Kassab et al., 1993). Briefly, the terminal arterioles (order 1), or those that give rise to the capillaries (order 0), were identified first. The higher-order arterioles were then identified. For each vessel, the diameter was expressed as the mean and SEM of three diameter measurements taken in areas adjacent to the vessel itself, and the length was measured with successive repeated measurements along the entire length of the vessel between one branch and the next. By plotting the lengths and diameters obtained on the monitor images in stop-frame conditions, it was possible to construct a map of each microvascular network studied. We evaluated the number and order of vessels in a window of 400 × 400 μm in all groups of animals. The increase of microvascular permeability, an indicator of compromised BBB integrity, was quantified by evaluating the fluorescent dextran leakage from blood vessels and expressed as normalized gray levels (NGLs): NGL = (I - Ib)/Ib, where, Ib was the baseline gray level at the microvasculature filling with fluorescence, and I was the value after 30 min of observation. To obtain the gray levels, the MIP image program was utilized, and the data reported were derived from the average of five windows measuring 50 x 50 μm (taken with the 10x objective) located outside the vessels. To identify the same regions of interest, a computer-assisted device for XY movement of the microscope table was used. The density of functional capillaries, a key indicator of tissue blood supply, was measured by a computerized method (MIP Image, CNR, Pisa) in an area of 150 μm^2, evaluated as $cm/cm^2 = cm{-}1$ and expressed in percentage. Extracellular Aβ deposition, a hallmark lesion of AD, was evaluated by Thioflavin-S (ThS) fluorescence. The pial layer was superfused with aCSF, containing 250 mM ThS at 37.0 ± 0.5°C. The ThS fluorescence intensity was assessed using an appropriate filter (550 nm) and quantified by NGL. A double-blind experimental procedure was conducted to remove bias from single-operator measurements. In every instance, the results were concordant.

2.2.8 Western blotting

After the sacrifice, the brain was isolated and stored at -80°C. The brain samples were homogenized in 8x volume of RIPA lysis buffer (Santa Cruz Biotechnology, Dallas, TX, USA) supplemented with phosphatase

and protease inhibitor cocktails, and protein concentration was measured with the Protein Assay Dye Reagent Concentrate (Bio-Rad Laboratories, Inc.). Subsequent procedures, including sample preparation, electrophoresis, and immunoblotting, were carried out as previously described in section 2.1.6 of this thesis, while the antibodies used are reported in **Table 5**.

Table 5. List of antibodies used for Western Blotting.

Antibody	Source	Catalogue	Blocking	Dilution
Rabbit monoclonal antibody anti-pNFκB (p65)	Abcam	ab76302	5% skimmed milk	1:1000
Rabbit polyclonal antibody anti-NFκB (p65)	Abcam	ab16502	5% skimmed milk	1:1000
Mouse monoclonal antibody anti-IL6	Santa Cruz	sc57315	5% skimmed milk	1:200
Rabbit monoclonal antibody anti-GFAP	Abcam	ab207165	5% skimmed milk	1:5000
Rabbit monoclonal antibody anti-Iba1	Abcam	ab178846	5% skimmed milk	1:500
Rabbit monoclonal antibody anti-HIF1α	Abcam	ab179483	5% skimmed milk	1:1000
Rabbit monoclonal antibody anti-VEGFA	Abcam	ab214424	5% skimmed milk	1:1000
Rabbit monoclonal antibody anti-iNOS	Abcam	ab178945	5% skimmed milk	1:1000
Rabbit polyclonal antibody anti-ZO1	Abcam	ab96587	5% skimmed milk	1:500
Rabbit monoclonal antibody anti-Occludin	Abcam	ab216327	5% skimmed milk	1:1000
Mouse monoclonal antibody anti-Claudin 5	Invitrogen	35-2500	5% skimmed milk	1:500
Rabbit monoclonal antibody anti-CD10	Abcam	ab256494	5% skimmed milk	1:1000
Rabbit polyclonal antibody anti-IDE	Abcam	ab32216	5% skimmed milk	1:1000
Mouse monoclonal antibody anti-β-actin	Sigma-Aldrich	A2228	5% skimmed milk	1:2500

2.2.9 ELISA

After the sacrifice, the brain was isolated and stored at -80°C. Subsequent procedures were carried out as previously described in section 2.1.7 of this thesis. The ELISA kit N. KMB3441 was used according to the manufacturer's protocol to measure the brain Aβ (1-42) levels.

2.2.10 Novel object recognition test

The NOR test was used to assess short- and long-term memory, based on the innate tendency of rodents to explore novel objects. The test followed a previously described protocol [0.3390/ph16091307]. Briefly, mice were habituated to the arena for 10 minutes in the absence of objects. In the training phase, two identical objects were presented, and animals were allowed to explore for 5 minutes. After a 3-hour retention interval, one object was replaced with a novel one, and exploration behavior was recorded for 5 minutes. The next day, 24 hours after training, the new object used in the 3 h test was replaced with a new one, and the exploration behavior was recorded again. Video recordings were analyzed using ToxTrac v2.98 to extract mobility parameters and trajectories, which were further processed with ImageJ-win32. Data analysis was performed using GraphPad Prism 9. The Discrimination Index: DI = (Tnovel − Tfamiliar)/(Tnovel + Tfamiliar)) and Recognition Index: RI = Tnovel/(Tnovel + Tfamiliar), were calculated to evaluate memory performance.

2.2.11 Gravimetric quantification of liver lipid

Liver lipid content was quantified using the gravimetric method originally developed by Folch et al., 1957, with minor modifications. Mouse liver tissue was homogenized after being mixed with equal volumes of water and methanol. The homogenate underwent three sequential extractions with chloroform, followed by two washes with 1 M KCl and water. The chloroform solution was then completely evaporated and subjected to extended drying until a constant weight was achieved. The lipid content was subsequently quantified and expressed as milligrams of lipids per gram of tissue (mg/g tissue).

2.2.12 Statistical analysis

Data were expressed as the mean ± SEM. Statistical significance was evaluated using the two-way ANOVA followed by Tukey's post-hoc multiple comparisons test. GraphPad Prism 9.0 software was used to analyze the data. $p < 0.05$ values were considered statistically significant.

3. RESULTS

3.1 Results on the retinal features

3.1.1 Retinal function of 5xFAD mice

The electroretinographic routine displayed in **Figure 1** was designed to obtain a comprehensive evaluation of the retinal function over time, including dark- and light-adapted photoreceptoral, post-photoreceptoral, and RGC activity in 5xFAD mice as compared to their WT counterparts. As depicted in **Figure 1A**, 5xFAD mice show retinal activity comparable with WT mice at 3 months of age, while far-reaching changes were observed at later ages. The analysis of scERG highlighted that the amplitude of the a-wave (**Figure 1B**), referring to the overall photoreceptoral activity, was significantly reduced in the 5xFAD mice at 9 months of age. In contrast, the b-wave (**Figure 1C**), reflecting the overall post-photoreceptoral response, including bipolar cell and Müller cell activity, displayed significantly lower amplitudes in 5xFAD retinas both at 6 and 9 months of age. Overall, the scERG data indicated that in 5xFAD mice, inner retinal neurons were affected before evident functional deficits appeared in retinal photoreceptors. The phERG b-wave amplitudes, which represent the post-photoreceptor activity mainly related to the cone pathway, did not show any significant variations between 5xFAD and WT mice either at 3 or at 6 months of age, but they were significantly reduced in 5xFAD animals at 9 months (**Figure 1D**). Regarding the phNR amplitude, generally related to RGC activity (Cvenkel et al., 2017), it was significantly reduced in 5xFAD mice, compared to WT, at both 6 and 9 months of age (**Figure 1E**). Overall, the phERG data were consistent with those of the scERG analysis and indicated that neurons of the inner retina (most likely RGCs) displayed pathological functional changes before cone photoreceptors. PERG responses were recorded to investigate the functional activity of RGCs. Similar to the phNR data, both the N35-P50 (**Figure 1F**) and the P50-N95 (**Figure 1G**) amplitudes were significantly decreased in 5xFAD mice compared to WT, at 6 and 9 months of age. Overall, the PERG data indicated an evident and progressive decrease in RGC function in 5XFAD mice starting at or slightly before 6 months of age.

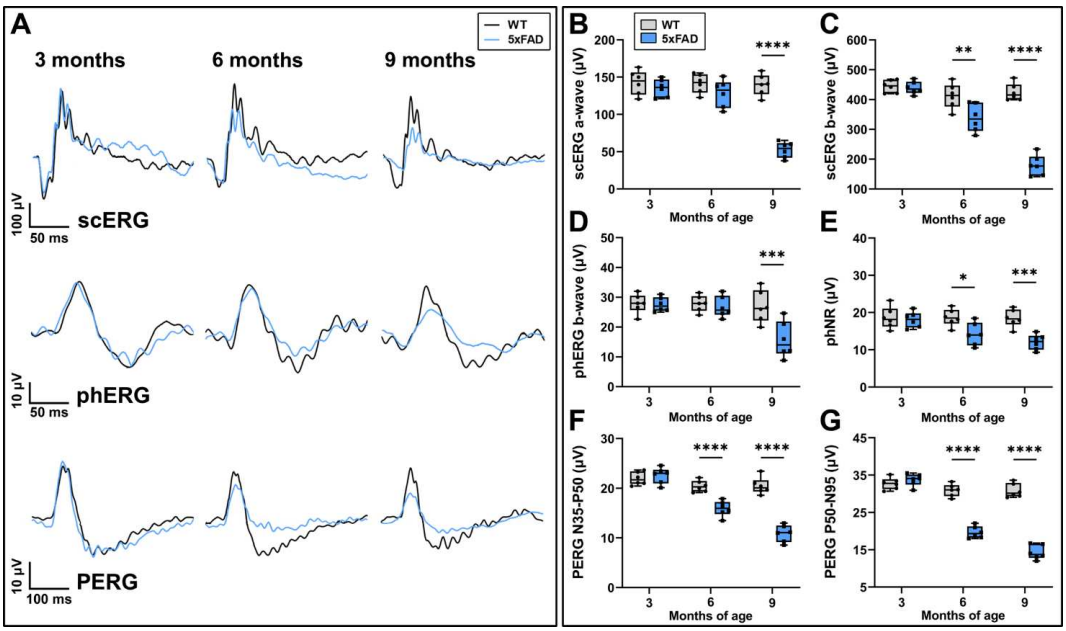

Figure 1. The retinal function of WT and 5xFAD mice at 3, 6, and 9 months of age was evaluated with ERG. (**A**) Representative scERG, phERG, and PERG waveforms. (**B-G**) Quantitative analyses of scERG a-wave (**B**), scERG b-wave (**C**), phERG b-wave (**D**), phNR (E), PERG N35-P50 (**F**), and PERG P50-N95 (**G**) amplitudes. Data were shown as box plots with minimum to maximum whiskers. Statistical significance was evaluated through Two-way ANOVA with Bonferroni post-hoc test (n = 6). * $p < 0.05$, ** $p < 0.01$, *** $p < 0.001$, **** $p < 0.0001$ versus age-matched WT. scERG, scotopic-ERG; phERG, photopic-ERG; PERG, Pattern-ERG.

The progressive worsening of retinal function was confirmed by the analysis of visual acuity with the Prusky water maze test. As shown in **Figure 2A**, at both 6 and 9 months, visual acuity in 5xFAD mice was significantly reduced with respect to that in WT mice. At these time points, the success rate of 5xFAD mice was lower than that of WT mice (**Figure 2B**). The observation that the response curves at low spatial frequencies and their slopes at higher frequencies were similar in both strains indicated that the poor performance of 5xFAD mice was related to the declining retinal function and not to the cognitive impairment that is observed starting at 4-6 months of age (Pádua et al., 2024).

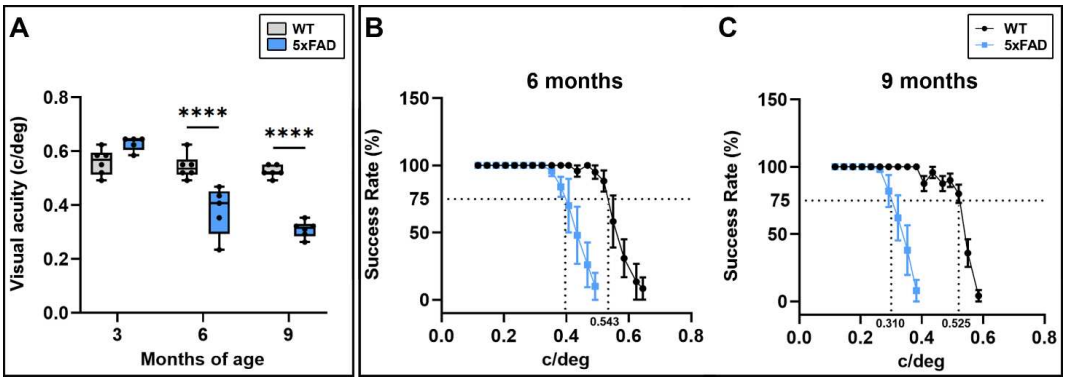

Figure 2. Visual acuity of WT and 5xFAD mice at 3, 6, and 9 months of age was evaluated by the Prusky water maze test. (**A**) Visual acuity, measured in cycles per degree. (**B-C**) Success rates (percentage of correct trials) for each group in response to each spatial frequency presented at 6 (left panel) and 9 (right panel) months. Data were shown as box plots with minimum to maximum whiskers. Statistical significance was evaluated through Two-way ANOVA followed by Bonferroni's multiple comparisons test (n = 6). **** $p < 0.001$ versus respective WT.

3.1.2 Retinal structure of 5xFAD mice

From a structural point of view, the OCT analysis revealed a significant decrease in the RNFL-GCL thickness at 9 months, which was compensated for by a concomitant increase in IPL thickness (**Figure 3A-B**).

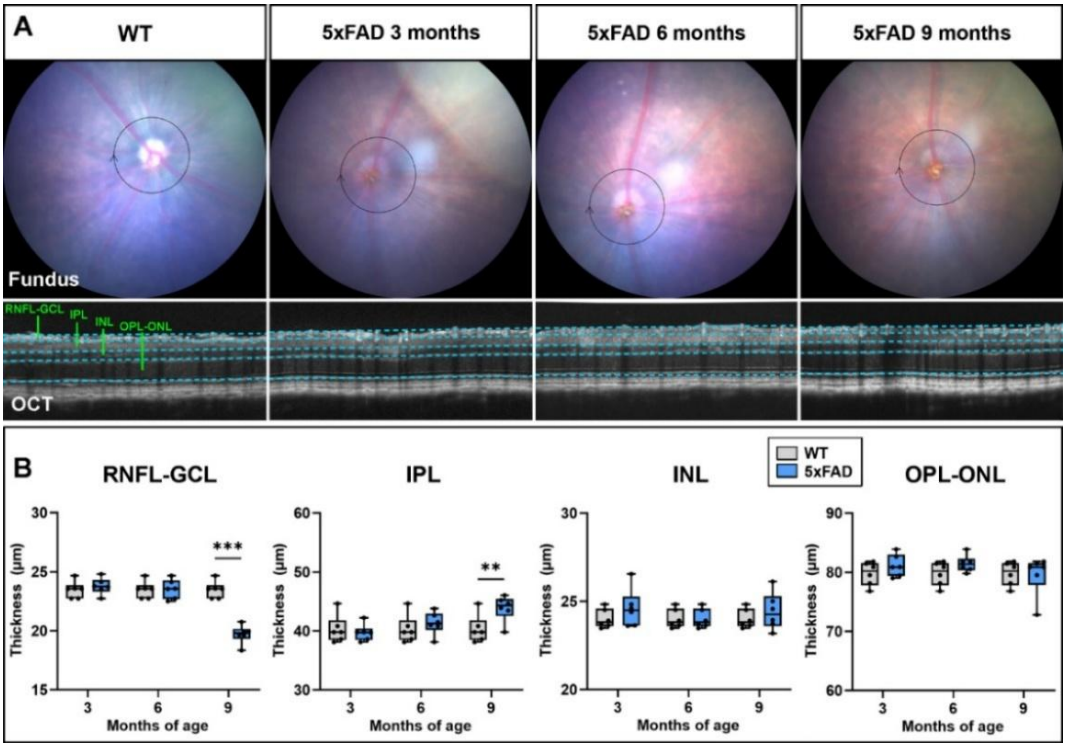

Figure 3. In vivo analysis of retinal morphology in WT and 5xFAD mice at 3, 6, and 9 months of age as assessed by image-guided OCT. (**A**) Fundus images (upper row) were used to center the scan area around the optic nerve head (500 µm). Circular B-scans of the central retina (lower row) were processed for segmentation of retinal layers. (**B**) Quantitative measurements of retinal layer thickness. The OCT scans in WT retinas were similar at all ages. Data were shown as box plots with minimum to maximum whiskers. Statistical significance was evaluated through Two-way ANOVA with Bonferroni post-hoc test (n = 6). ** $p < 0.01$, *** $p < 0.001$ versus age-matched WT. RNFL, retinal nerve fiber layer; GCL, ganglion cell layer; INL, inner nuclear layer; OPL, outer plexiform layer; ONL, outer nuclear layer.

3.1.3 Characterization of 5xFAD mouse retinas

The ERG data indicated that, in 5xFAD mice, RGCs displayed pathological functional changes beginning at 6 months of age. Consistently, Aβ deposits were observed in the GCL of 5xFAD retinas at 6 months, and they were further increased at 9 months, when infiltration of the deposits towards internal retinal layers was also observed (**Figure 4A-D**). As shown in **Figure 4I**, measurements of the retinal Aβ content with ELISA confirmed significant increases of Aβ (1-42) in 5xFAD retinas at 6 and 9 months of age. To ascertain whether the increased presence of Aβ deposits in the GCL might be associated with changes in RGC viability, the number of RBPMS-immunolabeled RGCs was evaluated over time in WT and 5xFAD retinal sections (**Figure 4E-H**). In line with the ERG recordings and with the data of Aβ immunofluorescence, a significant decrease in RGC number, compared to WT, was observed in 5xFAD retinas at 6 and 9 months of age (**Figure 4J**).

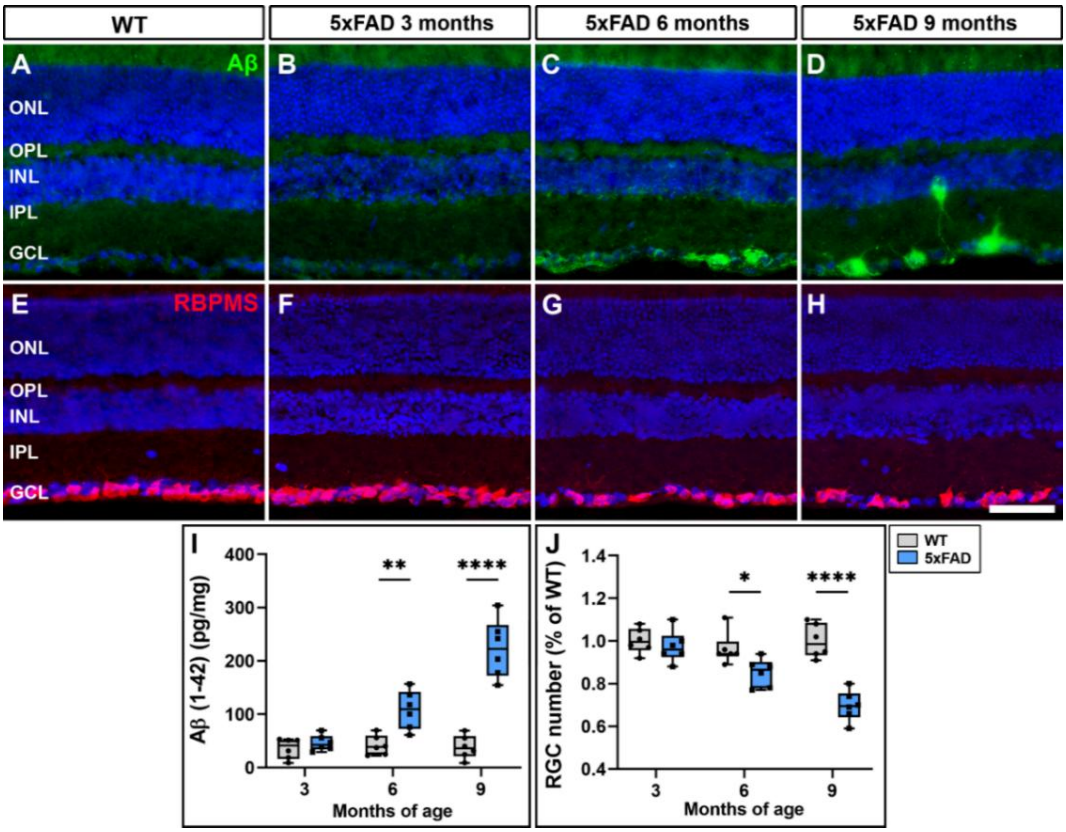

Figure 4. Evaluation of Aβ accumulation and loss of RGCs in WT and in 5xFAD mouse retinas at 3, 6, and 9 months of age. (**A-H**) Representative images of retinal cross-sections immunolabeled for Aβ (**A-D**) and RBPMS (**E-H**) with DAPI counterstain. The immunostaining patterns in WT retinas were similar at all ages; therefore, only one representative image of a WT retina is represented. Scale bar, 30 µm. (**I**) ELISA quantification of retinal Aβ (1-42) levels. (**J**) RGC numbers in the central retina expressed as a percentage of WT at 3 months of age. Data were shown as box plots with minimum to maximum whiskers. Statistical significance was evaluated through Two-way ANOVA with Bonferroni post-hoc test (n = 6). * $p < 0.05$, ** $p < 0.01$, **** $p < 0.0001$ versus age-matched WT. Aβ, amyloid beta; RBPMS, RNA-binding protein with multiple splicing; GCL, ganglion cell layer; INL, inner nuclear layer; OPL, outer plexiform layer; ONL, outer nuclear layer.

The ERG data and the analysis of RGC numbers suggested the occurrence of significant cell loss in 5xFAD mice between 6 and 9 months of age. Accordingly, observations of active caspase 3 immunofluorescence (**Figure 5A-D**) showed the presence of apoptotic cell profiles, mainly localized in GCL in 9-month-old 5xFAD retinas. A western blot analysis showed a significant increase in the Bax/Bcl-2 ratio in 9-month-old 5xFAD mice (**Figure 5E-F**), further supporting these findings.

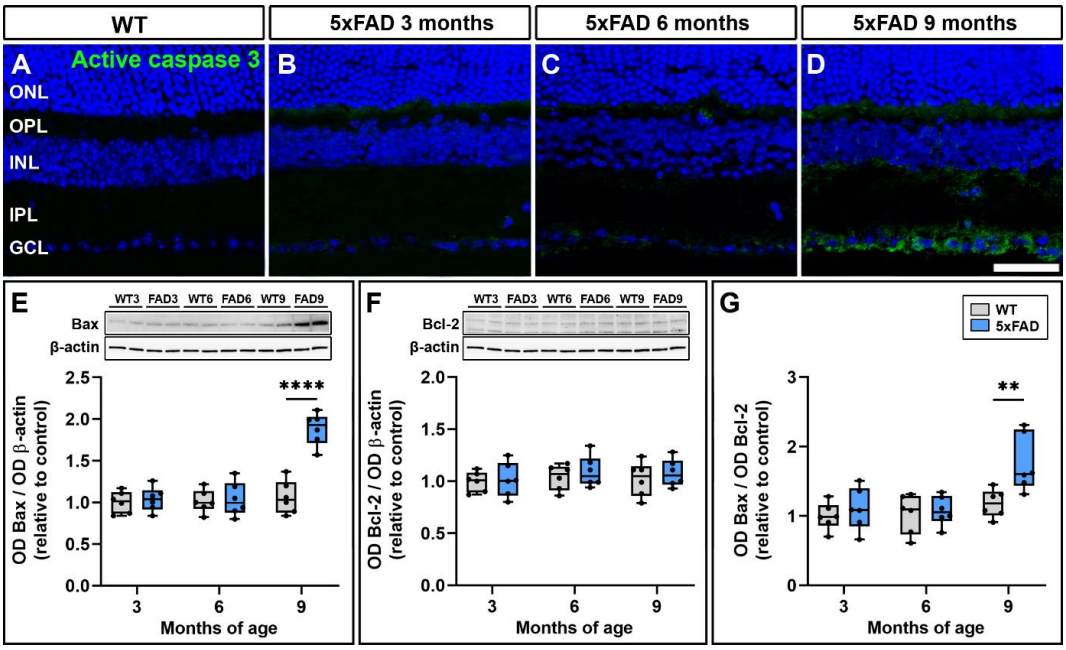

Figure 5. Evaluation of apoptosis in WT and in 5xFAD mouse retinas at 3, 6, and 9 months of age. (**A-D**) Representative images of retinal cross-sections immunolabeled for active caspase 3 with DAPI counterstain. The immunostaining patterns in WT retinas were similar at all ages; therefore, only one representative image of a WT retina is represented. Scale bar, 30 µm. (**E-G**) Western blotting and densitometric analysis of Bax (**E**), Bcl-2 (**F**), and Bax/Bcl-2 ratio (**G**). The levels of Bax and Bcl-2 were normalized to β-actin as well as to control (WT at 3 months of age). Data were shown as box plots with minimum to maximum whiskers. Statistical significance was evaluated through Two-way ANOVA with Bonferroni post-hoc test (n = 6). ** $p < 0.01$, **** $p < 0.0001$ versus age-matched WT. Bax, Bcl-2-associated X protein; Bcl-2, B-cell lymphoma 2; GCL, ganglion cell layer; INL, inner nuclear layer; OPL, outer plexiform layer; ONL, outer nuclear layer.

In addition to Aβ accumulation, the hallmark of AD is an increased rate of Tau protein phosphorylation. A significant increase in the protein content of both Tau (**Figure 6A**) and pTau (**Figure 6B**) was observed in 5xFAD retinas over time. In particular, as shown in Figure 6, the ratio pTau/Tau (**Figure 6C**) resulted significantly higher in 5xFAD retinas, compared to WT, at both 6 and 9 months of age, indicating a remarkable increase of Tau protein phosphorylation in 5xFAD retinas over time.

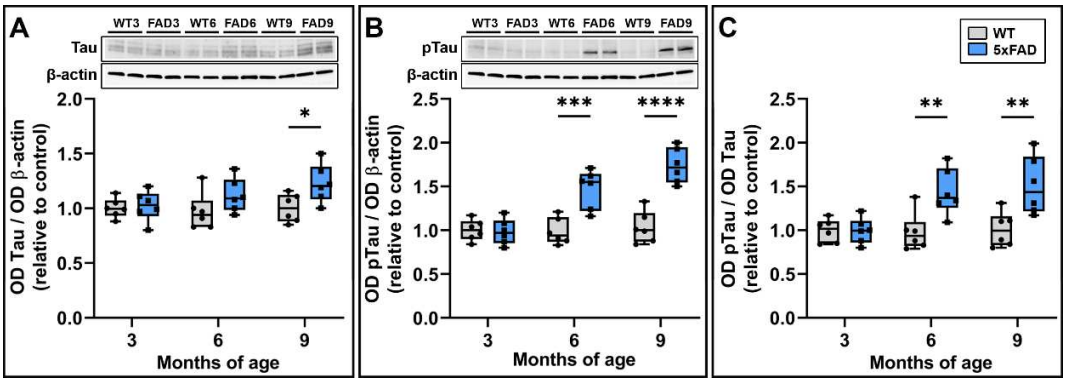

Figure 6. Evaluation of Tau protein phosphorylation in WT and in 5xFAD mouse retinas at 3, 6, and 9 months of age. Representative Western blotting and densitometric analysis of Tau protein (**A**), its phosphorylated form (**B**), and relative quantification of pTau/Tau ratio (**C**). The levels of pTau and Tau protein were normalized to β-actin as well as to the control (WT at 3 months of age). Data were shown as box plots with minimum to maximum whiskers. Statistical significance was evaluated through Two-way ANOVA with Bonferroni post-hoc test (n = 6). * $p < 0.05$, ** $p < 0.01$, *** $p < 0.001$, **** $p < 0.0001$ versus age-matched WT. pTau; phosphorylated Tau.

Increased inflammation and oxidative stress are likely to be involved in the pathological changes observed in the retinas of 5xFAD mice. As shown in **Figure 7A-C**, a marked increase in NFκB phosphorylation was observed in 5xFAD retinas at 9 months of age, and the protein content of IL-6 was significantly increased at the same age (**Figure 7D**). The pattern of oxidative stress markers Nrf2 (**Figure 7E**) and NQO1 (**Figure 7F**) was similar to that of NFκB phosphorylation and IL-6 protein content. Overall, these data indicated high levels of inflammation and oxidative stress in 5xFAD retinas at 9 months of age.

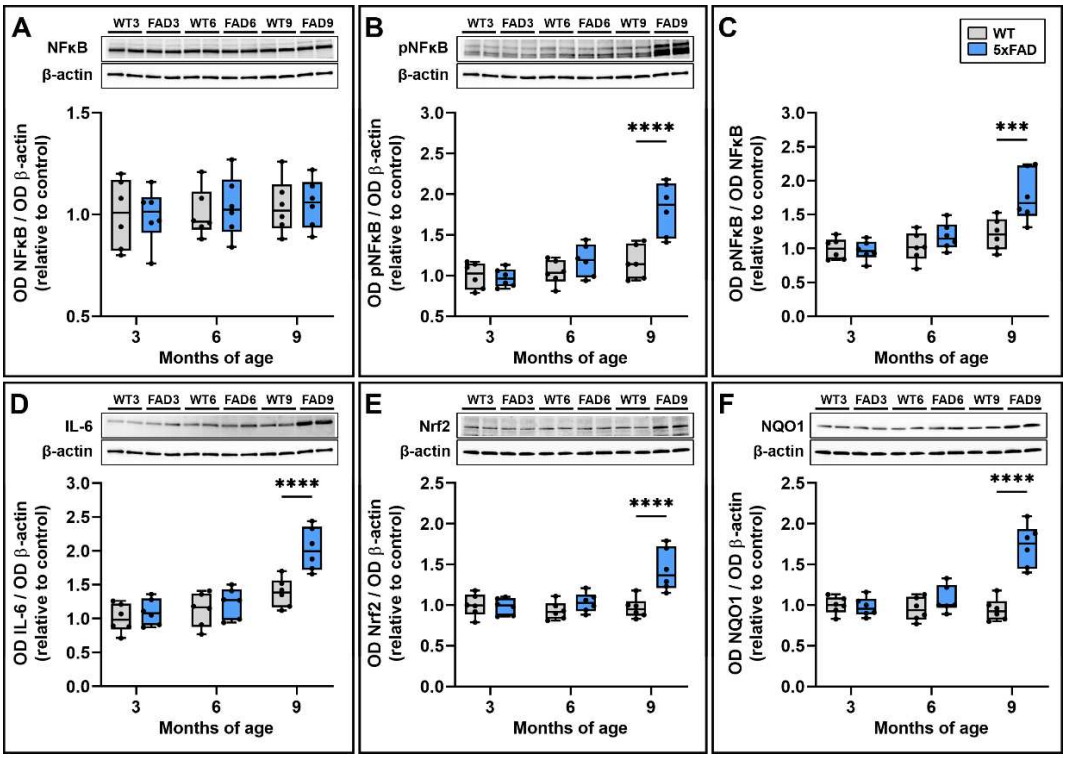

Figure 7. Evaluation of neuroinflammatory (**A-C**) and oxidative stress markers (**D-F**) in WT and 5xFAD mouse retinas at 3, 6, and 9 months of age. Western blotting and densitometric analysis of NFκB (**A**), pNFκB (**B**), IL-6 (**D**), Nrf2 (**E**), NQO1 (**F**), and relative quantification of pNFκB/NFκB ratio (**C**). The level of NFκB, pNFκB, IL-6, Nrf2, and NQO1 was normalized to β-actin as well as to control (WT at 3 months of age). Data were shown as box plots with minimum to

maximum whiskers. Statistical significance was evaluated through Two-way ANOVA with Bonferroni post-hoc test (n = 6). *** $p < 0.001$, **** $p < 0.0001$ versus age-matched WT. NFκB, Nuclear Factor kappa-light-chain-enhancer of activated B cells; pNFκB, phosphorylated NFκB; IL-6, interleukin-6; Nrf2, Nuclear factor erythroid 2-related factor 2; NQO1, NAD(P)H quinone dehydrogenase 1.

The glial cells of the retina were investigated using different immunohistochemical markers. To ascertain whether Müller cells were affected by the pathological conditions that develop in the 5xFAD retina over time, they were labeled with antibodies directed to GS. As illustrated in **Figure 8A-D**, no changes were observed in GS immunostaining in 5xFAD retinas, either with respect to WT retinas or over time. GFAP immunostaining was employed to visualize astrocytes and to ascertain the possible occurrence of glial reactivity (that is, GFAP staining in Müller cells) in 5xFAD retinas. **Figure 8E-H** clearly shows no changes in astrocyte appearance and the absence of any signs of glial reactivity. Finally, Iba1 immunostaining was used to visualize microglial cells. These cells were observed in WT and 5xFAD retinas at all ages. They were mainly localized within the IPL and the OPL and were characterized by long and ramified processes in both WT and 5xFAD retinas at 3 and 6 months of age (**Figure 8I-K**). At 9 months, Iba1 immunolabeled cells in 5xFAD retinas displayed shorter and less ramified processes, and some of them appeared to have almost completely lost their ramifications, assuming an amoeboid morphology typical of reactive or activated microglial cells (**Figure 8L**).

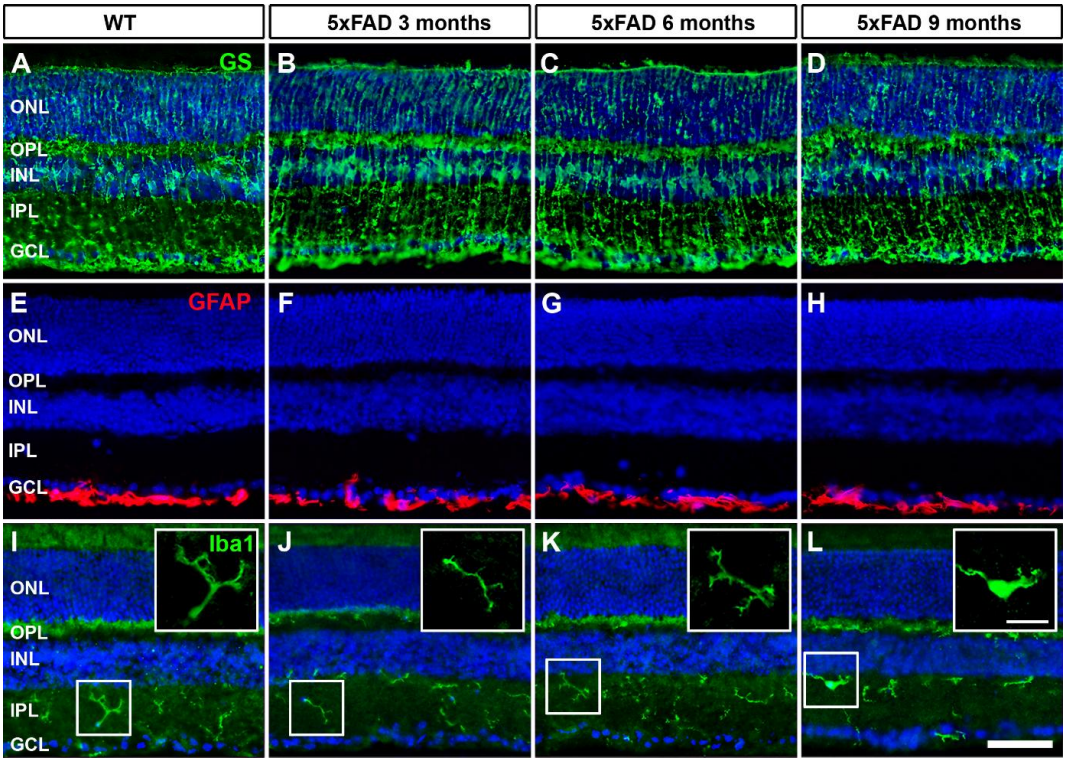

Figure 8. Evaluation of macro- and microgliosis in WT and 5xFAD mouse retinas at 3, 6, and 9 months of age. The immunohistochemical patterns in WT retinas were similar at all ages; therefore, only one representative image of a WT retina is represented. Representative images of retinal cross-sections immunolabeled for GS (**A-D**), GFAP (**E-H**), and Iba1 (**I-L**) with DAPI counterstain. The immunostaining patterns in WT retinas were similar at all ages. Scale bar, 30 µm. GS, Glutamine Synthetase; GFAP, glial fibrillary acidic protein; Iba1, Ionized calcium-binding adaptor molecule 1; GCL, ganglion cell layer; INL, inner nuclear layer; OPL, outer plexiform layer; ONL, outer nuclear layer.

3.1.4 Retinal miRNA profiling

To evaluate the possible involvement of miRNAs in the development of retinal morpho-functional and molecular alterations in 5xFAD mice, a retinal miRNA profiling of 5xFAD mice was performed using samples at 3, 6, and 9 months of age. WT mice of the same age were used as controls. As shown in **Figure 9A**, a PCA analysis of the samples collected at all time points suggested a batch effect due to samples collected at different times. Therefore, a differential expression analysis was performed over all time points after batch effect correction. Five differentially expressed miRNAs, downregulated in 5xFAD mice at 3, 6, or 9 months, were identified (**Figure 9B**), and their putative effectors were retrieved. The intersections among their putative effectors are shown in **Figure 9C**. Four out of five deregulated miRNAs (mmu-miR-12191-3p, mmu-miR-3963, mmu-miR-3968, and mmu-miR-124-5p) were then validated at 9 months through qRT-PCR, while validation failed for mmu-miR-3473f (**Figure 9D**).

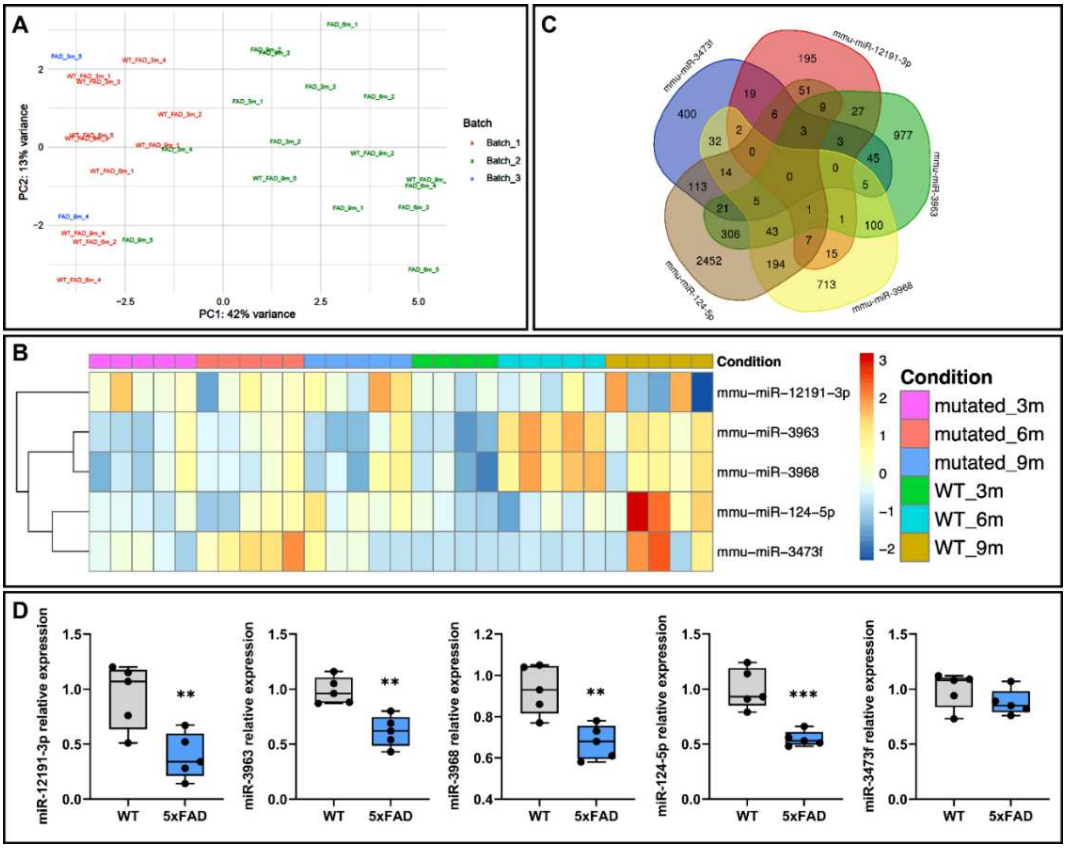

Figure 9. Batch effect and data processing. (**A**) Principal Component Analysis showing a batch effect. (**B**) Heatmap after batch correction representing the hierarchical clustering analysis of miRNome. The expression values of each miRNA are normalized across each row, where red and blue represent up- and down-regulation, respectively. Each miRNA expression value is represented by a single row of colored boxes, while columns represent different mice (mutated or wildtype) at different time points (3, 6, or 9 months). (**C**) Gene target intersections are represented with a Venn diagram. (**D**) Relative expression levels of the five differentially expressed miRNAs. Data were shown as box plots with minimum to maximum whiskers. Statistical significance was evaluated through Two-way ANOVA with Bonferroni post-hoc test (n = 6). ** $p < 0.01$, *** $p < 0.001$ versus age-matched WT.

Among the differentially expressed miRNAs validated through qRT-PCR, we focused our analysis on mmu-miR-3968 and mmu-miR-124-5p, whose expression is related to AD onset/progression. We found that they have 194 effector genes in common. The biological processes in which they are involved were investigated with an ORA analysis. The ORA revealed that the target genes were involved in processes such as apoptosis, inflammation, photoreceptor differentiation, neuronal and synaptic function, and eye development (**Figure 10**) (Wang et al., 2023; An et al., 2017), corroborating the previous morpho-functional and molecular analyses.

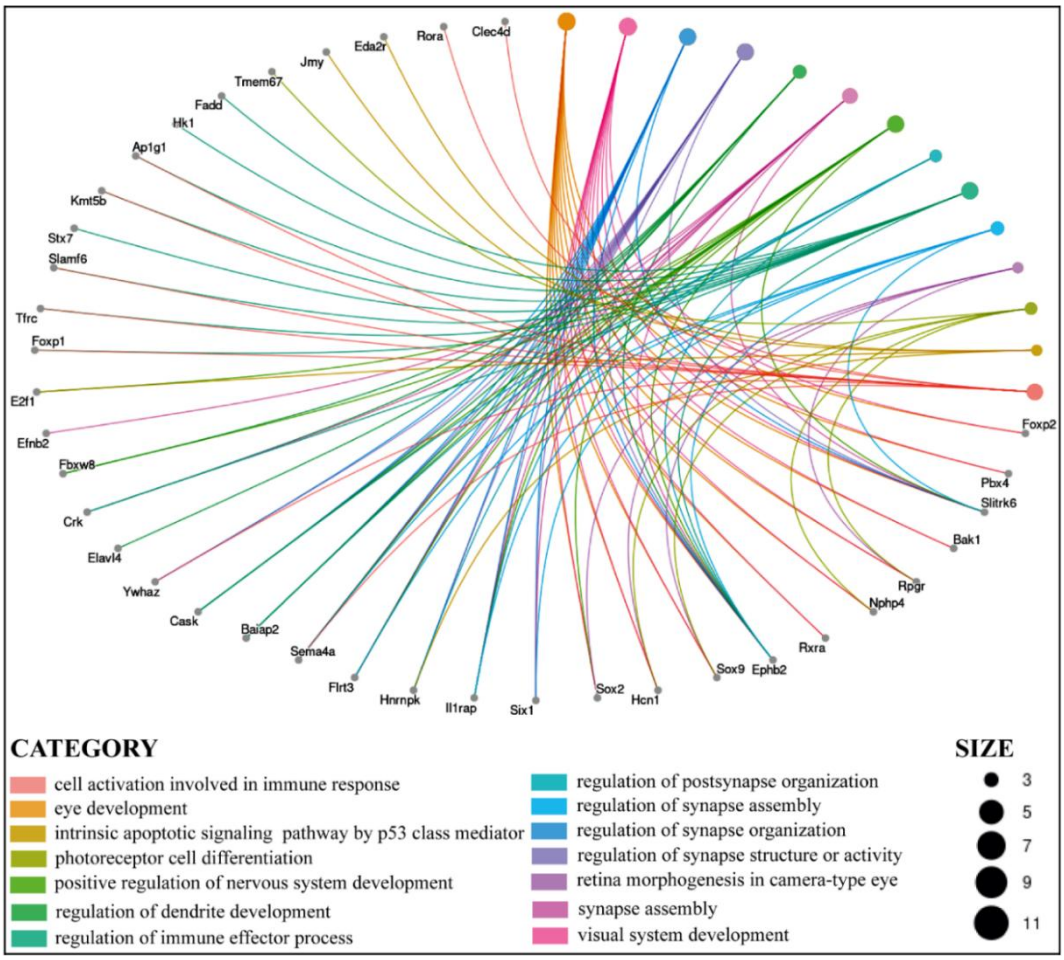

Figure 10. Enriched biological processes by common target genes of mmu-miR-124-5p and mmu-miR-3968 assessed through an over-representation analysis and visualized using the cnetplot function ClusterProfiler R package. The colored nodes represent the pathways, and the grey nodes are the differentially expressed genes associated with those pathways.

3.2 Results on the cerebral microcirculation parameters and dietary impact of the ACE oil supplementation

3.2.1 ACE oil-enriched diet prevents cerebral microcirculation alterations

Since cerebral microvasculature is affected in AD patients (Chwalisz, 2021; Attems and Jellinger, 2014; Nelson et al., 2012) and EVOO has been reported to positively impact the cerebral microvasculature in subjects with mild cognitive impairment (Kaddoumi et al., 2022), we evaluated the effect of the ACE oil-enriched diet on pial microcirculation. As shown in **Figure 11A-D**, when compared to their relative controls that did not exhibit any pathological changes, 5xFAD mice receiving a standard diet displayed far-reaching changes in arteriolar vessel morphology starting at 2 months. By Straler's method, for the first time used to classify microvascular networks in mice, it was possible to identify 3 orders of arterioles in all WT studied, while only 2 vessel orders were present in 5xFAD (reduction of arteriolar vessels) (**Table 6**). Interestingly, the order 2 vessels in 5xFAD mice were significantly longer than the order 2 vessels in WT, a finding due to pronounced tortuosity. These characteristics were associated with recurrent arteriovenous anastomoses. The ACE oil-enriched diet efficiently restored preserved alterations in the pial cerebral microcirculation in 5xFAD mice (**Figure 11E-H**). In particular, the arteriolar networks are made up of three orders of vessels, and the trend is linear as was observed in WT. The microvascular permeability, which increased in 5xFAD mice receiving the standard diet starting from 4 months, was significantly decreased by the ACE oil-enriched diet (**Figure 11I**). Moreover, the perfused capillary density, which was progressively reduced in 5xFAD mice receiving the standard diet starting from 2 months and reaching a reduction of about 50% at 6 months, was almost completely prevented by the ACE oil-enriched diet (**Figure 11J**).

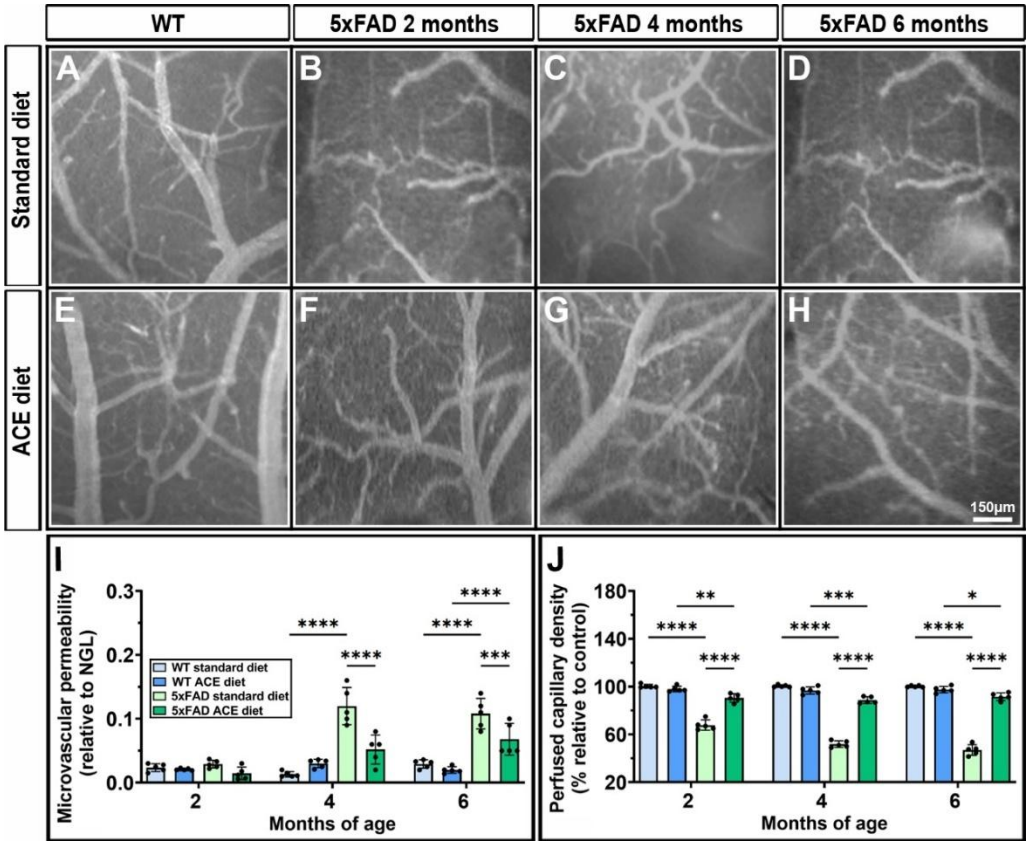

Figure 11. Effects of the ACE oil-enriched diet on pial microcirculation. (**A-H**) Representative images of pial microvasculature in WT (**A, E**) and 5xFAD (**B-D, F-H**) mice fed either a standard (**A-D**) or an ACE oil-enriched diet (**E-H**). WT mice displayed similar patterns across all ages; therefore, only one representative image is shown for each dietary condition. Scale bar, 150 µm. The microvascular permeability was measured and expressed as normalized grey levels (**I**), while the perfused capillary density was quantified and expressed as a percentage of control (WT receiving the standard diet at 2 months of age) (**J**). Data were shown as histogram columns with minimum to maximum whiskers. Statistical significance was evaluated through two-way ANOVA followed by Tukey's post-hoc multiple comparison test (n = 5 for each experimental group). * $p < 0.05$, ** $p < 0.01$, *** $p < 0.001$ and **** $p < 0.0001$. ACE, Acebuche, NGL, normalized grey levels.

Table 6. Strahler scheme for ordering the segments of a tree-like cerebrovascular network.

Experimental Group	Dietary	Order	Diameter (µm)	Length (µm)	Arterioles (n)
2-month-old WT	Standard	3	36.9 ± 2.4	587 ± 14.3	2.0 ± 1.0
		2	24.5 ± 1.7	325.7 ± 21.2	5.5 ± 1.0
		1	16.0 ± 0.9	174.5 ± 18.0	7.0 ± 2.0
2-month-old WT	ACE	3	36.3 ± 2.2	580 ± 15.5	2.0 ± 0.5
		2	25.7 ± 2.3	320.8 ± 20.2	4.0 ± 1.0
		1	17.1 ± 0.9	168.3 ± 17.0	8.0 ± 2.0
2-month-old 5xFAD	Standard	3	None	None	None
		2	26.3 ± 2.1	405.2 ± 16.8	2.5 ± 0.5
		1	15.5 ± 0.5	205.8 ± 12.5	4.5 ± 1.0
2-month-old 5xFAD	ACE	3	34.8 ± 2.3	489.1 ± 16.7	1.0 ± 0.5
		2	23.9 ± 1.4	384.4 ± 19.2	4.0 ± 1.5
		1	17.3 ± 0.2	168.7 ± 15.3	5.0 ± 1.0
4-month-old WT	Standard	3	36.6 ± 3.2	622.3 ± 12.2	2.0 ± 1.0
		2	25.8 ± 2.6	405.8 ± 17.6	5.0 ± 1.0
		1	16.7 ± 1.3	180.3 ± 16.0	6.0 ± 2.0

4-month-old WT	ACE	3	35.9 ± 2	657.4 ± 15.3	1.5 ± 0.5
		2	26.7 ± 1.9	397.2 ± 12.9	5.0 ± 1.5
		1	16.2 ± 1.7	195.3 ± 9.6	7.0 ± 1.0
4-month-old 5xFAD	Standard	3	None	None	None
		2	25.1 ± 3.6	478.1 ± 20.4	2.0 ± 0.5
		1	17.0 ± 1.4	189.0 ± 15.7	4.0 ± 1.0
4-month-old 5xFAD	ACE	3	35.2 ± 3.0	623.7 ± 15.4	1.0 ± 0.5
		2	24.8 ± 2.6	352.3 ± 17.2	4.0 ± 1.5
		1	16.7 ± 1.7	176.5 ± 14.7	6.0 ± 1.0
6-month-old WT	Standard	3	37.1 ± 3.0	635.7 ± 13.1	1.5 ± 1.0
		2	26.4 ± 1.8	373.6 ± 18.7	6.0 ± 0.5
		1	17.1 ± 0.3	202.5 ± 14.4	7.0 ± 1.5
6-month-old WT	ACE	3	36.8 ± 2.2	627.5 ± 13.8	2.0 ± 1.0
		2	25.1 ± 1.6	303.0 ± 15.9	6.5 ± 2.0
		1	16.7 ± 0.8	197.5 ± 15.8	8.0 ± 2.0
6-month-old 5xFAD	Standard	3	None	None	None
		2	27.2 ± 2.3	525.6 ± 17.3	1.5 ± 0.5
		1	15.9 ± 1.9	195.4 ± 11.1	3.5 ± 1.5
6-month-old 5xFAD	ACE	3	36.7 ± 2.5	503.7 ± 15.2	2.5 ± 1.0
		2	24.9 ± 2.7	408.1 ± 21.5	5.0 ± 1.0
		1	15.5 ± 0.8	188.4 ± 13.8	7.0 ± 2.0

3.2.2 ACE oil-enriched diet reduces cerebrovascular Aβ accumulation

ThS is a fluorescent dye commonly used to detect amyloid deposits, typically associated with neurodegenerative diseases such as AD. As shown in **Figure 12**, the ThS fluorescence intensity was evaluated in WT and 5xFAD mice fed either a standard diet (**Figure 12A-D**) or an ACE oil-enriched diet (**Figure 12E-H**). The data reveal the presence of widespread Aβ deposits in 5xFAD mice at 4 months (**Figure 12C**) and 6 months of age (**Figure 12D**), corresponding to a marked increase in ThS fluorescence intensity (**Figure 12I**). To corroborate these observations, we quantified brain Aβ levels in WT and 5xFAD mice under both dietary conditions. As illustrated in **Figure 12J**, 5xFAD mice exhibited a progressive accumulation of Aβ (1-42) starting at 4 months of age, consistent with enhanced APP processing in this model. Notably, dietary supplementation with ACE oil significantly lowered ThS fluorescence intensity (**Figure 12I**) and brain Aβ (1-42) levels (**Figure 12J**) in 5xFAD mice, suggesting a potential protective effect of ACE oil against amyloid pathology.

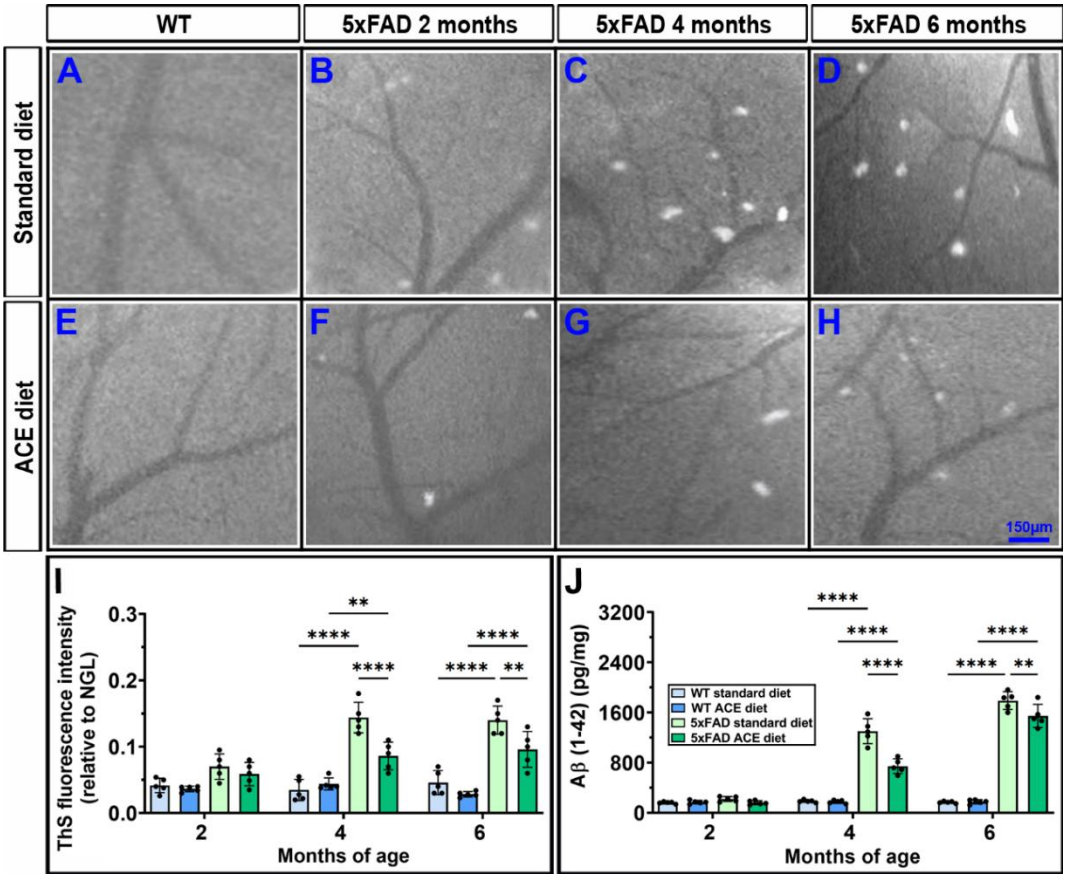

Figure 12. ACE oil-enriched diet decreased cerebrovascular Aβ accumulation in 5xFAD mice. Representative images of ThS fluorescent intensity in WT and 5xFAD mice fed with a standard diet (**A-D**) or an ACE oil-enriched diet (**E-H**). Scale bar, 150 µm. The ThS fluorescent intensity was measured and expressed as normalized gray levels (**I**). The levels of Aβ (1-42) were measured by ELISA in brain homogenates from WT and 5xFAD mice receiving the standard or the ACE oil-enriched diet (**J**). Data were shown as histogram columns with minimum to maximum whiskers. Statistical significance was evaluated by two-way ANOVA followed by Tukey's post-hoc multiple comparison test (n = 5 for each experimental group). **, $p < 0.01$, **** $p < 0.0001$. ACE, Acebuche; Aβ, amyloid beta; ThS, thioflavin S; NGL, normalized grey levels.

3.2.3 ACE oil-enriched diet prevents the downregulation of Aβ-degrading enzymes

Brain Aβ accumulation may result not only from increased production but also from impaired clearance; therefore, we evaluated the expression of two key Aβ-degrading enzymes, IDE and CD10, in the brain of both WT and 5xFAD mice fed either a standard or an ACE oil-enriched diet. As shown in **Figure 13**, levels of both IDE and CD10 were lower in 5xFAD compared to WT mice at 4 and 6 months. In 5xFAD mice, the ACE oil-enriched diet prevented the reduction of IDE and CD10 levels.

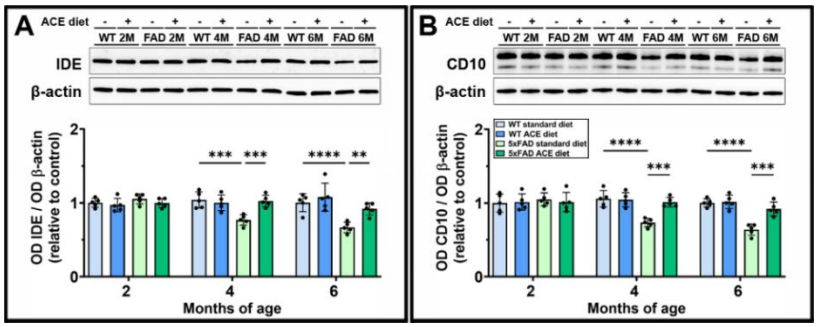

Figure 13. Effects of the ACE oil-enriched diet on the levels of Aβ-degrading enzymes. (**A, B**) Representative Western blots showing immunoreactive bands and relative densitometric analysis of IDE (**A**) and CD10 (**B**) levels in brain homogenates from WT and 5xFAD mice receiving the standard or the ACE oil-enriched diet. The level of IDE and CD10 was normalized to β-actin as well as to the control (WT receiving the standard diet at 2 months of age). Data are shown as histogram columns with minimum to maximum whiskers. Statistical significance was evaluated through two-way ANOVA followed by Tukey's post-hoc multiple comparison test (n = 5 for each experimental group). ** $p < 0.01$, *** $p < 0.001$, and **** $p < 0.0001$. ACE, Acebuche; IDE, Insulin-Degrading Enzyme; CD10, Cluster of Differentiation 10.

3.2.4 ACE oil-enriched diet prevents hypoxia and maintains BBB integrity

The presence of hypoxic conditions, likely resulting from vascular alterations, and the progressive breakdown of BBB integrity were assessed by Western blot analyses (**Figure 14**). Particularly, a marked increase in hypoxia-inducible factor (HIF)-1α (**Figure 14A**) and VEGF-A (**Figure 14B**) levels was found in 5xFAD mice starting from 2 months of age. The ACE oil-enriched diet restored both HIF-1α and VEGF-A levels at 2 and 4 months of age, but not in 6-month-old 5xFAD mice. Moreover, from 4 months onward, 5xFAD mice exhibited a significant reduction in cerebral claudin-5 expression (**Figure 14C**) that was restored by the ACE oil-enriched diet at 4 but not at 6 months. The levels of additional BBB markers, occludin (**Figure 14D**) and ZO-1 (**Figure 14E**), were not affected in 5xFAD mice.

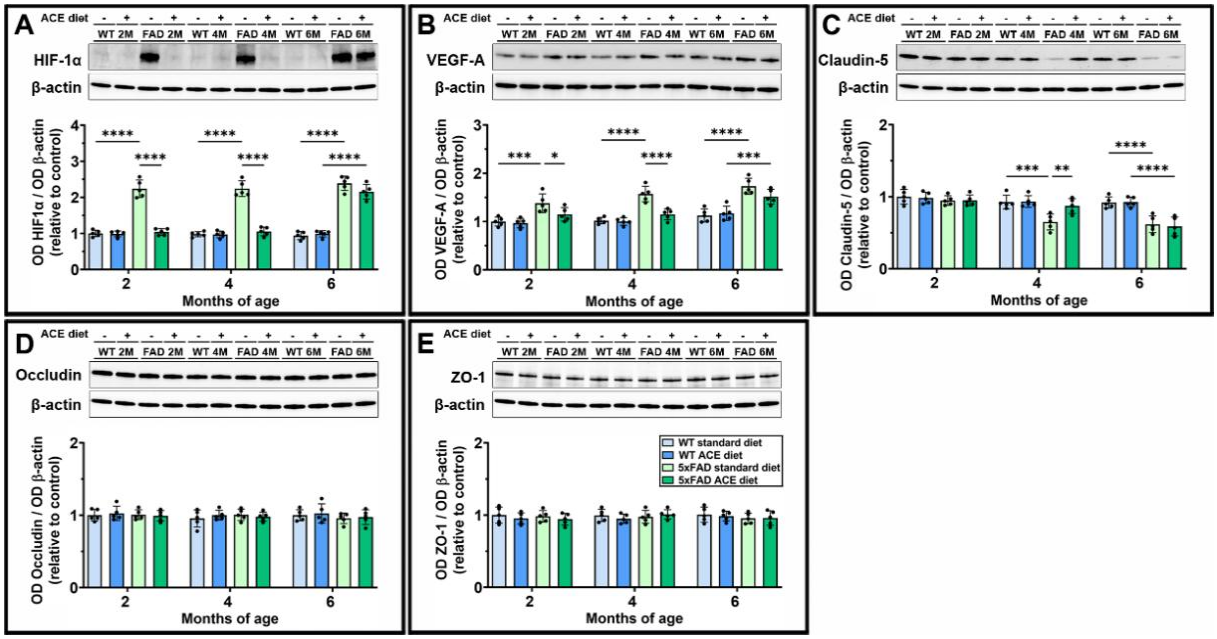

Figure 14. Effects of the ACE oil-enriched diet on the levels of hypoxia and blood-brain barrier (BBB) markers. (**A-E**) Representative Western blots showing immunoreactive bands and relative densitometric analysis of HIF-1α (**A**), VEGF-A (**B**), claudin-5 (**C**), occludin (**D**), and zonula occludens (ZO)-1 (**E**) levels in brain homogenates from WT and 5xFAD mice receiving the standard or the ACE oil-enriched diet. The level of HIF-1α, VEGF-A, claudin-5, occludin, and ZO-1 was normalized to β-actin as well as to the control (WT receiving the standard diet at 2 months of age). Data are shown as histogram columns with minimum to maximum whiskers. Statistical significance was evaluated through two-way ANOVA followed by Tukey's post-hoc multiple comparison test (n = 5 for each experimental group). * $p < 0.05$, ** $p < 0.01$, *** $p < 0.001$, and **** $p < 0.0001$. ACE, Acebuche; HIF-1α, Hypoxia-Inducible Factor 1-alpha; VEGF-A, Vascular Endothelial Growth Factor A; ZO-1, zonula occludens-1.

3.2.5 ACE oil-enriched diet reduces gliosis

To investigate whether BBB disruption and the Aβ accumulation might trigger a reactive gliosis and if this process might be counteracted by ACE oil, we evaluated the expression of acknowledged markers of micro- and macrogliosis, Iba1 and GFAP, respectively. As shown in **Figure 15**, both Iba1 (**Figure 15A**) and GFAP (**Figure 15B**) were upregulated in the brain of 5xFAD mice starting from 4 months. The ACE oil-enriched diet significantly attenuated gliosis in 4-month-old mice, with a partial loss of effectiveness at 6 months of age.

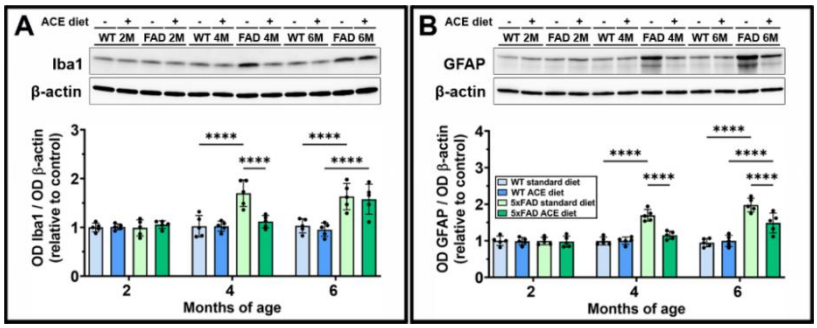

Figure 15. Effects of the ACE oil-enriched diet on the levels of micro- and macrogliosis markers. (**A, B**) Representative Western blots showing immunoreactive bands and relative densitometric analysis of Iba1 (**A**) and GFAP (**B**) levels in brain homogenates from WT and 5xFAD mice receiving the standard or the ACE oil-enriched diet. The level of Iba1 and GFAP was normalized to β-actin as well as to the control (WT receiving the standard diet at 2 months of age). Data are shown as histogram columns with minimum to maximum whiskers. Statistical significance was evaluated through two-way ANOVA followed by Tukey's post-hoc multiple comparison test (n = 5 for each experimental group). **** $p < 0.0001$. ACE, Acebuche; Iba1, Ionized calcium-binding adaptor molecule 1; GFAP, glial fibrillary acidic protein.

3.2.6 ACE oil-enriched diet delays the onset of neuroinflammatory processes

Cerebral gliosis is accompanied by the activation of neuroinflammatory processes. As shown in **Figure 16**, starting from 4 months, 5xFAD mice exhibited clear signs of neuroinflammation. This was evidenced by an increased ratio between the phosphorylated form of NF-kB (pNF-kB) and its total form (**Figure 16A-C**), elevated levels of the pro-inflammatory cytokine IL-6 (**Figure 16D**), and upregulation of the key player of the brain inflammatory response, inducible nitric oxide synthase (iNOS) (**Figure 16E**). The ACE oil-enriched diet significantly attenuated neuroinflammatory phenomena in 4-month-old mice, whereas this effect was no longer observed in 6-month-old 5xFAD mice.

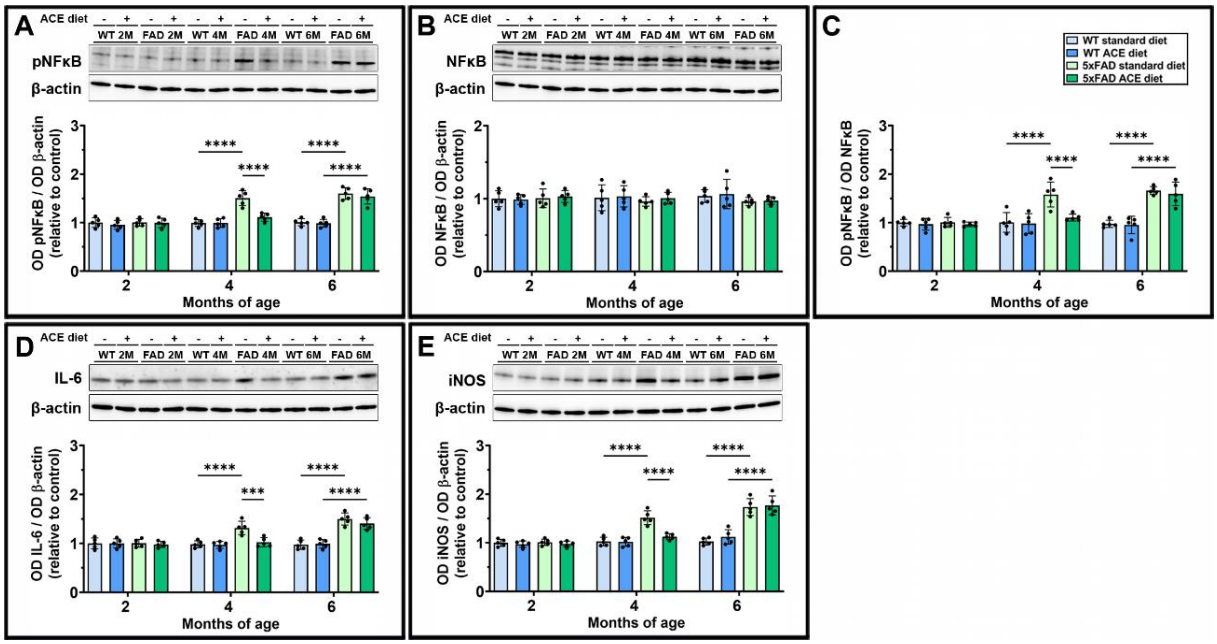

Figure 16. Effects of the ACE oil-enriched diet on the levels of neuroinflammatory markers. (**A, B**) Representative Western blots showing immunoreactive bands and relative densitometric analysis of the pNF-kB (**A**) and NF-kB (**B**) levels in brain homogenates from WT and 5xFAD mice receiving the standard or the ACE oil-enriched diet. (**C**) Ratio between the levels of pNF-kB and NF-kB. (**D, E**) Representative Western blots showing immunoreactive bands and relative densitometric analysis of IL-6 (**D**) and iNOS (**E**) in the same groups as in (**A, B**). The level of pNF-kB, NF-kB, IL-6, and iNOS was normalized to β-actin as well as to the control (WT receiving the standard diet at 2 months of age). Data are shown as histogram columns with minimum to maximum whiskers. Statistical significance was evaluated through two-way ANOVA followed by Tukey's post-hoc multiple comparison test (n = 5 for each experimental group). *** $p < 0.001$ and **** $p < 0.0001$. ACE, Acebuche; NFκB, Nuclear Factor kappa-light-chain-enhancer of activated B cells; pNFκB, phosphorylated NFκB; IL-6, interleukin-6; iNOS, inducible Nitric Oxide Synthase.

3.2.7 ACE oil-enriched diet ameliorates cognitive deficits

Cognitive decline in 5xFAD mice typically begins at 4 months of age, marking the onset of a prodromal phase that progresses to a symptomatic phase by approximately 6 months (Pádua et al., 2024). To investigate the potential neuroprotective effects of the ACE oil-enriched diet on cognitive function, 5xFAD mice were subjected to the NOR test by evaluating both short (3 h) and long-term (24 h) memory. As shown in **Figure 17**, the two-key metrics, DI and RI, were ameliorated by the ACE oil, with an effectiveness that was lost at 6 months. In particular, when tested at 3 h, DI and RI were increased at 4 months, while when tested at 24 h, DI and RI resulted in increased values at both 2 and 4 months.

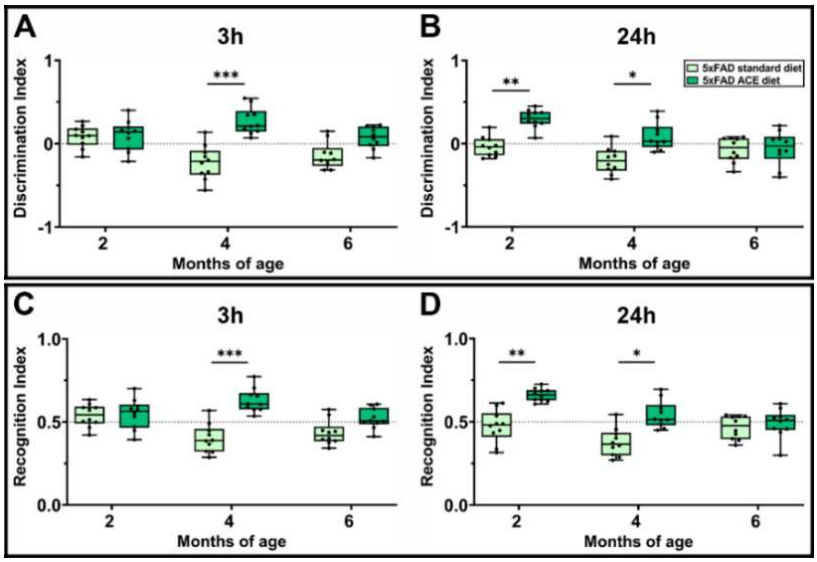

Figure 17. Effects of the ACE oil-enriched diet on cognitive functions. Cognitive functions in 5xFAD mice receiving the standard or ACE oil-enriched diet were assessed by the NOR test. (A-D) Discrimination index (**A, B**) and recognition index (**C, D**) were evaluated at 3 h (**A, C**) and 24 h (**B, D**) after training. Data are shown as box plots with minimum to maximum whiskers. Statistical significance was evaluated through two-way ANOVA followed by Tukey's post-hoc multiple comparison test (n = 10 for each experimental group). * $p < 0.05$, ** $p < 0.01$, *** $p < 0.001$. ACE, Acebuche.

3.2.8 Effects of the ACE oil-enriched diet on metabolic parameters

We monitored the effects of the ACE oil-enriched diet on metabolic parameters. As shown in **Figure 18**, no differences were observed in water consumption (**Figure 18A**), food intake (**Figure 18B**), and blood glucose level (**Figure 18C**) among the experimental groups over time. Conversely, body weight was significantly increased at 6 months in both WT and 5xFAD mice receiving the ACE oil-enriched diet (**Figure 18D**).

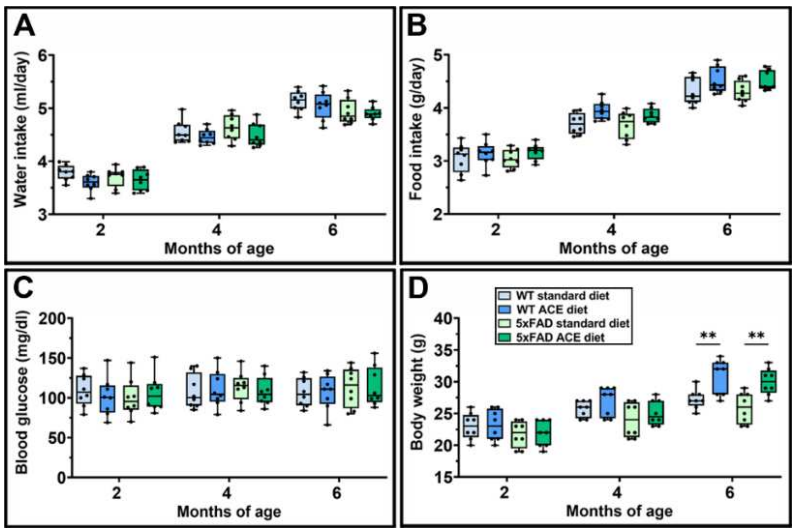

Figure 18. Effects of the ACE oil-enriched diet on metabolic parameters. Water intake (**A**), food intake (**B**), blood glucose (**C**), and body weight (**D**) were measured longitudinally in WT and 5xFAD mice receiving either the standard or ACE oil-enriched diet. Data were shown as box plots with minimum to maximum whiskers. Statistical significance was evaluated through two-way ANOVA followed by Tukey's post-hoc multiple comparison test (n = 8 for each experimental group). ** $p < 0.01$. ACE, Acebuche.

At 2 and 4 months of age, no difference in adipose tissue content was observed in WT and 5xFAD mice fed with a standard or ACE oil-enriched diet. In contrast, at 6 months of age, both WT and 5xFAD mice receiving the ACE oil-enriched diet exhibited a significantly increased amount of adipose tissue compared to their respective counterparts fed with a standard diet (**Figure 19**).

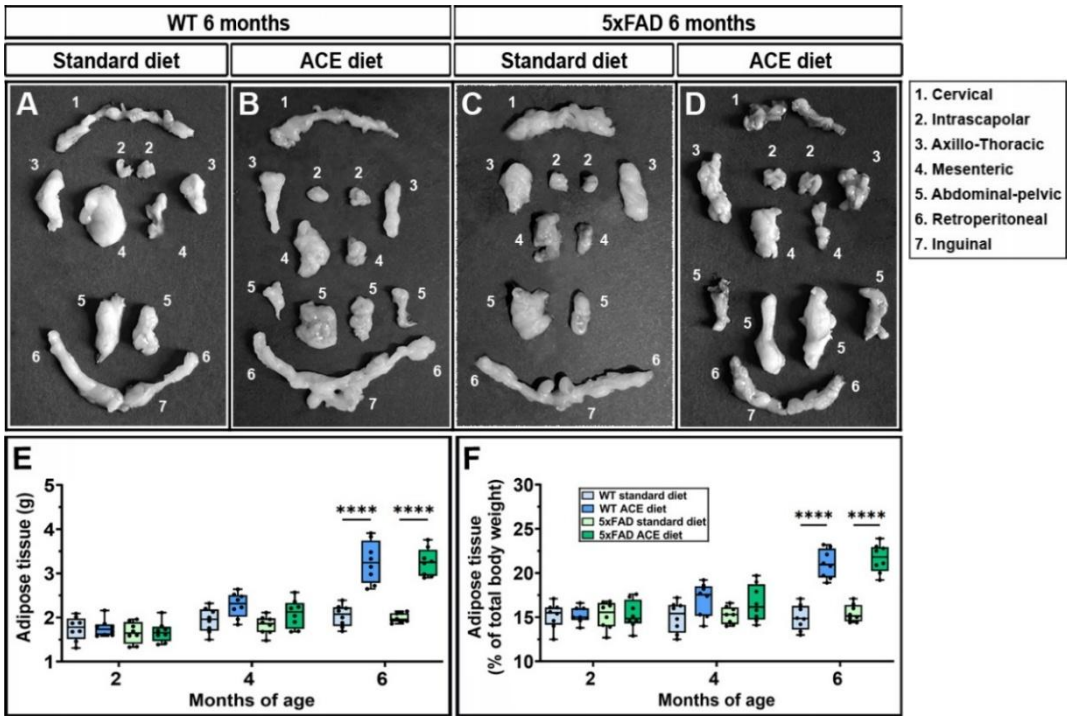

Figure 19. Effects of the ACE oil-enriched diet on adiposity. (**A-D**) Representative images of adipose tissue harvested from 6-month-old WT and 5xFAD mice receiving the standard or the ACE oil-enriched diet. (**E, F**) The adipose tissue was weighed and expressed as absolute weight (**E**) or as a percentage of the body weight (**F**). Data were shown as box plots with minimum to maximum whiskers. Statistical significance was evaluated through two-way ANOVA followed by Tukey's post-hoc multiple comparison test (n = 8 for each experimental group). **** $p < 0.0001$. ACE, Acebuche.

Serum biochemical analyses were conducted to evaluate cholesterol levels (**Figure 20A-C**), as well as the levels of some key hepatic enzymes (**Figure 20D-F**). No significant differences were observed in total cholesterol (**Figure 20A**), LDL (**Figure 20B**), or HDL (**Figure 20C**) levels among the experimental groups. Conversely, serum levels of hepatic enzymes, including ALP (**Figure 20D**), GGT (**Figure 20E**), and GPT (**Figure 20F**), were considerably increased in both 6-month-old WT and 5xFAD mice receiving the ACE oil-enriched diet.

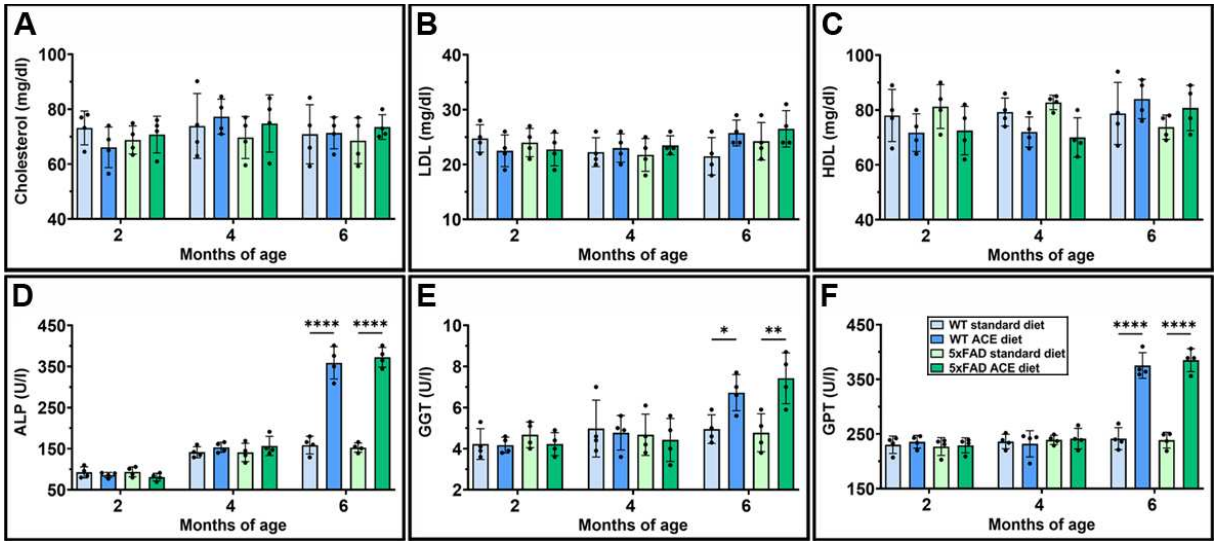

Figure 20. Effects of the ACE oil-enriched diet on serum levels of cholesterol and hepatic enzymes. (**A-F**) Serum levels of total cholesterol (**A**), LDL (**B**), HDL (**C**), ALP (**D**), GGT (**E**), and GPT (**F**) were measured. Data are shown as histogram columns with minimum to maximum whiskers. Statistical significance was evaluated through two-way ANOVA followed by Tukey's post-hoc multiple comparison test (n = 4 for each experimental group). * $p < 0.05$, ** $p < 0.01$ and **** $p < 0.0001$. ACE, Acebuche; LDL, low-density lipoprotein; HDL, high-density lipoprotein; ALP, Alkaline Phosphatase; GGT, Gamma-glutamyl transferase; GPT, Glutamic-Pyruvic Transaminase.

Although no differences in hepatic lipid content were apparently observed in 2- and 4-month-old WT and 5xFAD fed with standard or ACE oil-enriched diet, histological analysis revealed marked lipid accumulation in the liver of 6-month-old animals receiving ACE oil-enriched diet (**Figure 21A-D**). This qualitative data was supported by gravimetric analysis (**Figure 21E**), which confirmed the presence of a higher amount of hepatic lipids in both 6-month-old WT and 5xFAD mice receiving the ACE oil-enriched diet.

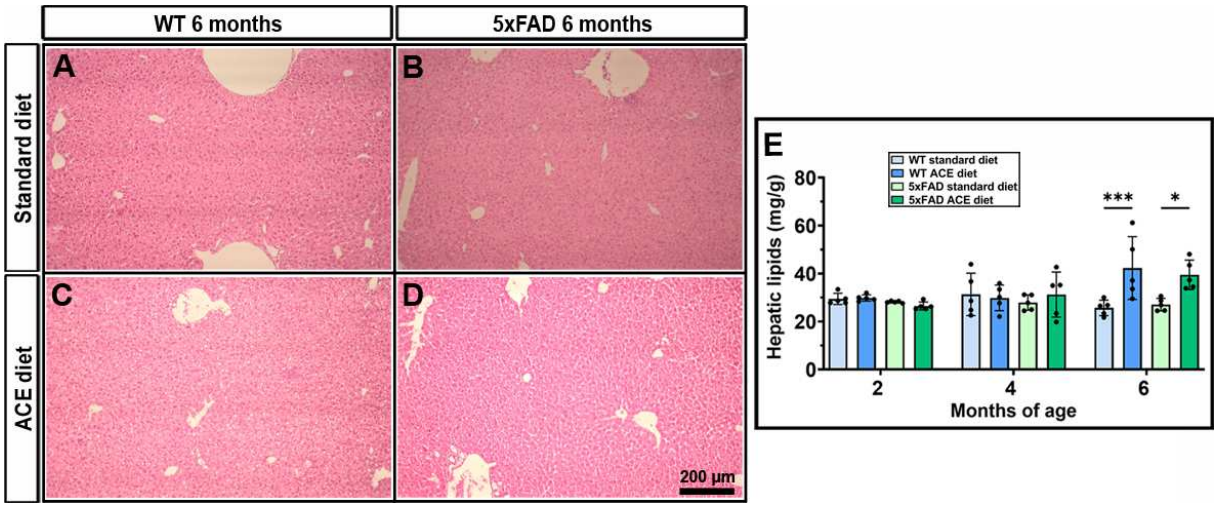

Figure 21. Effects of the ACE oil-enriched diet on hepatic lipid content. (**A-D**) Haematoxylin and eosin staining of liver tissue from 6-month-old WT and 5xFAD mice receiving the standard or the ACE oil-enriched diet. Scale bar, 200 µm. (**E**) Total hepatic lipid content is expressed as milligrams of lipids per gram of tissue. Data are shown as histogram columns with minimum to maximum whiskers. Statistical significance was evaluated through two-way ANOVA followed by Tukey's post-hoc multiple comparison test (n = 5 for each experimental group). * $p < 0.05$ and *** $p < 0.001$. ACE, Acebuche.

4. DISCUSSION

This PhD thesis presents two distinct yet complementary research projects, both rooted in the study of AD using the 5xFAD murine model. While each project focuses on a different anatomical and functional domain, the retina and the cerebral microcirculation, they converge in their aim to elucidate the early pathological mechanisms of AD and explore novel diagnostic and therapeutic strategies.

The first project provides a comprehensive morpho-functional and molecular characterization of the retina in 5xFAD mice, positioning the retina not only as a passive target of neurodegeneration but as a potential site for early AD diagnosis. Our findings indicate profound alterations in retinal function, structure, and molecular signaling, beginning as early as six months of age. Electroretinographic data revealed significant deficits involving both the inner and outer retinal layers, alongside a progressive decline in visual acuity and RGC function (Lynn et al., 2025; McCool et al., 2025; McAnany et al., 2021; Zhang et al., 2021; Lim et al., 2020). Generally, photoreceptor anomalies remain unclear in AD, but a progressive degeneration of rods and cones was reported in some AD murine models, in which impaired expression of phototransduction proteins, photoreceptor morphological alterations, functional deficits, and cell death caused by apoptosis, necroptosis, or senescence were reported (Zhang et al., 2021; Haruta et al., 2009). In line with the alterations evidenced by ERG recordings, here we show that visual acuity in 5xFAD mice progressively fades starting at 6 months, in agreement with previous studies using an optomotor test (Zhang et al., 2021). Our data demonstrate a marked impairment of RGC function in 5xFAD mice starting at 6 months of age, according to previous literature (Araya-Arriagada et al., 2021; Lim et al., 2020). Concurrently, immunofluorescence and OCT analyses showed a significant reduction of RGC number and GCL/RNFL thickness in 5xFAD retinas compared to WT, in accordance with previous findings (Matei et al., 2022; Lim et al., 2020), and the presence of active caspase 3 immunostaining in RGCs of 9-month-old 5xFAD mice suggested RGC death by apoptosis. This is not surprising, since it is widely known that RGCs are heavily affected in different neurodegenerative diseases such as Parkinson's disease, Huntington's disease, and AD, due to the pathological accumulation of α-synuclein, mutant huntingtin, and different Aβ isoforms, respectively (Yang et al., 2024; La Morgia et al., 2017; Normando et al., 2016). APP processing through the amyloidogenic pathway produces different Aβ isoforms. Due to their low solubility, Aβ (1-42) monomers may form high-order assemblies ranging from low molecular weight to midrange- and high-molecular-weight oligomers, fibrils, and senile plaques. Among them, Aβ oligomers seem to be the most toxic form, as they can interact with different types of receptors expressed by neuronal, glial, and endothelial cells, inducing neuroinflammation, oxidative stress, synapse loss, Tau protein hyperphosphorylation, and cell death (Cline et al., 2018; Chen et al., 2017; Gu et al., 2013). In 5xFAD mouse retinas, we identified the presence of extensive Aβ deposits at both 6- and 9-months of age, concurrent with an increase in Aβ (1-42) levels. Although the mechanisms need to be clarified, it has been demonstrated that Aβ may induce neuronal apoptosis both indirectly, triggering neuroinflammatory processes and oxidative stress, or directly altering the levels of some antiapoptotic or proapoptotic factors such as Bcl2 or Bax (Goel et al., 2022; Yao et al., 2005). In this respect, our data show higher levels of neuroinflammation and oxidative stress markers, as well as an increased Bax/Bcl2 ratio in 9-month-old 5xFAD mice, together with the presence

of active caspase-3 immunoreactive profiles mainly localized in the GCL. We cannot exclude RGC loss also due to non-apoptotic cell death mechanisms that are typically present in AD, such as ferroptosis, pyroptosis, or necroptosis (Silva-Llanes et al., 2025; Balusu et al., 2024). Together with neuroinflammation and oxidative stress, we also observed massive microgliosis with evident microglial phenotypical changes, suggesting a shift from a surveillant to an activated state in 5xFAD mouse retinas. This increased microglial reactivity was concurrent with Aβ accumulation. During AD progression, microglial cells may play a dual role, displaying neuroprotective or neurotoxic functions depending on the disease stage and contextual factors (Sun et al., 2024). On the one hand, activated microglial cells may cluster around Aβ deposits, acting positively through the formation of a dense barrier that limits Aβ dissemination or by promoting Aβ phagocytosis and protease release. On the other hand, prolonged microglial activation may lead to chronic neuroinflammation, exacerbating neuronal damage (Baligács et al., 2024; Chen et al., 2022; Hickman et al., 2008). Indeed, the oligomeric forms of Aβ have been shown to interact with various receptors expressed by microglial cells, among which the receptor expressed on myeloid cells 2, the CD36, CD47, the receptor for advanced glycation end-products, and the α-6/β-1 integrin, initiating a signaling cascade that leads to microglial activation with subsequent Aβ phagocytosis and progressive release of pro-inflammatory cytokines and chemokines, such as IL-6 and IL-1β (Cai et al., 2022). Noteworthy, it has been demonstrated recently that Aβ (1-42) may also interact with the Dectin-1 receptor expressed by microglial cells, inducing activation of the NFκB signaling pathway and subsequent expression of pro-inflammatory factors, such as IL-6 (Zhao et al., 2023). Not surprisingly, we also found an evident increase in NFκB phosphorylation and IL-6 levels in 9-month-old 5xFAD mice. The simultaneous presence of Aβ deposits and reactive microglial cells may cause IPL thickening, as observed in 9-month-old 5xFAD mice (Lim et al., 2020), but further evaluation will be necessary. Conversely, no macroglial reactivity was observed in the retina of 5xFAD mice, at variance with previous data reporting an increase of GFAP immunoreactivity (Zhang et al., 2021). While both microgliosis and macrogliosis are associated with the production of an inflammatory milieu in the AD brain (Maggiore et al., 2024), the presence of activated macroglia in the retina is not so obvious. For instance, different studies reported either increased or decreased GFAP immunoreactivity in the retina of AD patients as well as in the retina of mouse models of AD (Palko et al., 2024; Xu et al., 2022; Chidlow et al., 2017; Edwards et al., 2014; Blanks et al., 1996). In addition to Aβ accumulation, we also observed an increase in Tau protein phosphorylation in the retinas of both 6- and 9-month-old 5xFAD mice, which is likely to play a key role in retinal degeneration. Normally, the main biological functions of the Tau protein are associated with self-assembly and stabilization of the microtubule network (Alonso et al., 2018). During AD progression, Tau protein may undergo hyperphosphorylation in the brain and retinal cells, generating toxic oligomeric forms and NFTs, causing microtubule destabilization with subsequent synaptic dysfunction and neuronal death (Davis et al., 2025). Tau protein pathology is closely related to neuroinflammation, considering that sustained and increased neuronal and glial inflammatory responses may exacerbate the Tau protein pathology, which further aggravates the inflammatory process (Chen et al., 2023). The pTau intracellular accumulation may induce activation of the NFκB pathway and subsequent release of pro-inflammatory cytokines, which, in turn,

stimulate microglia activation, leading to a further increase of inflammation and cell death (Dong et al., 2022). The present literature indicates that miRNAs play a key role in the regulation of several genes involved in AD. In this regard, murine models represent an effective tool both to validate miRNA targets in vivo and to provide relevant information about the role of specific miRNA-dependent gene pathways in AD (Wang et al., 2019; Delay et al., 2011). Numerous studies on murine models of AD identified and validated different dysregulated miRNAs involved in Aβ accumulation, Tau protein phosphorylation, neuroinflammation, neuronal apoptosis, neurogenesis, cognitive function, mitochondrial dynamics, and synapse activity (Li et al., 2024; Barros-Viegas et al., 2020; Wang et al., 2019; Delay et al., 2011). Our contribution regarded the identification of two dysregulated miRNAs in the 5xFAD retinas, miR-3968 and miR-124-5p. These miRNAs are implicated in biological processes such as apoptosis, inflammation, photoreceptoral differentiation, as well as neuronal and synaptic function. For instance, miR-124 has been identified as a negative regulator of both NF-kB (Jeong et al., 2015) and Bax (Xu et al., 2019) expression, while miR-3968 downregulation has been reported to be associated with inflammatory responses (Mahajan et al., 2024), suggesting that the downregulation of these miRNAs in the 5xFAD retina may be directly linked to increased neuroinflammation and apoptosis. MiR-3968 and miR-124-5p are also known to be correlated to AD, as miR-124 acts by regulating the activity of BACE and subsequent Aβ burden, while miR-3968 was associated with the presence of NFT, synaptic dysfunction, and memory loss (Counts et al., 2025; Hatzimanolis et al., 2025; Wang et al., 2023; Ouyang et al., 2022; An et al., 2017). Consistent with the present findings, miR-124 has been reported to be downregulated in both in vitro and in vivo models of AD (Al-Sawasany et al., 2025; An et al., 2017), while miR-3968 was downregulated in the APP/PS1 mouse model (Wang et al., 2023).

The second project shifts focus to the cerebral microcirculation, providing a detailed profile of the main brain molecular features of the 5xFAD murine model, as well as new evidence supporting the protective effect of ACE oil against AD-related neurovascular and molecular changes. Under physiological conditions, the proper functioning of cerebral vasculature plays a pivotal role in maintaining CNS homeostasis by supplying oxygen and nutrients to the brain, removing metabolic waste products, and regulating the exchange of cells and a wide range of molecules between the intravascular space, interstitial compartment, and cerebrospinal fluid (Eisenmenger et al., 2023; Braun and Iliff, 2020). A growing body of evidence suggests that cerebrovascular dysfunction is a key factor in the development of various neurodegenerative disorders, including Parkinson's disease, Huntington's disease, amyotrophic lateral sclerosis, multiple sclerosis, spinocerebellar ataxias, and AD (Garcia and Heiman, 2025; Sweeney et al., 2018). In line with this, fluorescence microscopy analyses reveal clear morpho-functional impairments in the cerebral pial microcirculation of 5xFAD mice as early as 2 months of age, consistent with current literature (Jullienne et al., 2023; Szu and Obenaus, 2021; Anh et al., 2018; Giannoni et al., 2016; Kook et al., 2012). These vascular abnormalities are characterized by reduced arteriolar density and pronounced vascular tortuosity, along with the presence of aberrant arteriovenous anastomoses, perfused capillary rarefaction, and increased microvascular permeability, hallmark signs of compromised brain circulation and early loss of neurovascular homeostasis. In addition to the observed cerebrovascular changes, 5xFAD mice show lower levels of claudin-5 at both 4 and 6 months of age compared

to age-matched WT controls. Claudin-5, one of the most abundantly expressed tight junction proteins in the CNS, is widely recognized as a core regulator of BBB integrity (Jia et al., 2025; Vázquez-Liébanas et al., 2024; Zhu et al., 2022; Greene et al., 2019). Its deficiency has been strongly associated with increased BBB permeability and heightened vulnerability to circulating neurotoxic substances, contributing to neurodegenerative disease progression such as AD (Greene et al., 2019). Consistent with our observations, reduced levels of claudin-5 have already been reported in various cerebral regions of some murine models of AD (Shibly et al., 2024; Wang et al., 2022; Zhu et al., 2022) and in the post-mortem brains of AD patients (Yamazaki et al., 2019). Alongside claudin-5, other critical tight junction components, such as occludin and ZO-1, also play important roles in maintaining the BBB structure and function (Sugiyama et al., 2023; Liu et al., 2012). However, no significant differences in occludin and ZO-1 levels can be observed in 5xFAD mice at the examined time points, suggesting that BBB dysfunction and consequent increased microvascular permeability may be primarily driven by claudin-5 downregulation during early disease stages. This aligns with existing literature, which reports that 5xFAD mice show decreased levels of occludin and ZO-1 starting from 9-12 months of age (Jullienne et al., 2023; Anh et al., 2018). Besides that, increased brain levels of HIF-1α and VEGF-A can be observed starting from 2 months, indicating the presence of hypoxic conditions, a well-recognized feature of AD pathology typically resulting from vascular dysfunction and impaired oxygen delivery (Tao et al., 2024; Villareal et al., 2016; Daulatzai, 2010). Particularly, hypoxia exerts a dual role. In the early phases of AD, it promotes the stabilization of HIF-1α that allows the transcriptional activity of HIF-1, which subsequently induces VEGF-A expression as part of a protective compensatory mechanism aimed at restoring oxygen homeostasis and stimulating angiogenesis (Lin et al., 2024). The long-lasting activation of these factors becomes detrimental, leading to the development of inflammatory processes and neurovascular alterations (Choi, 2024; Grammas et al., 2011). HIF-1 has also been reported to downregulate Aβ-degrading enzymes and concurrently stimulate BACE and γ-secretase enzymatic complex activity, thereby exacerbating Aβ accumulation and accelerating AD progression (Bonnar et al., 2025; Choi et al., 2024; Lynch et al., 2022; Salminen et al., 2016; Zhang and Le, 2010; Weller et al., 2008). Some of the main catabolic enzymes involved in Aβ degradation include IDE and CD10 (Chen et al., 2017). On the one hand, CD10 is a membrane-bound endopeptidase predominantly localized on the neuronal surface, especially in pre- and post-synaptic terminal regions (Morito et al., 2025; Zhou et al., 2017), while IDE is a zinc-binding metalloprotease mainly expressed in the cytosol of neurons and glial cells (Corraliza-Gomez et al., 2023). Our data highlight a marked reduction of both CD10 and IDE expression in 5xFAD mice starting from 4 months of age, suggesting their potential involvement in the progression of the disease. Consistent with these findings, many studies have reported that reduced levels of CD10 are likely a primary cause of AD (Sasaguri et al., 2021), while the role of IDE remains less well-defined, even if a progressive increment of Aβ accompanied by spatial and memory deficits was found in mice having a deficiency of IDE, underscoring its importance in AD pathogenesis (Corraliza-Gomez et al., 2023; Farris et al., 2003; Miller et al., 2003). As expected, the simultaneous presence of hypoxia, along with decreased levels of CD10 and IDE, coincides with increased cerebral Aβ levels. Particularly, ELISA assays and ThS staining, a method using a non-specific fluorescent probe commonly used to detect Aβ deposits

(MacKeigan et al., 2023; Urbanc et al., 2002), reveal increasing levels of Aβ (1-40) and Aβ (1-42) isoforms in 5xFAD mice starting from 4 months. The appearance of Aβ deposits occurs later than the onset of vascular damage, aligning with the widely supported "two-hit vascular hypothesis", which proposes a 2-step positive feedback loop in which an initial vascular insult compromises BBB integrity and Aβ clearance mechanisms, thereby creating a permissive environment for subsequent Aβ accumulation and neurodegeneration (Eisenmenger et al., 2023; Solis et al., 2021; Nelson et al., 2016). As they accumulate in the brain, numerous Aβ isoforms of varying molecular size and solubility can aggregate into a variety of assemblies, including oligomers, fibrils, and plaques, each with distinct structural and pathological properties (Chen et al., 2017). Specifically, Aβ oligomers can interact with a wide range of receptors expressed by neurons and glial cells, thereby triggering neuroinflammatory phenomena, gliosis, synaptic dysfunction, and neuronal death (Fanlo-Ucar et al., 2024; Chen et al., 2017). Furthermore, Aβ accumulation in the perivascular spaces can result in a gradual narrowing of the vascular lumen, ultimately leading to hypoxia and activation of HIF-1, which further exacerbates the neuroinflammatory response and contributes to subsequent vascular damage (Hai et al., 2024; Jung et al., 2023). A fundamental role in the development of AD-related neuroinflammatory processes is played by the transcription factor NF-κB, which orchestrates the expression of a wide range of pro-inflammatory mediators in response to pathological stimuli, including Aβ peptide (Sun et al., 2022; Chen et al., 2017). Moreover, NF-κB can transcriptionally regulate BACE expression, thus affecting the amyloidogenic pathway and subsequent cerebral Aβ accumulation (Lazic et al., 2019; Chami and Checler, 2012; Chen et al., 2012). Not by chance, the ratio pNF-κB/NF-κB, along with the expression of IL-6 and iNOS, was increased in 4- and 6-month-old 5xFAD mice compared with the age-matched WT controls, supporting previous observations reported in AD models (Lindsay et al., 2021; Wang et al., 2019; Lazic et al., 2019; Colton et al., 2006). The progressive formation of Aβ deposits in the brain may also promote the recruitment and consequent activation of astrocytes and microglia (Fanlo-Ucar et al., 2024). In the early stages of AD, glial reactivity plays a protective role by enhancing receptor-mediated phagocytosis of Aβ. However, chronic activation leads to an impaired phagocytic capacity, accompanied by a shift toward a pro-inflammatory phenotype, contributing to neuroinflammation, synaptic dysfunction, and cognitive deficits (Yu et al., 2024; Fanlo-Ucar et al., 2024; Uddin and Lim, 2022). Consistent with current literature (Jung-Shin et al., 2024; Ko et al., 2024; Angeli et al., 2020), beyond the neuroinflammatory milieu, an increased expression of GFAP and Iba1 can be observed in 5xFAD mice starting from 4 months of age, reflecting astrogliosis and microglial reactivity, respectively. As expected, the concomitant presence of an altered microvascular network and marked molecular alterations led to the progressive memory loss starting from 4-month-old 5xFAD mice compared with age-matched WT controls, confirming the findings of previous studies (Sánchez et al., 2023; Zhang et al., 2021; Li et al., 2021). Besides drug therapies and genetic approaches (Tartaglia and Ingelsson, 2024; Peng et al., 2023; Van Dyck et al., 2022; Chen et al., 2017), a growing body of evidence suggests that regular consumption of foods rich in anti-inflammatory compounds, antioxidants, B-group vitamins, and polyunsaturated fatty acids, such as EVOO, may exert beneficial effects in slowing down AD progression (Kaddoumi et al., 2022; Lauretti et al., 2017; Qosa et al., 2015). The administration of an enriched diet of ACE oil, well-known for its neuroprotective

properties (Lucchesi et al., 2024; Santana-Garrido et al., 2024), effectively prevents the onset of cerebral microcirculatory abnormalities in 5xFAD mice as early as 2 months of age, by preserving a microvascular architecture and function comparable to age-matched WT controls. ACE oil also significantly alleviates the hypoxic condition observed in 5xFAD mice by suppressing the upregulation of HIF-1α and VEGF-A. Moreover, 5xFAD mice receiving ACE oil exhibit levels of claudin-5, CD10, and IDE similar to WT controls, along with a marked reduction of brain Aβ and neuroinflammatory markers. A significant improvement in cognitive function can also be observed starting from 4 months of age. Despite ACE oil administration conferring a marked protection against early neurovascular and molecular alterations, its efficacy is reduced at 6 months, being ACE oil still capable of preventing some AD-related brain alterations but not others. The reduced effectiveness of the ACE oil coincides with increased body weight, total adipose tissue, and hepatic lipid content, along with higher serum levels of some liver functionality-related enzymes, suggesting that the development of a systemic dysmetabolic state characterized by hepatic steatosis may have overridden the initial protective effects of ACE oil. In this respect, metabolic imbalance in the liver has been associated with AD (Song et al., 2025), indicating that alterations of the liver-brain crosstalk may play a role in AD pathogenesis. In addition, mice with hepatic steatosis show an increased accumulation of APP in the liver that decreases the scavenging action of the liver towards Aβ, potentially enhancing Aβ accumulation in the periphery, including the brain, thus promoting AD (Garcia et al., 2022). However, the hepatic damage may not be the only explanation for the reduced effectiveness of the diet at 6 months. Indeed, this may also be related to the fact that the 5xFAD mouse, carrying 5 AD-linked mutations, is a model with a rapid onset of AD phenotype, in particular when compared with other mouse models of AD (Zhong et al., 2024). Therefore, it is plausible that the anti-inflammatory components of the ACE oil may face such a high burden of metabolic stress that they lose efficacy after months of administration. Although this hypothesis needs to be verified, for instance, using a model with a milder AD-related phenotype, the present findings are proof of concept that the introduction in the diet of an EVOO rich in anti-inflammatory components may be protective against AD-related damage. On the other hand, the metabolic imbalance after months of the ACE oil-enriched diet was expected since the lipid content of the standard diet is roughly 6% whereas the content in the ACE oil-enriched diet is about 17%. In a translational perspective, therefore, to maintain long-term efficacy of the diet, alternative strategies could be based on a reduced dietary concentration of ACE oil that would make long-term dietary treatments feasible.

Collectively, these two projects underscore the multifaceted nature of AD, highlighting both retinal and cerebrovascular compartments as early and vulnerable targets of AD pathology. The findings support the use of the retina as a surrogate site for early diagnosis and molecular monitoring and emphasize the cerebral microcirculation as a therapeutic target for intervention. While distinct in anatomical focus, both studies reveal common pathological mechanisms, including Aβ accumulation, inflammatory activation, and gliosis, reinforcing the systemic and interconnected character of AD. Moreover, both projects explore non-invasive or minimally invasive approaches, retinal biomarkers, and nutritional therapy, offering promising avenues for early diagnosis and prevention in translational contexts. Ultimately, this thesis contributes novel insights into

the pathophysiology of AD and opens new perspectives for integrated, multi-targeted strategies in the fight against neurodegeneration.

5. CONCLUSION

In conclusion, the two research projects presented in this doctoral thesis provide complementary insights into the early AD pathological mechanisms, emphasizing the importance of adopting a systemic, multi-organ approach in the study of neurodegeneration. The retinal investigation confirmed that the eye, and in particular the retina, can serve as a sensitive and accessible site for detecting early AD-related changes. The functional, structural, and molecular alterations observed in the 5xFAD retina, including Aβ and pTau accumulation, RGC degeneration, microgliosis, and miRNA dysregulation, reflect key hallmarks of AD and open new perspectives for the development of non-invasive retinal biomarkers for early diagnosis and disease monitoring. At the same time, the study of cerebral microcirculation revealed that vascular dysfunction is not merely a secondary consequence but rather an early and active contributor to AD pathogenesis. The identification of BBB disruption, hypoxia, impaired Aβ clearance, and inflammatory activation at early time points reinforces the "two-hit vascular hypothesis", as well as the critical role of the vascular system as a target in both pathophysiological research and treatment development. Notably, the protective effect of ACE oil supplementation highlights the therapeutic potential of nutritional interventions targeting vascular and inflammatory pathways in the early phases of AD. While some limitations related to metabolic side effects emerged over time, these findings provide a valuable proof of concept and encourage further research into personalized and balanced nutritional approaches to support brain health.

Taken together, these two projects converge on several central themes, including Aβ toxicity, neuroinflammation, and cell death, demonstrating how different biological systems, such as the retina and brain vasculature, can be interrogated in parallel to better understand the complexity of AD. This integrated approach not only broadens our understanding of disease mechanisms but also lays the groundwork for multifactorial strategies aimed at early detection, prevention, and intervention. Moving forward, further studies are needed to explore the temporal relationship between retinal and cerebral changes, to validate retinal biomarkers in translational settings, and to refine nutritional strategies that can offer long-term neuroprotection without systemic metabolic burden. Nonetheless, the present findings significantly advance the field and contribute to a more comprehensive understanding of AD.

6. REFERENCES

- A Armstrong R. Risk factors for Alzheimer's disease. Folia Neuropathol. 2019;57(2):87-105. doi: 10.5114/fn.2019.85929. PMID: 31556570.
- Afford S, Randhawa S. Apoptosis. Mol Pathol. 2000 Apr;53(2):55-63. doi: 10.1136/mp.53.2.55. PMID: 10889903; PMCID: PMC1186906.
- Ahn KC, Learman CR, Dunbar GL, Maiti P, Jang WC, Cha HC, Song MS. Characterization of Impaired Cerebrovascular Structure in APP/PS1 Mouse Brains. Neuroscience. 2018 Aug 10;385:246-254. doi: 10.1016/j.neuroscience.2018.05.002. Epub 2018 May 17. PMID: 29777753.
- Ahn KC, Learman CR, Dunbar GL, Maiti P, Jang WC, Cha HC, Song MS. Characterization of Impaired Cerebrovascular Structure in APP/PS1 Mouse Brains. Neuroscience. 2018 Aug 10;385:246-254. doi: 10.1016/j.neuroscience.2018.05.002. Epub 2018 May 17. PMID: 29777753.
- Akiyama H, Barger S, Barnum S, Bradt B, Bauer J, Cole GM, Cooper NR, Eikelenboom P, Emmerling M, Fiebich BL, Finch CE, Frautschy S, Griffin WS, Hampel H, Hull M, Landreth G, Lue L, Mrak R, Mackenzie IR, McGeer PL, O'Banion MK, Pachter J, Pasinetti G, Plata-Salaman C, Rogers J, Rydel R, Shen Y, Streit W, Strohmeyer R, Tooyoma I, Van Muiswinkel FL, Veerhuis R, Walker D, Webster S, Wegrzyniak B, Wenk G, Wyss-Coray T. Inflammation and Alzheimer's disease. Neurobiol Aging. 2000 May-Jun;21(3):383-421. doi: 10.1016/s0197-4580(00)00124-x. PMID: 10858586; PMCID: PMC3887148.
- Al Rihani SB, Darakjian LI, Kaddoumi A. Oleocanthal-Rich Extra-Virgin Olive Oil Restores the Blood-Brain Barrier Function through NLRP3 Inflammasome Inhibition Simultaneously with Autophagy Induction in TgSwDI Mice. ACS Chem Neurosci. 2019 Aug 21;10(8):3543-3554. doi: 10.1021/acschemneuro.9b00175. Epub 2019 Jun 25. PMID: 31244050; PMCID: PMC6703911.
- Alkhalifa AE, Al-Ghraiybah NF, Kaddoumi A. Extra-Virgin Olive Oil in Alzheimer's Disease: A Comprehensive Review of Cellular, Animal, and Clinical Studies. Int J Mol Sci. 2024 Feb 5;25(3):1914. doi: 10.3390/ijms25031914. PMID: 38339193; PMCID: PMC10856527.
- Alonso AD, Cohen LS, Corbo C, Morozova V, ElIdrissi A, Phillips G, Kleiman FE. Hyperphosphorylation of Tau Associates With Changes in Its Function Beyond Microtubule Stability. Front Cell Neurosci. 2018 Oct 9;12:338. doi: 10.3389/fncel.2018.00338. PMID: 30356756; PMCID: PMC6189415.
- Al-Sawasany AS, Fayed HM, Mahmoud BF, Elblehi SS, Ghazal NA. Evaluation of the Neurotherapeutic Effect of Quercetin on Neuronal miR-124 and β-Site Amyloid Precursor Protein Cleaving Enzyme 1 (BACE1) in an Experimental Alzheimer's Disease Model. J Biochem Mol Toxicol. 2025 May;39(5):e70290. doi: 10.1002/jbt.70290. PMID: 40341631.
- An F, Gong G, Wang Y, Bian M, Yu L, Wei C. MiR-124 acts as a target for Alzheimer's disease by regulating BACE1. Oncotarget. 2017 Dec 9;8(69):114065-114071. doi: 10.18632/oncotarget.23119. Erratum in: Oncotarget. 2018 May 15;9(37):24871. doi: 10.18632/oncotarget.25461. PMID: 29371969; PMCID: PMC5768386.

- An F, Gong G, Wang Y, Bian M, Yu L, Wei C. MiR-124 acts as a target for Alzheimer's disease by regulating BACE1. Oncotarget. 2017 Dec 9;8(69):114065-114071. doi: 10.18632/oncotarget.23119. Erratum in: Oncotarget. 2018 May 15;9(37):24871. doi: 10.18632/oncotarget.25461. PMID: 29371969; PMCID: PMC5768386.
- Anderton BH, Betts J, Blackstock WP, Brion JP, Chapman S, Connell J, Dayanandan R, Gallo JM, Gibb G, Hanger DP, Hutton M, Kardalinou E, Leroy K, Lovestone S, Mack T, Reynolds CH, Van Slegtenhorst M. Sites of phosphorylation in tau and factors affecting their regulation. Biochem Soc Symp. 2001;(67):73-80. doi: 10.1042/bss0670073. PMID: 11447841.
- Angeli S, Kousiappa I, Stavrou M, Sargiannidou I, Georgiou E, Papacostas SS, Kleopa KA. Altered Expression of Glial Gap Junction Proteins Cx43, Cx30, and Cx47 in the 5XFAD Model of Alzheimer's Disease. Front Neurosci. 2020 Oct 7;14:582934. doi: 10.3389/fnins.2020.582934. PMID: 33117125; PMCID: PMC7575794.
- Angeloni C, Malaguti M, Barbalace MC, Hrelia S. Bioactivity of Olive Oil Phenols in Neuroprotection. Int J Mol Sci. 2017 Oct 25;18(11):2230. doi: 10.3390/ijms18112230. PMID: 29068387; PMCID: PMC5713200.
- Araya-Arriagada J, Bello F, Shivashankar G, Neira D, Durán-Aniotz C, Acosta ML, Escobar MJ, Hetz C, Chacón M, Palacios AG. Retinal Ganglion Cells Functional Changes in a Mouse Model of Alzheimer's Disease Are Linked with Neurotransmitter Alterations. J Alzheimers Dis. 2021;82(s1):S5-S18. doi: 10.3233/JAD-201195. PMID: 33749647.
- Ashraf G, McGuinness M, Khan MA, Obtinalla C, Hadoux X, van Wijngaarden P. Retinal imaging biomarkers of Alzheimer's disease: A systematic review and meta-analysis of studies using brain amyloid beta status for case definition. Alzheimers Dement (Amst). 2023 May 25;15(2):e12421. doi: 10.1002/dad2.12421. PMID: 37250908; PMCID: PMC10210353.
- Attems J, Jellinger KA. The overlap between vascular disease and Alzheimer's disease--lessons from pathology. BMC Med. 2014 Nov 11;12:206. doi: 10.1186/s12916-014-0206-2. PMID: 25385447; PMCID: PMC4226890.
- Baligács N, Albertini G, Borrie SC, Serneels L, Pridans C, Balusu S, De Strooper B. Homeostatic microglia initially seed and activated microglia later reshape amyloid plaques in Alzheimer's Disease. Nat Commun. 2024 Dec 5;15(1):10634. doi: 10.1038/s41467-024-54779-w. PMID: 39639016; PMCID: PMC11621353.
- Balusu S, De Strooper B. The necroptosis cell death pathway drives neurodegeneration in Alzheimer's disease. Acta Neuropathol. 2024 Jun 9;147(1):96. doi: 10.1007/s00401-024-02747-5. PMID: 38852117; PMCID: PMC11162975.
- Bandyopadhyay S, Goldstein LE, Lahiri DK, Rogers JT. Role of the APP non-amyloidogenic signaling pathway and targeting alpha-secretase as an alternative drug target for treatment of Alzheimer's disease. Curr Med Chem. 2007;14(27):2848-64. doi: 10.2174/092986707782360060. PMID: 18045131.

- Bär T. The vascular system of the cerebral cortex. Adv Anat Embryol Cell Biol. 1980;59:I-VI,1-62. doi: 10.1007/978-3-642-67432-7. PMID: 6996438.
- Barnham KJ, Masters CL, Bush AI. Neurodegenerative diseases and oxidative stress. Nat Rev Drug Discov. 2004 Mar;3(3):205-14. doi: 10.1038/nrd1330. PMID: 15031734.
- Barros-Viegas AT, Carmona V, Ferreiro E, Guedes J, Cardoso AM, Cunha P, Pereira de Almeida L, Resende de Oliveira C, Pedro de Magalhães J, Peça J, Cardoso AL. miRNA-31 Improves Cognition and Abolishes Amyloid-β Pathology by Targeting APP and BACE1 in an Animal Model of Alzheimer's Disease. Mol Ther Nucleic Acids. 2020 Mar 6;19:1219-1236. doi: 10.1016/j.omtn.2020.01.010. Epub 2020 Jan 17. PMID: 32069773; PMCID: PMC7031139.
- Basinger H, Hogg JP. Neuroanatomy, Brainstem. 2023 Jul 4. In: StatPearls [Internet]. Treasure Island (FL): StatPearls Publishing; 2025 Jan–. PMID: 31335017.
- Batarseh YS, Kaddoumi A. Oleocanthal-rich extra-virgin olive oil enhances donepezil effect by reducing amyloid-β load and related toxicity in a mouse model of Alzheimer's disease. J Nutr Biochem. 2018 May;55:113-123. doi: 10.1016/j.jnutbio.2017.12.006. Epub 2017 Dec 27. PMID: 29413486; PMCID: PMC5936648.
- Bayir H. Reactive oxygen species. Crit Care Med. 2005 Dec;33(12 Suppl):S498-501. doi: 10.1097/01.ccm.0000186787.64500.12. PMID: 16340433.
- Bishop GM, Robinson SR. Physiological roles of amyloid-beta and implications for its removal in Alzheimer's disease. Drugs Aging. 2004;21(10):621-30. doi: 10.2165/00002512-200421100-00001. PMID: 15287821.
- Blanks JC, Torigoe Y, Hinton DR, Blanks RH. Retinal pathology in Alzheimer's disease. I. Ganglion cell loss in foveal/parafoveal retina. Neurobiol Aging. 1996 May-Jun;17(3):377-84. doi: 10.1016/0197-4580(96)00010-3. PMID: 8725899.
- Bonnar O, Eyre B, van Veluw SJ. Perivascular brain clearance as a therapeutic target in cerebral amyloid angiopathy and Alzheimer's disease. Neurotherapeutics. 2025 Apr;22(3):e00535. doi: 10.1016/j.neurot.2025.e00535. Epub 2025 Jan 30. PMID: 39890534; PMCID: PMC12047398.
- Botella Lucena P, Heneka MT. Inflammatory aspects of Alzheimer's disease. Acta Neuropathol. 2024 Aug 28;148(1):31. doi: 10.1007/s00401-024-02790-2. PMID: 39196440.
- Braun M, Iliff JJ. The impact of neurovascular, blood-brain barrier, and glymphatic dysfunction in neurodegenerative and metabolic diseases. Int Rev Neurobiol. 2020;154:413-436. doi: 10.1016/bs.irn.2020.02.006. Epub 2020 Jul 14. PMID: 32739013.
- Brunden KR, Zhang B, Carroll J, Yao Y, Potuzak JS, Hogan AM, Iba M, James MJ, Xie SX, Ballatore C, Smith AB 3rd, Lee VM, Trojanowski JQ. Epothilone D improves microtubule density, axonal integrity, and cognition in a transgenic mouse model of tauopathy. J Neurosci. 2010 Oct 13;30(41):13861-6. doi: 10.1523/JNEUROSCI.3059-10.2010. PMID: 20943926; PMCID: PMC2958430.
- Butterfield DA, Lauderback CM. Lipid peroxidation and protein oxidation in Alzheimer's disease brain: potential causes and consequences involving amyloid beta-peptide-associated free radical oxidative stress.

Free Radic Biol Med. 2002 Jun 1;32(11):1050-60. doi: 10.1016/s0891-5849(02)00794-3. PMID: 12031889.

- Cai Y, Liu J, Wang B, Sun M, Yang H. Microglia in the Neuroinflammatory Pathogenesis of Alzheimer's Disease and Related Therapeutic Targets. Front Immunol. 2022 Apr 26;13:856376. doi: 10.3389/fimmu.2022.856376. PMID: 35558075; PMCID: PMC9086828.
- Carelli V, La Morgia C, Valentino ML, Barboni P, Ross-Cisneros FN, Sadun AA. Retinal ganglion cell neurodegeneration in mitochondrial inherited disorders. Biochim Biophys Acta. 2009 May;1787(5):518-28. doi: 10.1016/j.bbabio.2009.02.024. Epub 2009 Mar 5. PMID: 19268652.
- Carey MR. The cerebellum. Curr Biol. 2024 Jan 8;34(1):R7-R11. doi: 10.1016/j.cub.2023.11.048. PMID: 38194930.
- Chami L, Checler F. BACE1 is at the crossroad of a toxic vicious cycle involving cellular stress and β-amyloid production in Alzheimer's disease. Mol Neurodegener. 2012 Oct 5;7:52. doi: 10.1186/1750-1326-7-52. PMID: 23039869; PMCID: PMC3507664.
- Chandra S, Sisodia SS, Vassar RJ. The gut microbiome in Alzheimer's disease: what we know and what remains to be explored. Mol Neurodegener. 2023 Feb 1;18(1):9. doi: 10.1186/s13024-023-00595-7. PMID: 36721148; PMCID: PMC9889249.
- Cheignon C, Tomas M, Bonnefont-Rousselot D, Faller P, Hureau C, Collin F. Oxidative stress and the amyloid beta peptide in Alzheimer's disease. Redox Biol. 2018 Apr;14:450-464. doi: 10.1016/j.redox.2017.10.014. Epub 2017 Oct 18. PMID: 29080524; PMCID: PMC5680523.
- Chen CH, Zhou W, Liu S, Deng Y, Cai F, Tone M, Tone Y, Tong Y, Song W. Increased NF-κB signalling up-regulates BACE1 expression and its therapeutic potential in Alzheimer's disease. Int J Neuropsychopharmacol. 2012 Feb;15(1):77-90. doi: 10.1017/S1461145711000149. Epub 2011 Feb 18. PMID: 21329555.
- Chen GF, Xu TH, Yan Y, Zhou YR, Jiang Y, Melcher K, Xu HE. Amyloid beta: structure, biology and structure-based therapeutic development. Acta Pharmacol Sin. 2017 Sep;38(9):1205-1235. doi: 10.1038/aps.2017.28. Epub 2017 Jul 17. PMID: 28713158; PMCID: PMC5589967.
- Chen GF, Xu TH, Yan Y, Zhou YR, Jiang Y, Melcher K, Xu HE. Amyloid beta: structure, biology and structure-based therapeutic development. Acta Pharmacol Sin. 2017 Sep;38(9):1205-1235. doi: 10.1038/aps.2017.28. Epub 2017 Jul 17. PMID: 28713158; PMCID: PMC5589967.
- Chen Y, Xia Q, Zeng Y, Zhang Y, Zhang M. Regulations of Retinal Inflammation: Focusing on Müller Glia. Front Cell Dev Biol. 2022 Apr 27;10:898652. doi: 10.3389/fcell.2022.898652. PMID: 35573676; PMCID: PMC9091449.
- Cheng Y, He CY, Tian DY, Chen SH, Ren JR, Sun HL, Xu MY, Tan CR, Fan DY, Jian JM, Sun PY, Zeng GH, Shen YY, Shi AY, Jin WS, Bu XL, Liu HM, Xu YM, Wang J, Wang YJ. Physiological β-amyloid clearance by the liver and its therapeutic potential for Alzheimer's disease. Acta Neuropathol. 2023 Jun;145(6):717-731. doi: 10.1007/s00401-023-02559-z. Epub 2023 Mar 25. PMID: 36964213.

- Chidlow G, Wood JP, Manavis J, Finnie J, Casson RJ. Investigations into Retinal Pathology in the Early Stages of a Mouse Model of Alzheimer's Disease. J Alzheimers Dis. 2017;56(2):655-675. doi: 10.3233/JAD-160823. PMID: 28035930; PMCID: PMC5271427.
- Choi YK. Detrimental Roles of Hypoxia-Inducible Factor-1α in Severe Hypoxic Brain Diseases. Int J Mol Sci. 2024 Apr 18;25(8):4465. doi: 10.3390/ijms25084465. PMID: 38674050; PMCID: PMC11050730.
- Chong ZZ, Lin SH, Li F, Maiese K. The sirtuin inhibitor nicotinamide enhances neuronal cell survival during acute anoxic injury through AKT, BAD, PARP, and mitochondrial associated "anti-apoptotic" pathways. Curr Neurovasc Res. 2005 Oct;2(4):271-85. doi: 10.2174/156720205774322584. PMID: 16181120; PMCID: PMC1986682.
- Chwalisz BK. Cerebral amyloid angiopathy and related inflammatory disorders. J Neurol Sci. 2021 May 15;424:117425. doi: 10.1016/j.jns.2021.117425. Epub 2021 Mar 27. PMID: 33840507.
- Claassen JA. New cardiovascular targets to prevent late onset Alzheimer disease. Eur J Pharmacol. 2015 Sep 15;763(Pt A):131-4. doi: 10.1016/j.ejphar.2015.05.022. Epub 2015 May 15. PMID: 25987416.
- Cline EN, Bicca MA, Viola KL, Klein WL. The Amyloid-β Oligomer Hypothesis: Beginning of the Third Decade. J Alzheimers Dis. 2018;64(s1):S567-S610. doi: 10.3233/JAD-179941. PMID: 29843241; PMCID: PMC6004937.
- Cobley JN, Fiorello ML, Bailey DM. 13 reasons why the brain is susceptible to oxidative stress. Redox Biol. 2018 May;15:490-503. doi: 10.1016/j.redox.2018.01.008. Epub 2018 Feb 3. PMID: 29413961; PMCID: PMC5881419.
- Colton CA, Vitek MP, Wink DA, Xu Q, Cantillana V, Previti ML, Van Nostrand WE, Weinberg JB, Dawson H. NO synthase 2 (NOS2) deletion promotes multiple pathologies in a mouse model of Alzheimer's disease. Proc Natl Acad Sci U S A. 2006 Aug 22;103(34):12867-72. doi: 10.1073/pnas.0601075103. Epub 2006 Aug 14. Erratum in: Proc Natl Acad Sci U S A. 2006 Oct 10;103(41):15273. Weinberg, B [corrected to Weinberg, JB]. PMID: 16908860; PMCID: PMC1550768.
- Coronel R, Bernabeu-Zornoza A, Palmer C, Muñiz-Moreno M, Zambrano A, Cano E, Liste I. Role of Amyloid Precursor Protein (APP) and Its Derivatives in the Biology and Cell Fate Specification of Neural Stem Cells. Mol Neurobiol. 2018 Sep;55(9):7107-7117. doi: 10.1007/s12035-018-0914-2. Epub 2018 Jan 30. PMID: 29383688.
- Corraliza-Gomez M, Bermejo T, Lilue J, Rodriguez-Iglesias N, Valero J, Cozar-Castellano I, Arranz E, Sanchez D, Ganfornina MD. Insulin-degrading enzyme (IDE) as a modulator of microglial phenotypes in the context of Alzheimer's disease and brain aging. J Neuroinflammation. 2023 Oct 11;20(1):233. doi: 10.1186/s12974-023-02914-7. PMID: 37817156; PMCID: PMC10566021.
- Corsi F, Galante A, Maggi MA, Mazziotti R, Bisti S, Piano I, Gargini C. The efficacy of Saffron Repron® in counteracting the progression of retinitis pigmentosa: Neuroprotection and resilience. Asia Pac J Ophthalmol (Phila). 2025 May-Jun;14(3):100192. doi: 10.1016/j.apjo.2025.100192. Epub 2025 Mar 22. PMID: 40122468.

- Counts SE, Beck JS, Maloney B, Malek-Ahmadi M, Ginsberg SD, Mufson EJ, Lahiri DK. Posterior cingulate cortex microRNA dysregulation differentiates cognitive resilience, mild cognitive impairment, and Alzheimer's disease. Alzheimers Dement. 2025 Feb;21(2):e70019. doi: 10.1002/alz.70019. PMID: 40008917; PMCID: PMC11863362.
- Cvenkel B, Sustar M, Perovšek D. Ganglion cell loss in early glaucoma, as assessed by photopic negative response, pattern electroretinogram, and spectral-domain optical coherence tomography. Doc Ophthalmol. 2017;135(1):17-28.
- D'Angelo E. Physiology of the cerebellum. Handb Clin Neurol. 2018;154:85-108. doi: 10.1016/B978-0-444-63956-1.00006-0. PMID: 29903454.
- Dao P, Ye F, Liu Y, Du ZY, Zhang K, Dong CZ, Meunier B, Chen H. Development of Phenothiazine-Based Theranostic Compounds That Act Both as Inhibitors of β-Amyloid Aggregation and as Imaging Probes for Amyloid Plaques in Alzheimer's Disease. ACS Chem Neurosci. 2017 Apr 19;8(4):798-806. doi: 10.1021/acschemneuro.6b00380. Epub 2017 Feb 2. PMID: 28097868.
- Daulatzai MA. Early stages of pathogenesis in memory impairment during normal senescence and Alzheimer's disease. J Alzheimers Dis. 2010;20(2):355-67. doi: 10.3233/JAD-2010-1374. PMID: 20164576.
- Davis MR, Robinson E, Koronyo Y, Salobrar-Garcia E, Rentsendorj A, Gaire BP, Mirzaei N, Kayed R, Sadun AA, Ljubimov AV, Schneider LS, Hawes D, Black KL, Fuchs DT, Koronyo-Hamaoui M. Retinal ganglion cell vulnerability to pathogenic tau in Alzheimer's disease. bioRxiv [Preprint]. 2024 Sep 21:2024.09.17.613293. doi: 10.1101/2024.09.17.613293. Update in: Acta Neuropathol Commun. 2025 Feb 15;13(1):31. doi: 10.1186/s40478-025-01935-y. PMID: 39345568; PMCID: PMC11430098.
- de Hoz R, Rojas B, Ramírez AI, Salazar JJ, Gallego BI, Triviño A, Ramírez JM. Retinal Macroglial Responses in Health and Disease. Biomed Res Int. 2016;2016:2954721. doi: 10.1155/2016/2954721. Epub 2016 May 18. PMID: 27294114; PMCID: PMC4887628.
- De Plano LM, Calabrese G, Rizzo MG, Oddo S, Caccamo A. The Role of the Transcription Factor Nrf2 in Alzheimer's Disease: Therapeutic Opportunities. Biomolecules. 2023 Mar 17;13(3):549. doi: 10.3390/biom13030549. PMID: 36979483; PMCID: PMC10046499.
- Deardorff WJ, Grossberg GT. Behavioral and psychological symptoms in Alzheimer's dementia and vascular dementia. Handb Clin Neurol. 2019;165:5-32. doi: 10.1016/B978-0-444-64012-3.00002-2. PMID: 31727229.
- Delay C, Hébert SS. MicroRNAs and Alzheimer's Disease Mouse Models: Current Insights and Future Research Avenues. Int J Alzheimers Dis. 2011;2011:894938. doi: 10.4061/2011/894938. Epub 2011 Jul 31. PMID: 21826259; PMCID: PMC3150778.
- Dhana K, Evans DA, Rajan KB, Bennett DA, Morris MC. Healthy lifestyle and the risk of Alzheimer dementia: Findings from 2 longitudinal studies. Neurology. 2020 Jul 28;95(4):e374-e383. doi: 10.1212/WNL.0000000000009816. Epub 2020 Jun 17. PMID: 32554763; PMCID: PMC7455318.

- Dong Y, Yu H, Li X, Bian K, Zheng Y, Dai M, Feng X, Sun Y, He Y, Yu B, Zhang H, Wu J, Yu X, Wu H, Kong W. Hyperphosphorylated tau mediates neuronal death by inducing necroptosis and inflammation in Alzheimer's disease. J Neuroinflammation. 2022 Aug 15;19(1):205. doi: 10.1186/s12974-022-02567-y. PMID: 35971179; PMCID: PMC9377071.
- Doody RS, Gavrilova SI, Sano M, Thomas RG, Aisen PS, Bachurin SO, Seely L, Hung D; dimebon investigators. Effect of dimebon on cognition, activities of daily living, behaviour, and global function in patients with mild-to-moderate Alzheimer's disease: a randomised, double-blind, placebo-controlled study. Lancet. 2008 Jul 19;372(9634):207-15. doi: 10.1016/S0140-6736(08)61074-0. PMID: 18640457.
- Duan Y, Ye T, Qu Z, Chen Y, Miranda A, Zhou X, Lok KC, Chen Y, Fu AKY, Gradinaru V, Ip NY. Brain-wide Cas9-mediated cleavage of a gene causing familial Alzheimer's disease alleviates amyloid-related pathologies in mice. Nat Biomed Eng. 2022 Feb;6(2):168-180. doi: 10.1038/s41551-021-00759-0. Epub 2021 Jul 26. PMID: 34312508.
- Dubois B, von Arnim CAF, Burnie N, Bozeat S, Cummings J. Biomarkers in Alzheimer's disease: role in early and differential diagnosis and recognition of atypical variants. Alzheimers Res Ther. 2023 Oct 13;15(1):175. doi: 10.1186/s13195-023-01314-6. PMID: 37833762; PMCID: PMC10571241.
- Duffy AM, Bouchier-Hayes DJ, Harmey JH. Vascular Endothelial Growth Factor (VEGF) and Its Role in Non-Endothelial Cells: Autocrine Signalling by VEGF. In: Madame Curie Bioscience Database [Internet]. Austin (TX): Landes Bioscience; 2000-2013. Doi: 10.1007/978-1-4419-9148-5_13.
- Dumont M, Stack C, Elipenahli C, Jainuddin S, Gerges M, Starkova N, Calingasan NY, Yang L, Tampellini D, Starkov AA, Chan RB, Di Paolo G, Pujol A, Beal MF. Bezafibrate administration improves behavioral deficits and tau pathology in P301S mice. Hum Mol Genet. 2012 Dec 1;21(23):5091-105. doi: 10.1093/hmg/dds355. Epub 2012 Aug 24. PMID: 22922230; PMCID: PMC3490516.
- Edwards MM, Rodríguez JJ, Gutierrez-Lanza R, Yates J, Verkhratsky A, Lutty GA. Retinal macroglia changes in a triple transgenic mouse model of Alzheimer's disease. Exp Eye Res. 2014 Oct;127:252-60. doi: 10.1016/j.exer.2014.08.006. Epub 2014 Aug 19. PMID: 25149907; PMCID: PMC4175519.
- Eimer WA, Vassar R. Neuron loss in the 5XFAD mouse model of Alzheimer's disease correlates with intraneuronal Aβ42 accumulation and Caspase-3 activation. Mol Neurodegener. 2013 Jan 14;8:2. doi: 10.1186/1750-1326-8-2. PMID: 23316765; PMCID: PMC3552866.
- Eisenmenger LB, Peret A, Famakin BM, Spahic A, Roberts GS, Bockholt JH, Johnson KM, Paulsen JS. Vascular contributions to Alzheimer's disease. Transl Res. 2023 Apr;254:41-53. doi: 10.1016/j.trsl.2022.12.003. Epub 2022 Dec 15. PMID: 36529160; PMCID: PMC10481451.
- Elmore S. Apoptosis: a review of programmed cell death. Toxicol Pathol. 2007 Jun;35(4):495-516. doi: 10.1080/01926230701320337. PMID: 17562483; PMCID: PMC2117903.
- Elmore S. Apoptosis: a review of programmed cell death. Toxicol Pathol. 2007 Jun;35(4):495-516. doi: 10.1080/01926230701320337. PMID: 17562483; PMCID: PMC2117903.

- Estrada LD, Ahumada P, Cabrera D, Arab JP. Liver Dysfunction as a Novel Player in Alzheimer's Progression: Looking Outside the Brain. Front Aging Neurosci. 2019 Jul 17;11:174. doi: 10.3389/fnagi.2019.00174. PMID: 31379558; PMCID: PMC6650779.
- Fan W, Huang W, Chen J, Li N, Mao L, Hou S. Retinal microglia: Functions and diseases. Immunology. 2022 Jul;166(3):268-286. doi: 10.1111/imm.13479. Epub 2022 Apr 22. PMID: 35403700.
- Fan W, Huang W, Chen J, Li N, Mao L, Hou S. Retinal microglia: Functions and diseases. Immunology. 2022 Jul;166(3):268-286. doi: 10.1111/imm.13479. Epub 2022 Apr 22. PMID: 35403700.
- Fanlo-Ucar H, Picón-Pagès P, Herrera-Fernández V, Ill-Raga G, Muñoz FJ. The Dual Role of Amyloid Beta-Peptide in Oxidative Stress and Inflammation: Unveiling Their Connections in Alzheimer's Disease Etiopathology. Antioxidants (Basel). 2024 Oct 8;13(10):1208. doi: 10.3390/antiox13101208. PMID: 39456461; PMCID: PMC11505517.
- Farkas E, Luiten PG. Cerebral microvascular pathology in aging and Alzheimer's disease. Prog Neurobiol. 2001 Aug;64(6):575-611. doi: 10.1016/s0301-0082(00)00068-x. PMID: 11311463. Mehta JL, Nichols WW, Mehta P. Neutrophils as potential participants in acute myocardial ischemia: relevance to reperfusion. J Am Coll Cardiol. 1988 Jun;11(6):1309-16. doi: 10.1016/0735-1097(88)90297-5. PMID: 3284944.
- Farris W, Mansourian S, Chang Y, Lindsley L, Eckman EA, Frosch MP, Eckman CB, Tanzi RE, Selkoe DJ, Guenette S. Insulin-degrading enzyme regulates the levels of insulin, amyloid beta-protein, and the beta-amyloid precursor protein intracellular domain in vivo. Proc Natl Acad Sci U S A. 2003 Apr 1;100(7):4162-7. doi: 10.1073/pnas.0230450100. Epub 2003 Mar 12. PMID: 12634421; PMCID: PMC153065.
- Fernández-Sánchez L, Lax P, Campello L, Pinilla I, Cuenca N. Astrocytes and Müller Cell Alterations During Retinal Degeneration in a Transgenic Rat Model of Retinitis Pigmentosa. Front Cell Neurosci. 2015 Dec 22;9:484. doi: 10.3389/fncel.2015.00484. PMID: 26733810; PMCID: PMC4686678.
- Folch J, Lees M, Sloane Stanley GH. A simple method for the isolation and purification of total lipides from animal tissues. J Biol Chem. 1957 May;226(1):497-509. PMID: 13428781.
- Forner S, Kawauchi S, Balderrama-Gutierrez G, Kramár EA, Matheos DP, Phan J, Javonillo DI, Tran KM, Hingco E, da Cunha C, Rezaie N, Alcantara JA, Baglietto-Vargas D, Jansen C, Neumann J, Wood MA, MacGregor GR, Mortazavi A, Tenner AJ, LaFerla FM, Green KN. Systematic phenotyping and characterization of the 5xFAD mouse model of Alzheimer's disease. Sci Data. 2021 Oct 15;8(1):270. doi: 10.1038/s41597-021-01054-y. PMID: 34654824; PMCID: PMC8519958.
- Gail Canter R, Huang WC, Choi H, Wang J, Ashley Watson L, Yao CG, Abdurrob F, Bousleiman SM, Young JZ, Bennett DA, Delalle I, Chung K, Tsai LH. 3D mapping reveals network-specific amyloid progression and subcortical susceptibility in mice. Commun Biol. 2019 Oct 4;2:360. doi: 10.1038/s42003-019-0599-8. PMID: 31602409; PMCID: PMC6778135.
- Gaire BP, Koronyo Y, Fuchs DT, Shi H, Rentsendorj A, Danziger R, Vit JP, Mirzaei N, Doustar J, Sheyn J, Hampel H, Vergallo A, Davis MR, Jallow O, Baldacci F, Verdooner SR, Barron E, Mirzaei M, Gupta

VK, Graham SL, Tayebi M, Carare RO, Sadun AA, Miller CA, Dumitrascu OM, Lahiri S, Gao L, Black KL, Koronyo-Hamaoui M. Alzheimer's disease pathophysiology in the Retina. Prog Retin Eye Res. 2024 Jul;101:101273. doi: 10.1016/j.preteyeres.2024.101273. Epub 2024 May 15. PMID: 38759947; PMCID: PMC11285518.

- Garcia FJ, Heiman M. Molecular and cellular characteristics of cerebrovascular cell types and their contribution to neurodegenerative diseases. Mol Neurodegener. 2025 Jan 29;20(1):13. doi: 10.1186/s13024-025-00799-z. PMID: 39881338; PMCID: PMC11780804.
- Garcia J, Chang R, Steinberg RA, Arce A, Yang J, Van Der Eb P, Abdullah T, Chandrashekar DV, Eck SM, Meza P, Liu ZX, Cadenas E, Cribbs DH, Kaplowitz N, Sumbria RK, Han D. Modulation of hepatic amyloid precursor protein and lipoprotein receptor-related protein 1 by chronic alcohol intake: Potential link between liver steatosis and amyloid-β. Front Physiol. 2022 Sep 15;13:930402. doi: 10.3389/fphys.2022.930402. PMID: 36187787; PMCID: PMC9520570.
- García-Bermúdez MY, Freude KK, Mouhammad ZA, van Wijngaarden P, Martin KK, Kolko M. Glial Cells in Glaucoma: Friends, Foes, and Potential Therapeutic Targets. Front Neurol. 2021 Mar 16;12:624983. doi: 10.3389/fneur.2021.624983. PMID: 33796062; PMCID: PMC8007906.
- Gauthier S, Feldman HH, Schneider LS, Wilcock GK, Frisoni GB, Hardlund JH, Moebius HJ, Bentham P, Kook KA, Wischik DJ, Schelter BO, Davis CS, Staff RT, Bracoud L, Shamsi K, Storey JM, Harrington CR, Wischik CM. Efficacy and safety of tau-aggregation inhibitor therapy in patients with mild or moderate Alzheimer's disease: a randomised, controlled, double-blind, parallel-arm, phase 3 trial. Lancet. 2016 Dec 10;388(10062):2873-2884. doi: 10.1016/S0140-6736(16)31275-2. Epub 2016 Nov 16. PMID: 27863809; PMCID: PMC5164296.
- George M, Tharakan M, Culberson J, Reddy AP, Reddy PH. Role of Nrf2 in aging, Alzheimer's and other neurodegenerative diseases. Ageing Res Rev. 2022 Dec;82:101756. doi: 10.1016/j.arr.2022.101756. Epub 2022 Oct 13. PMID: 36243357.
- Giannoni P, Arango-Lievano M, Neves ID, Rousset MC, Baranger K, Rivera S, Jeanneteau F, Claeysen S, Marchi N. Cerebrovascular pathology during the progression of experimental Alzheimer's disease. Neurobiol Dis. 2016 Apr;88:107-17. doi: 10.1016/j.nbd.2016.01.001. Epub 2016 Jan 8. PMID: 26774030.
- Goel P, Chakrabarti S, Goel K, Bhutani K, Chopra T, Bali S. Neuronal cell death mechanisms in Alzheimer's disease: An insight. Front Mol Neurosci. 2022 Aug 25;15:937133. doi: 10.3389/fnmol.2022.937133. PMID: 36090249; PMCID: PMC9454331.
- Goode BL, Feinstein SC. Identification of a novel microtubule binding and assembly domain in the developmentally regulated inter-repeat region of tau. J Cell Biol. 1994 Mar;124(5):769-82. doi: 10.1083/jcb.124.5.769. PMID: 8120098; PMCID: PMC2119949.
- Gozes I. NAP (davunetide) provides functional and structural neuroprotection. Curr Pharm Des. 2011;17(10):1040-4. doi: 10.2174/138161211795589373. PMID: 21524250.

- Grammas P, Tripathy D, Sanchez A, Yin X, Luo J. Brain microvasculature and hypoxia-related proteins in Alzheimer's disease. Int J Clin Exp Pathol. 2011 Aug 15;4(6):616-27. Epub 2011 Jun 18. PMID: 21904637; PMCID: PMC3160613.
- Greene C, Hanley N, Campbell M. Claudin-5: gatekeeper of neurological function. Fluids Barriers CNS. 2019 Jan 29;16(1):3. doi: 10.1186/s12987-019-0123-z. PMID: 30691500; PMCID: PMC6350359.
- Grigoryan EN. Self-Organization of the Retina during Eye Development, Retinal Regeneration In Vivo, and in Retinal 3D Organoids In Vitro. Biomedicines. 2022 Jun 20;10(6):1458. doi: 10.3390/biomedicines10061458. PMID: 35740479; PMCID: PMC9221005.
- Grimaldi A, Pediconi N, Oieni F, Pizzarelli R, Rosito M, Giubettini M, Santini T, Limatola C, Ruocco G, Ragozzino D, Di Angelantonio S. Neuroinflammatory Processes, A1 Astrocyte Activation and Protein Aggregation in the Retina of Alzheimer's Disease Patients, Possible Biomarkers for Early Diagnosis. Front Neurosci. 2019 Sep 4;13:925. doi: 10.3389/fnins.2019.00925. PMID: 31551688; PMCID: PMC6737046.
- Grimes WN, Berson DM, Sabnis A, Hoon M, Sinha R, Tian H, Diamond JS. The retina's neurovascular unit: Müller glial sheaths and neuronal contacts. bioRxiv [Preprint]. 2024 May 1:2024.04.30.591885. doi: 10.1101/2024.04.30.591885. PMID: 38903067; PMCID: PMC11188116.
- Gu L, Guo Z. Alzheimer's Aβ42 and Aβ40 peptides form interlaced amyloid fibrils. J Neurochem. 2013 Aug;126(3):305-11. doi: 10.1111/jnc.12202. Epub 2013 Mar 12. PMID: 23406382; PMCID: PMC3716832.
- Guo Q, Jin Y, Chen X, Ye X, Shen X, Lin M, Zeng C, Zhou T, Zhang J. NF-κB in biology and targeted therapy: new insights and translational implications. Signal Transduct Target Ther. 2024 Mar 4;9(1):53. doi: 10.1038/s41392-024-01757-9. PMID: 38433280; PMCID: PMC10910037.
- Guo S, Wang H, Yin Y. Microglia Polarization From M1 to M2 in Neurodegenerative Diseases. Front Aging Neurosci. 2022 Feb 16;14:815347. doi: 10.3389/fnagi.2022.815347. PMID: 35250543; PMCID: PMC8888930.
- Guo T, Noble W, Hanger DP. Roles of tau protein in health and disease. Acta Neuropathol. 2017 May;133(5):665-704. doi: 10.1007/s00401-017-1707-9. Epub 2017 Apr 6. PMID: 28386764; PMCID: PMC5390006.
- Gupta VB, Chitranshi N, den Haan J, Mirzaei M, You Y, Lim JK, Basavarajappa D, Godinez A, Di Angelantonio S, Sachdev P, Salekdeh GH, Bouwman F, Graham S, Gupta V. Retinal changes in Alzheimer's disease- integrated prospects of imaging, functional and molecular advances. Prog Retin Eye Res. 2021 May;82:100899. doi: 10.1016/j.preteyeres.2020.100899. Epub 2020 Sep 2. PMID: 32890742.
- György B, Lööv C, Zaborowski MP, Takeda S, Kleinstiver BP, Commins C, Kastanenka K, Mu D, Volak A, Giedraitis V, Lannfelt L, Maguire CA, Joung JK, Hyman BT, Breakefield XO, Ingelsson M. CRISPR/Cas9 Mediated Disruption of the Swedish APP Allele as a Therapeutic Approach for Early-Onset Alzheimer's Disease. Mol Ther Nucleic Acids. 2018 Jun 1;11:429-440. doi: 10.1016/j.omtn.2018.03.007. Epub 2018 Mar 16. PMID: 29858078; PMCID: PMC5992788.

- Hadi Alijanvand S, Peduzzo A, Buell AK. Secondary Nucleation and the Conservation of Structural Characteristics of Amyloid Fibril Strains. Front Mol Biosci. 2021 Apr 16;8:669994. doi: 10.3389/fmolb.2021.669994. PMID: 33937341; PMCID: PMC8085410.
- Hai Y, Ren K, Zhang Y, Yang L, Cao H, Yuan X, Su L, Li H, Feng X, Liu D. HIF-1α serves as a co-linker between AD and T2DM. Biomed Pharmacother. 2024 Feb;171:116158. doi: 10.1016/j.biopha.2024.116158. Epub 2024 Jan 18. PMID: 38242039.
- Hampel H, Hardy J, Blennow K, Chen C, Perry G, Kim SH, Villemagne VL, Aisen P, Vendruscolo M, Iwatsubo T, Masters CL, Cho M, Lannfelt L, Cummings JL, Vergallo A. The Amyloid-β Pathway in Alzheimer's Disease. Mol Psychiatry. 2021 Oct;26(10):5481-5503. doi: 10.1038/s41380-021-01249-0. Epub 2021 Aug 30. PMID: 34456336; PMCID: PMC8758495.
- Haruta M, Bush RA, Kjellstrom S, Vijayasarathy C, Zeng Y, Le YZ, Sieving PA. Depleting Rac1 in mouse rod photoreceptors protects them from photo-oxidative stress without affecting their structure or function. Proc Natl Acad Sci U S A. 2009 Jun 9;106(23):9397-402. doi: 10.1073/pnas.0808940106. Epub 2009 May 21. PMID: 19470639; PMCID: PMC2685247.
- Hatzimanolis, O., Sykes, A.M. & Cristino, A.S. Circular RNAs in neurological conditions – computational identification, functional validation, and potential clinical applications. Mol Psychiatry 30, 1652–1675 (2025). https://doi.org/10.1038/s41380-025-02925-1.
- Heneka MT, van der Flier WM, Jessen F, Hoozemanns J, Thal DR, Boche D, Brosseron F, Teunissen C, Zetterberg H, Jacobs AH, Edison P, Ramirez A, Cruchaga C, Lambert JC, Laza AR, Sanchez-Mut JV, Fischer A, Castro-Gomez S, Stein TD, Kleineidam L, Wagner M, Neher JJ, Cunningham C, Singhrao SK, Prinz M, Glass CK, Schlachetzki JCM, Butovsky O, Kleemann K, De Jaeger PL, Scheiblich H, Brown GC, Landreth G, Moutinho M, Grutzendler J, Gomez-Nicola D, McManus RM, Andreasson K, Ising C, Karabag D, Baker DJ, Liddelow SA, Verkhratsky A, Tansey M, Monsonego A, Aigner L, Dorothée G, Nave KA, Simons M, Constantin G, Rosenzweig N, Pascual A, Petzold GC, Kipnis J, Venegas C, Colonna M, Walter J, Tenner AJ, O'Banion MK, Steinert JR, Feinstein DL, Sastre M, Bhaskar K, Hong S, Schafer DP, Golde T, Ransohoff RM, Morgan D, Breitner J, Mancuso R, Riechers SP. Neuroinflammation in Alzheimer disease. Nat Rev Immunol. 2025 May;25(5):321-352. doi: 10.1038/s41577-024-01104-7. Epub 2024 Dec 9. PMID: 39653749.
- Hickman SE, Allison EK, El Khoury J. Microglial dysfunction and defective beta-amyloid clearance pathways in aging Alzheimer's disease mice. J Neurosci. 2008 Aug 13;28(33):8354-60. doi: 10.1523/JNEUROSCI.0616-08.2008. PMID: 18701698; PMCID: PMC2597474.
- Howarth C. The contribution of astrocytes to the regulation of cerebral blood flow. Front Neurosci. 2014 May 9;8:103. doi: 10.3389/fnins.2014.00103. PMID: 24847203; PMCID: PMC4023041.
- Huang WJ, Zhang X, Chen WW. Role of oxidative stress in Alzheimer's disease. Biomed Rep. 2016 May;4(5):519-522. doi: 10.3892/br.2016.630. Epub 2016 Mar 15. PMID: 27123241; PMCID: PMC4840676.

- Hufnagle JJ, Tadi P. Neuroanatomy, Brain Veins. 2025 Jun 25. In: StatPearls [Internet]. Treasure Island (FL): StatPearls Publishing; 2025 Jan–. PMID: 31536212.
- Hussey KA, Hadyniak SE, Johnston RJ Jr. Patterning and Development of Photoreceptors in the Human Retina. Front Cell Dev Biol. 2022 Apr 14;10:878350. doi: 10.3389/fcell.2022.878350. PMID: 35493094; PMCID: PMC9049932.
- Iadecola C. Neurovascular regulation in the normal brain and in Alzheimer's disease. Nat Rev Neurosci. 2004 May;5(5):347-60. doi: 10.1038/nrn1387. PMID: 15100718.
- Imamoto Y, Shichida Y. Cone visual pigments. Biochim Biophys Acta. 2014 May;1837(5):664-73. doi: 10.1016/j.bbabio.2013.08.009. Epub 2013 Sep 7. PMID: 24021171.
- Jahn H. Memory loss in Alzheimer's disease. Dialogues Clin Neurosci. 2013 Dec;15(4):445-54. doi: 10.31887/DCNS.2013.15.4/hjahn. PMID: 24459411; PMCID: PMC3898682.
- Jakubczyk K, Dec K, Kałduńska J, Kawczuga D, Kochman J, Janda K. Reactive oxygen species - sources, functions, oxidative damage. Pol Merkur Lekarski. 2020 Apr 22;48(284):124-127. PMID: 32352946.
- Jawabri KH, Sharma S. Physiology, Cerebral Cortex Functions. 2023 Apr 24. In: StatPearls [Internet]. Treasure Island (FL): StatPearls Publishing; 2025 Jan–. PMID: 30860731.
- Jawhar S, Trawicka A, Jenneckens C, Bayer TA, Wirths O. Motor deficits, neuron loss, and reduced anxiety coinciding with axonal degeneration and intraneuronal Aβ aggregation in the 5XFAD mouse model of Alzheimer's disease. Neurobiol Aging. 2012 Jan;33(1):196.e29-40. doi: 10.1016/j.neurobiolaging.2010.05.027. Epub 2010 Jul 9. PMID: 20619937.
- Jeong D, Kim J, Nam J, Sun H, Lee YH, Lee TJ, Aguiar RC, Kim SW. MicroRNA-124 links p53 to the NF-κB pathway in B-cell lymphomas. Leukemia. 2015 Sep;29(9):1868-74. doi: 10.1038/leu.2015.101. Epub 2015 Apr 27. PMID: 25915824.
- Jia R, Solé-Guardia G, Verweij V, Snabel JM, Geenen B, Tuladhar AM, Kleemann R, Kiliaan AJ, Wiesmann M. Identification and Characterization of a Translational Mouse Model for Blood-Brain Barrier Leakage in Cerebral Small Vessel Disease. Int J Mol Sci. 2025 Jul 12;26(14):6706. doi: 10.3390/ijms26146706. PMID: 40724955; PMCID: PMC12294681.
- Jiang C, Li G, Huang P, Liu Z, Zhao B. The Gut Microbiota and Alzheimer's Disease. J Alzheimers Dis. 2017;58(1):1-15. doi: 10.3233/JAD-161141. PMID: 28372330.
- Jiang ZL, Kassab GS, Fung YC. Diameter-defined Strahler system and connectivity matrix of the pulmonary arterial tree. J Appl Physiol (1985). 1994 Feb;76(2):882-92. doi: 10.1152/jappl.1994.76.2.882. PMID: 8175603.
- Jullienne A, Szu JI, Quan R, Trinh MV, Norouzi T, Noarbe BP, Bedwell AA, Eldridge K, Persohn SC, Territo PR, Obenaus A. Cortical cerebrovascular and metabolic perturbations in the 5xFAD mouse model of Alzheimer's disease. Front Aging Neurosci. 2023 Jul 18;15:1220036. doi: 10.3389/fnagi.2023.1220036. PMID: 37533765; PMCID: PMC10392850.

- Jung J, Lee SN, Her SH, Yoo KD, Moon KW, Moon D, Jang WY. Long-Term Clinical Impact of Patients with Multi-Vessel Non-Obstructive Coronary Artery Disease. Life (Basel). 2023 Oct 26;13(11):2119. doi: 10.3390/life13112119. PMID: 38004259; PMCID: PMC10671936.
- Kaddoumi A, Denney TS Jr, Deshpande G, Robinson JL, Beyers RJ, Redden DT, Praticò D, Kyriakides TC, Lu B, Kirby AN, Beck DT, Merner ND. Extra-Virgin Olive Oil Enhances the Blood-Brain Barrier Function in Mild Cognitive Impairment: A Randomized Controlled Trial. Nutrients. 2022 Dec 1;14(23):5102. doi: 10.3390/nu14235102. PMID: 36501136; PMCID: PMC9736478.
- Kadry H, Noorani B, Cucullo L. A blood-brain barrier overview on structure, function, impairment, and biomarkers of integrity. Fluids Barriers CNS. 2020 Nov 18;17(1):69. doi: 10.1186/s12987-020-00230-3. PMID: 33208141; PMCID: PMC7672931.
- Kandel ER, Dudai Y, Mayford MR. The molecular and systems biology of memory. Cell. 2014 Mar 27;157(1):163-86. doi: 10.1016/j.cell.2014.03.001. PMID: 24679534.
- Kassab GS, Imoto K, White FC, Rider CA, Fung YC, Bloor CM. Coronary arterial tree remodeling in right ventricular hypertrophy. Am J Physiol. 1993 Jul;265(1 Pt 2):H366-75. doi: 10.1152/ajpheart.1993.265.1.H366. PMID: 8342653.
- Kassab GS, Lin DH, Fung YC. Consequences of pruning in morphometry of coronary vasculature. Ann Biomed Eng. 1994 Jul-Aug;22(4):398-403. doi: 10.1007/BF02368246. PMID: 7998685.
- Kim US, Mahroo OA, Mollon JD, Yu-Wai-Man P. Retinal Ganglion Cells-Diversity of Cell Types and Clinical Relevance. Front Neurol. 2021 May 21;12:661938. doi: 10.3389/fneur.2021.661938. PMID: 34093409; PMCID: PMC8175861.
- Kimura R, Ohno M. Impairments in remote memory stabilization precede hippocampal synaptic and cognitive failures in 5XFAD Alzheimer mouse model. Neurobiol Dis. 2009 Feb;33(2):229-35. doi: 10.1016/j.nbd.2008.10.006. Epub 2008 Nov 5. PMID: 19026746; PMCID: PMC2741400.
- Kinney JW, Bemiller SM, Murtishaw AS, Leisgang AM, Salazar AM, Lamb BT. Inflammation as a central mechanism in Alzheimer's disease. Alzheimers Dement (N Y). 2018 Sep 6;4:575-590. doi: 10.1016/j.trci.2018.06.014. PMID: 30406177; PMCID: PMC6214864.
- Kisler K, Nelson AR, Montagne A, Zlokovic BV. Cerebral blood flow regulation and neurovascular dysfunction in Alzheimer disease. Nat Rev Neurosci. 2017 Jul;18(7):419-434. doi: 10.1038/nrn.2017.48. Epub 2017 May 18. PMID: 28515434; PMCID: PMC5759779.
- Klein G, Delmar P, Voyle N, Rehal S, Hofmann C, Abi-Saab D, Andjelkovic M, Ristic S, Wang G, Bateman R, Kerchner GA, Baudler M, Fontoura P, Doody R. Gantenerumab reduces amyloid-β plaques in patients with prodromal to moderate Alzheimer's disease: a PET substudy interim analysis. Alzheimers Res Ther. 2019 Dec 12;11(1):101. doi: 10.1186/s13195-019-0559-z. PMID: 31831056; PMCID: PMC6909550.
- Ko YS, Ryu YK, Han S, Park HJ, Choi M, Kim BC, Jeong HS, Jang S, Jo J, Lee S, Choi WS, Cho HH. Hearing modulation affects Alzheimer's disease progression linked to brain inflammation: a study in

mouse models. Mol Med. 2024 Dec 26;30(1):276. doi: 10.1186/s10020-024-01040-1. PMID: 39725872; PMCID: PMC11670416.

- Kobat SG, Turgut B. Importance of Müller Cells. Beyoglu Eye J. 2020 Jul 29;5(2):59-63. doi: 10.14744/bej.2020.28290. PMID: 35098065; PMCID: PMC8784480.
- Komiya Y, Sugiyama M, Koyama C, Kameshima S, Ochiai M, Adachi Y, Yokoyama I, Fukasawa H, Yoshioka K, Arihara K. Dietary olive oil intake induces female-specific hepatic lipid accumulation without metabolic impairment in mice. Nutr Res. 2023 Apr;112:11-19. doi: 10.1016/j.nutres.2023.02.001. Epub 2023 Feb 23. PMID: 36934523.
- Konstantinidis E, Molisak A, Perrin F, Streubel-Gallasch L, Fayad S, Kim DY, Petri K, Aryee MJ, Aguilar X, György B, Giedraitis V, Joung JK, Pattanayak V, Essand M, Erlandsson A, Berezovska O, Ingelsson M. CRISPR-Cas9 treatment partially restores amyloid-β 42/40 in human fibroblasts with the Alzheimer's disease PSEN1 M146L mutation. Mol Ther Nucleic Acids. 2022 Mar 28;28:450-461. doi: 10.1016/j.omtn.2022.03.022. PMID: 35505961; PMCID: PMC9043867.
- Kook SY, Hong HS, Moon M, Ha CM, Chang S, Mook-Jung I. $A\beta_{1-42}$-RAGE interaction disrupts tight junctions of the blood-brain barrier via Ca^{2+}-calcineurin signaling. J Neurosci. 2012 Jun 27;32(26):8845-54. doi: 10.1523/JNEUROSCI.6102-11.2012. PMID: 22745485; PMCID: PMC6622350.
- Koronyo Y, Rentsendorj A, Mirzaei N, Regis GC, Sheyn J, Shi H, Barron E, Cook-Wiens G, Rodriguez AR, Medeiros R, Paulo JA, Gupta VB, Kramerov AA, Ljubimov AV, Van Eyk JE, Graham SL, Gupta VK, Ringman JM, Hinton DR, Miller CA, Black KL, Cattaneo A, Meli G, Mirzaei M, Fuchs DT, Koronyo-Hamaoui M. Retinal pathological features and proteome signatures of Alzheimer's disease. Acta Neuropathol. 2023 Apr;145(4):409-438. doi: 10.1007/s00401-023-02548-2. Epub 2023 Feb 11. PMID: 36773106; PMCID: PMC10020290.
- Korte N, Nortley R, Attwell D. Cerebral blood flow decrease as an early pathological mechanism in Alzheimer's disease. Acta Neuropathol. 2020 Dec;140(6):793-810. doi: 10.1007/s00401-020-02215-w. Epub 2020 Aug 31. PMID: 32865691; PMCID: PMC7666276.
- Kotredes KP, Pandey RS, Persohn S, Elderidge K, Burton CP, Miner EW, Haynes KA, Santos DFS, Williams SP, Heaton N, Ingraham CM, Lloyd C, Garceau D, O'Rourke R, Herrick S, Rangel-Barajas C, Maharjan S, Wang N, Sasner M, Lamb BT, Territo PR, Sukoff Rizzo SJ, Carter GW, Howell GR, Oblak AL. Characterizing molecular and synaptic signatures in mouse models of late-onset Alzheimer's disease independent of amyloid and tau pathology. Alzheimers Dement. 2024 Jun;20(6):4126-4146. doi: 10.1002/alz.13828. Epub 2024 May 12. PMID: 38735056; PMCID: PMC11180851.
- Kozomara A, Birgaoanu M, Griffiths-Jones S. miRBase: from microRNA sequences to function. Nucleic Acids Res. 2019 Jan 8;47(D1):D155-D162. doi: 10.1093/nar/gky1141. PMID: 30423142; PMCID: PMC6323917.
- Krasodomska K, Lubiński W, Potemkowski A, Honczarenko K. Pattern electroretinogram (PERG) and pattern visual evoked potential (PVEP) in the early stages of Alzheimer's disease. Doc Ophthalmol. 2010

Oct;121(2):111-21. doi: 10.1007/s10633-010-9238-x. Epub 2010 Jun 13. PMID: 20549299; PMCID: PMC2941083.

- Krasovec G, Horkan HR, Quéinnec É, Chambon JP. Intrinsic apoptosis is evolutionarily divergent among metazoans. Evol Lett. 2023 Nov 16;8(2):267-282. doi: 10.1093/evlett/qrad057. PMID: 38525035; PMCID: PMC10959488.
- Krause G, Winkler L, Mueller SL, Haseloff RF, Piontek J, Blasig IE. Structure and function of claudins. Biochim Biophys Acta. 2008 Mar;1778(3):631-45. doi: 10.1016/j.bbamem.2007.10.018. Epub 2007 Oct 25. PMID: 18036336.
- Kumar A, Sidhu J, Lui F, Tsao JW. Alzheimer Disease. 2024 Feb 12. In: StatPearls [Internet]. Treasure Island (FL): StatPearls Publishing; 2025 Jan–. PMID: 29763097.
- Kumari S, Dhapola R, Reddy DH. Apoptosis in Alzheimer's disease: insight into the signaling pathways and therapeutic avenues. Apoptosis. 2023 Aug;28(7-8):943-957. doi: 10.1007/s10495-023-01848-y. Epub 2023 Apr 26. PMID: 37186274.
- La Morgia C, Di Vito L, Carelli V, Carbonelli M. Patterns of Retinal Ganglion Cell Damage in Neurodegenerative Disorders: Parvocellular vs Magnocellular Degeneration in Optical Coherence Tomography Studies. Front Neurol. 2017 Dec 22;8:710. doi: 10.3389/fneur.2017.00710. PMID: 29312131; PMCID: PMC5744067.
- La Morgia C, Ross-Cisneros FN, Koronyo Y, Hannibal J, Gallassi R, Cantalupo G, Sambati L, Pan BX, Tozer KR, Barboni P, Provini F, Avanzini P, Carbonelli M, Pelosi A, Chui H, Liguori R, Baruzzi A, Koronyo-Hamaoui M, Sadun AA, Carelli V. Melanopsin retinal ganglion cell loss in Alzheimer's disease. Ann Neurol. 2016 Jan;79(1):90-109. doi: 10.1002/ana.24548. Epub 2015 Dec 18. PMID: 26505992; PMCID: PMC4737313.
- Lapi D, Di Maro M, Mastantuono T, Starita N, Ursino M, Colantuoni A. Arterial Network Geometric Characteristics and Regulation of Capillary Blood Flow in Hamster Skeletal Muscle Microcirculation. Front Physiol. 2019 Jan 18;9:1953. doi: 10.3389/fphys.2018.01953. PMID: 30713505; PMCID: PMC6345695.
- Lapi D, Scuri R, Colantuoni A. Trigeminal Cardiac Reflex and Cerebral Blood Flow Regulation. Front Neurosci. 2016 Oct 20;10:470. doi: 10.3389/fnins.2016.00470. PMID: 27812317; PMCID: PMC5071330.
- Lapi D, Stornaiuolo M, Sabatino L, Sommella E, Tenore G, Daglia M, Scuri R, Di Maro M, Colantuoni A, Novellino E. The Pomace Extract Taurisolo Protects Rat Brain From Ischemia-Reperfusion Injury. Front Cell Neurosci. 2020 Jan 28;14:3. doi: 10.3389/fncel.2020.00003. PMID: 32063837; PMCID: PMC6997812.
- LaRocca TJ, Cavalier AN, Roberts CM, Lemieux MR, Ramesh P, Garcia MA, Link CD. Amyloid beta acts synergistically as a pro-inflammatory cytokine. Neurobiol Dis. 2021 Nov;159:105493. doi: 10.1016/j.nbd.2021.105493. Epub 2021 Aug 28. PMID: 34464705; PMCID: PMC8502211.

- Lauffer MC, van Roon-Mom W, Aartsma-Rus A; N = 1 Collaborative. Possibilities and limitations of antisense oligonucleotide therapies for the treatment of monogenic disorders. Commun Med (Lond). 2024 Jan 5;4(1):6. doi: 10.1038/s43856-023-00419-1. PMID: 38182878; PMCID: PMC10770028.
- Lauretti E, Iuliano L, Praticò D. Extra-virgin olive oil ameliorates cognition and neuropathology of the 3xTg mice: role of autophagy. Ann Clin Transl Neurol. 2017 Jun 21;4(8):564-574. doi: 10.1002/acn3.431. PMID: 28812046; PMCID: PMC5553230.
- Lauretti E, Nenov M, Dincer O, Iuliano L, Praticò D. Extra virgin olive oil improves synaptic activity, short-term plasticity, memory, and neuropathology in a tauopathy model. Aging Cell. 2020 Jan;19(1):e13076. doi: 10.1111/acel.13076. Epub 2019 Nov 24. PMID: 31762202; PMCID: PMC6974729.
- Lawrence T. The nuclear factor NF-kappaB pathway in inflammation. Cold Spring Harb Perspect Biol. 2009 Dec;1(6):a001651. doi: 10.1101/cshperspect.a001651. Epub 2009 Oct 7. PMID: 20457564; PMCID: PMC2882124.
- Lazic D, Sagare AP, Nikolakopoulou AM, Griffin JH, Vassar R, Zlokovic BV. 3K3A-activated protein C blocks amyloidogenic BACE1 pathway and improves functional outcome in mice. J Exp Med. 2019 Feb 4;216(2):279-293. doi: 10.1084/jem.20181035. Epub 2019 Jan 15. PMID: 30647119; PMCID: PMC6363429.
- Leri M, Bertolini A, Stefani M, Bucciantini M. EVOO Polyphenols Relieve Synergistically Autophagy Dysregulation in a Cellular Model of Alzheimer's Disease. Int J Mol Sci. 2021 Jul 5;22(13):7225. doi: 10.3390/ijms22137225. PMID: 34281279; PMCID: PMC8267626.
- Li LY, Luo X, Wang X. Endonuclease G is an apoptotic DNase when released from mitochondria. Nature. 2001 Jul 5;412(6842):95-9. doi: 10.1038/35083620. PMID: 11452314.
- Li Y, Zhu K, Li N, Wang X, Xiao X, Li L, Li L, He Y, Zhang J, Wo J, Cui Y, Huang H, Zhang J, Wang W, Wang X, Zheng Y. Reversible GABAergic dysfunction involved in hippocampal hyperactivity predicts early-stage Alzheimer disease in a mouse model. Alzheimers Res Ther. 2021 Jun 14;13(1):114. doi: 10.1186/s13195-021-00859-8. PMID: 34127063; PMCID: PMC8204558.
- Li YB, Fu Q, Guo M, Du Y, Chen Y, Cheng Y. MicroRNAs: pioneering regulators in Alzheimer's disease pathogenesis, diagnosis, and therapy. Transl Psychiatry. 2024 Sep 10;14(1):367. doi: 10.1038/s41398-024-03075-8. PMID: 39256358; PMCID: PMC11387755.
- Liao C, Xu J, Chen Y, Ip NY. Retinal Dysfunction in Alzheimer's Disease and Implications for Biomarkers. Biomolecules. 2021 Aug 16;11(8):1215. doi: 10.3390/biom11081215. PMID: 34439882; PMCID: PMC8394950.
- Lim JKH, Li QX, He Z, Vingrys AJ, Chinnery HR, Mullen J, Bui BV, Nguyen CTO. Retinal Functional and Structural Changes in the 5xFAD Mouse Model of Alzheimer's Disease. Front Neurosci. 2020 Aug 13;14:862. doi: 10.3389/fnins.2020.00862. PMID: 32903645; PMCID: PMC7438734.

- Lin TK, Huang CR, Lin KJ, Hsieh YH, Chen SD, Lin YC, Chao AC, Yang DI. Potential Roles of Hypoxia-Inducible Factor-1 in Alzheimer's Disease: Beneficial or Detrimental? Antioxidants (Basel). 2024 Nov 11;13(11):1378. doi: 10.3390/antiox13111378. PMID: 39594520; PMCID: PMC11591038.
- Lindsay H, Tröger J, König A. Language Impairment in Alzheimer's Disease-Robust and Explainable Evidence for AD-Related Deterioration of Spontaneous Speech Through Multilingual Machine Learning. Front Aging Neurosci. 2021 May 19;13:642033. doi: 10.3389/fnagi.2021.642033. PMID: 34093165; PMCID: PMC8170097.
- Liu CC, Liu CC, Kanekiyo T, Xu H, Bu G. Apolipoprotein E and Alzheimer disease: risk, mechanisms and therapy. Nat Rev Neurol. 2013 Feb;9(2):106-18. doi: 10.1038/nrneurol.2012.263. Epub 2013 Jan 8. Erratum in: Nat Rev Neurol. 2013. doi: 10.1038/nmeurol.2013.32. Liu, Chia-Chan [corrected to Liu, Chia-Chen]. PMID: 23296339; PMCID: PMC3726719.
- Liu H, Le W. Epigenetic modifications of chronic hypoxia-mediated neurodegeneration in Alzheimer's disease. Transl Neurodegener. 2014 Mar 20;3(1):7. doi: 10.1186/2047-9158-3-7. PMID: 24650677; PMCID: PMC3994488.
- Liu J, Jin X, Liu KJ, Liu W. Matrix metalloproteinase-2-mediated occludin degradation and caveolin-1-mediated claudin-5 redistribution contribute to blood-brain barrier damage in early ischemic stroke stage. J Neurosci. 2012 Feb 29;32(9):3044-57. doi: 10.1523/JNEUROSCI.6409-11.2012. PMID: 22378877; PMCID: PMC3339570.
- Liu Q, Ying G, Hu C, Du L, Zhang H, Wang Z, Yue H, Yetisen AK, Wang G, Shen Y, Jiang N. Engineering in vitro vascular microsystems. Microsyst Nanoeng. 2025 May 22;11(1):100. doi: 10.1038/s41378-025-00956-w. PMID: 40399285; PMCID: PMC12095634.
- Liu T, Zhang L, Joo D, Sun SC. NF-κB signaling in inflammation. Signal Transduct Target Ther. 2017;2:17023–. doi: 10.1038/sigtrans.2017.23. Epub 2017 Jul 14. PMID: 29158945; PMCID: PMC5661633.
- Love MI, Huber W, Anders S. Moderated estimation of fold change and dispersion for RNA-seq data with DESeq2. Genome Biol. 2014;15(12):550. doi: 10.1186/s13059-014-0550-8. PMID: 25516281; PMCID: PMC4302049.
- Lovestone S, Boada M, Dubois B, Hüll M, Rinne JO, Huppertz HJ, Calero M, Andrés MV, Gómez-Carrillo B, León T, del Ser T; ARGO investigators. A phase II trial of tideglusib in Alzheimer's disease. J Alzheimers Dis. 2015;45(1):75-88. doi: 10.3233/JAD-141959. PMID: 25537011.
- Lucchesi M, Marracci S, Amato R, Lapi D, Santana-Garrido Á, Espinosa-Martín P, Vázquez CM, Mate A, Dal Monte M. The Anti-Inflammatory and Antioxidant Properties of Acebuche Oil Exert a Retinoprotective Effect in a Murine Model of High-Tension Glaucoma. Nutrients. 2024 Jan 30;16(3):409. doi: 10.3390/nu16030409. PMID: 38337691; PMCID: PMC10857689.
- Lynch M, Pham W, Sinclair B, O'Brien TJ, Law M, Vivash L. Perivascular spaces as a potential biomarker of Alzheimer's disease. Front Neurosci. 2022 Oct 18;16:1021131. doi: 10.3389/fnins.2022.1021131. PMID: 36330347; PMCID: PMC9623161.

- Lynn SA, Pandi SPS, Sanchez-Bretano A, Muir AM, Parker L, Chatelet DS, Newall T, Scott JA, Keeling E, Smyth NR, Self JE, Lotery AJ, Lee H, Ratnayaka JA. A longitudinal study of the 5xFAD mouse retina delineates Amyloid beta (Aβ)-mediated retinal pathology from age-related changes. Alzheimers Res Ther. 2025 Jun 19;17(1):136. doi: 10.1186/s13195-025-01784-w. PMID: 40537856; PMCID: PMC12177965.
- MacKeigan, T.P.; Morgan, M.L.; Stys, P.K. Quantitation of Tissue Amyloid via Fluorescence Spectroscopy Using Controlled Concentrations of Thioflavin-S. Molecules 2023, 28, 4483. https: doi.org/10.3390/molecules28114483.
- Maggiore A, Latina V, D'Erme M, Amadoro G, Coccurello R. Non-canonical pathways associated to Amyloid beta and tau protein dyshomeostasis in Alzheimer's disease: A narrative review. Ageing Res Rev. 2024 Dec;102:102578. doi: 10.1016/j.arr.2024.102578. Epub 2024 Nov 13. PMID: 39542177.
- Mahajan N, Luo Q, Abhyankar S, Bhatwadekar AD. Transcriptomic Profile of Lin-Sca1+c-kit (LSK) cells in db/db mice with long-standing diabetes. BMC Genomics. 2024 Aug 12;25(1):782. doi: 10.1186/s12864-024-10679-3. PMID: 39134978; PMCID: PMC11318115.
- Makhaeva GF, Kovaleva NV, Boltneva NP, Lushchekina SV, Rudakova EV, Stupina TS, Terentiev AA, Serkov IV, Proshin AN, Radchenko EV, Palyulin VA, Bachurin SO, Richardson RJ. Conjugates of tacrine and 1,2,4-thiadiazole derivatives as new potential multifunctional agents for Alzheimer's disease treatment: Synthesis, quantum-chemical characterization, molecular docking, and biological evaluation. Bioorg Chem. 2020 Mar;96:103563. doi: 10.1016/j.bioorg.2019.103563. PMID: 31735356.
- Maldonado KA, Alsayouri K. Physiology, Brain. 2023 Mar 17. In: StatPearls [Internet]. Treasure Island (FL): StatPearls Publishing; 2025 Jan–. PMID: 31869182.
- Martin, Marcel. Cutadapt removes adapter sequences from high-throughput sequencing reads. EMBnet.journal, [S.l.], v. 17, n. 1, p. pp. 10-12, May 2011. ISSN 2226-6089. Available at: <https://journal.embnet.org/index.php/embnetjournal/article/view/200>. Date accessed: 02 Oct. 2025. doi:https://doi.org/10.14806/ej.17.1.200.
- Masland RH. The neuronal organization of the retina. Neuron. 2012 Oct 18;76(2):266-80. doi: 10.1016/j.neuron.2012.10.002. Epub 2012 Oct 17. PMID: 23083731; PMCID: PMC3714606.
- Masters CL, Bateman R, Blennow K, Rowe CC, Sperling RA, Cummings JL. Alzheimer's disease. Nat Rev Dis Primers. 2015 Oct 15;1:15056. doi: 10.1038/nrdp.2015.56. PMID: 27188934.
- Matei N, Leahy S, Blair NP, Burford J, Rahimi M, Shahidi M. Retinal Vascular Physiology Biomarkers in a 5XFAD Mouse Model of Alzheimer's Disease. Cells. 2022 Aug 4;11(15):2413. doi: 10.3390/cells11152413. PMID: 35954257; PMCID: PMC9368483.
- Mavilio A, Sisto D, Prete F, Guadalupi V, Dammacco R, Alessio G. RE-PERG in early-onset Alzheimer's disease: A double-blind, electrophysiological pilot study. PLoS One. 2020 Aug 13;15(8):e0236568. doi: 10.1371/journal.pone.0236568. PMID: 32790788; PMCID: PMC7425894.
- Mayhan WG, Heistad DD. Role of veins and cerebral venous pressure in disruption of the blood-brain barrier. Circ Res. 1986 Aug;59(2):216-20. doi: 10.1161/01.res.59.2.216. PMID: 3742745.

- McAnany JJ, Matei N, Chen YF, Liu K, Park JC, Shahidi M. Rod pathway and cone pathway retinal dysfunction in the 5xFAD mouse model of Alzheimer's disease. Sci Rep. 2021 Mar 1;11(1):4824. doi: 10.1038/s41598-021-84318-2. PMID: 33649406; PMCID: PMC7921657.
- McCool S, Smith JC, Sladek A, Fan S, Van Hook MJ. Retinal and thalamic alterations in the 5xFAD mouse model of Alzheimer's disease. PLoS One. 2025 Mar 3;20(3):e0319397. doi: 10.1371/journal.pone.0319397. PMID: 40029927; PMCID: PMC11875347.
- McCool S, Smith JC, Sladek A, Fan S, Van Hook MJ. Retinal and thalamic alterations in the 5xFAD mouse model of Alzheimer's disease. PLoS One. 2025 Mar 3;20(3):e0319397. doi: 10.1371/journal.pone.0319397. PMID: 40029927; PMCID: PMC11875347.
- McGleenon BM, Dynan KB, Passmore AP. Acetylcholinesterase inhibitors in Alzheimer's disease. Br J Clin Pharmacol. 1999 Oct;48(4):471-80. doi: 10.1046/j.1365-2125.1999.00026.x. PMID: 10583015; PMCID: PMC2014378.
- Mendez MF, Chavez D, Akhlaghipour G. Bilingualism Delays Expression of Alzheimer's Clinical Syndrome. Dement Geriatr Cogn Disord. 2019;48(5-6):281-289. doi: 10.1159/000505872. Epub 2020 Feb 11. PMID: 32045913; PMCID: PMC7195235.
- Merighi S, Nigro M, Travagli A, Gessi S. Microglia and Alzheimer's Disease. Int J Mol Sci. 2022 Oct 27;23(21):12990. doi: 10.3390/ijms232112990. PMID: 36361780; PMCID: PMC9657945.
- Miller BC, Eckman EA, Sambamurti K, Dobbs N, Chow KM, Eckman CB, Hersh LB, Thiele DL. Amyloid-beta peptide levels in brain are inversely correlated with insulysin activity levels in vivo. Proc Natl Acad Sci U S A. 2003 May 13;100(10):6221-6. doi: 10.1073/pnas.1031520100. Epub 2003 May 5. PMID: 12732730; PMCID: PMC156353.
- Molday RS, Moritz OL. Photoreceptors at a glance. J Cell Sci. 2015 Nov 15;128(22):4039-45. doi: 10.1242/jcs.175687. PMID: 26574505; PMCID: PMC4712787.
- Moreira PI, Carvalho C, Zhu X, Smith MA, Perry G. Mitochondrial dysfunction is a trigger of Alzheimer's disease pathophysiology. Biochim Biophys Acta. 2010 Jan;1802(1):2-10. doi: 10.1016/j.bbadis.2009.10.006. Epub 2009 Oct 21. PMID: 19853658.
- Morito T, Hashimoto S, Takamura R, Watamura N, Kakiya N, Fujioka R, Mihara N, Sekiguchi M, Watanabe-Iwata K, Kamano N, Qi M, Matsuba Y, Tsubuki S, Saito T, Iwata N, Sasaguri H, Saido TC. The Role of Neprilysin and Insulin-Degrading Enzyme in the Etiology of Sporadic Alzheimer's Disease. J Neurosci. 2025 Jun 4;45(23):e2152242025. doi: 10.1523/JNEUROSCI.2152-24.2025. PMID: 40300834; PMCID: PMC12139590.
- Murayi R, Chittiboina P. Glucocorticoids in the management of peritumoral brain edema: a review of molecular mechanisms. Child's Nerv Syst. 2016 Dec;32(12):2293-2302. doi: 10.1007/s00381-016-3240-x. Epub 2016 Sep 9. PMID: 27613642; PMCID: PMC5136308.
- Mure LS. Intrinsically Photosensitive Retinal Ganglion Cells of the Human Retina. Front Neurol. 2021 Mar 25;12:636330. doi: 10.3389/fneur.2021.636330. PMID: 33841306; PMCID: PMC8027232.

- Nair P, Lu M, Petersen S, Ashkenazi A. Apoptosis initiation through the cell-extrinsic pathway. Methods Enzymol. 2014;544:99-128. doi: 10.1016/B978-0-12-417158-9.00005-4. PMID: 24974288.
- Nelson AR, Sweeney MD, Sagare AP, Zlokovic BV. Neurovascular dysfunction and neurodegeneration in dementia and Alzheimer's disease. Biochim Biophys Acta. 2016 May;1862(5):887-900. doi: 10.1016/j.bbadis.2015.12.016. Epub 2015 Dec 17. PMID: 26705676; PMCID: PMC4821735.
- Nelson PT, Alafuzoff I, Bigio EH, Bouras C, Braak H, Cairns NJ, Castellani RJ, Crain BJ, Davies P, Del Tredici K, Duyckaerts C, Frosch MP, Haroutunian V, Hof PR, Hulette CM, Hyman BT, Iwatsubo T, Jellinger KA, Jicha GA, Kövari E, Kukull WA, Leverenz JB, Love S, Mackenzie IR, Mann DM, Masliah E, McKee AC, Montine TJ, Morris JC, Schneider JA, Sonnen JA, Thal DR, Trojanowski JQ, Troncoso JC, Wisniewski T, Woltjer RL, Beach TG. Correlation of Alzheimer disease neuropathologic changes with cognitive status: a review of the literature. J Neuropathol Exp Neurol. 2012 May;71(5):362-81. doi: 10.1097/NEN.0b013e31825018f7. PMID: 22487856; PMCID: PMC3560290.
- Nelson R, Connaughton V. Bipolar Cell Pathways in the Vertebrate Retina. 2007 May 24 [updated 2012 Jan 20]. In: Kolb H, Fernandez E, Jones B, Nelson R, editors. Webvision: The Organization of the Retina and Visual System [Internet]. Salt Lake City (UT): University of Utah Health Sciences Center; 1995–. PMID: 21413382.
- Nicoll JAR, Buckland GR, Harrison CH, Page A, Harris S, Love S, Neal JW, Holmes C, Boche D. Persistent neuropathological effects 14 years following amyloid-β immunization in Alzheimer's disease. Brain. 2019 Jul 1;142(7):2113-2126. doi: 10.1093/brain/awz142. PMID: 31157360; PMCID: PMC6598630.
- Niewiadomska G, Niewiadomski W, Steczkowska M, Gasiorowska A. Tau Oligomers Neurotoxicity. Life (Basel). 2021 Jan 6;11(1):28. doi: 10.3390/life11010028. PMID: 33418848; PMCID: PMC7824853.
- Nilsen J, Chen S, Irwin RW, Iwamoto S, Brinton RD. Estrogen protects neuronal cells from amyloid beta-induced apoptosis via regulation of mitochondrial proteins and function. BMC Neurosci. 2006 Nov 3;7:74. doi: 10.1186/1471-2202-7-74. PMID: 17083736; PMCID: PMC1636062.
- Normando, E.M., Davis, B.M., De Groef, L. et al. The retina as an early biomarker of neurodegeneration in a rotenone-induced model of Parkinson's disease: evidence for a neuroprotective effect of rosiglitazone in the eye and brain. acta Neuropathol Commun 4, 86 (2016). Doi:10.1186/s40478-016-0346-z.
- Oakley H, Cole SL, Logan S, Maus E, Shao P, Craft J, Guillozet-Bongaarts A, Ohno M, Disterhoft J, Van Eldik L, Berry R, Vassar R. Intraneuronal beta-amyloid aggregates, neurodegeneration, and neuron loss in transgenic mice with five familial Alzheimer's disease mutations: potential factors in amyloid plaque formation. J Neurosci. 2006 Oct 4;26(40):10129-40. doi: 10.1523/JNEUROSCI.1202-06.2006. PMID: 17021169; PMCID: PMC6674618.
- Obermeier B, Daneman R, Ransohoff RM. Development, maintenance and disruption of the blood-brain barrier. Nat Med. 2013 Dec;19(12):1584-96. doi: 10.1038/nm.3407. Epub 2013 Dec 5. PMID: 24309662; PMCID: PMC4080800.

- Oblak AL, Lin PB, Kotredes KP, Pandey RS, Garceau D, Williams HM, Uyar A, O'Rourke R, O'Rourke S, Ingraham C, Bednarczyk D, Belanger M, Cope ZA, Little GJ, Williams SG, Ash C, Bleckert A, Ragan T, Logsdon BA, Mangravite LM, Sukoff Rizzo SJ, Territo PR, Carter GW, Howell GR, Sasner M, Lamb BT. Comprehensive Evaluation of the 5XFAD Mouse Model for Preclinical Testing Applications: A MODEL-AD Study. Front Aging Neurosci. 2021 Jul 23;13:713726. doi: 10.3389/fnagi.2021.713726. PMID: 34366832; PMCID: PMC8346252.
- Ogawa S. Nutritional management of older adults with cognitive decline and dementia. Geriatr Gerontol Int. 2014 Apr;14 Suppl 2:17-22. doi: 10.1111/ggi.12252. PMID: 24650061.
- Osama A, Zhang J, Yao J, Yao X, Fang J. Nrf2: a dark horse in Alzheimer's disease treatment. Ageing Res Rev. 2020 Dec;64:101206. doi: 10.1016/j.arr.2020.101206. Epub 2020 Nov 2. PMID: 33144124.
- Ostrowitzki S, Bittner T, Sink KM, Mackey H, Rabe C, Honig LS, Cassetta E, Woodward M, Boada M, van Dyck CH, Grimmer T, Selkoe DJ, Schneider A, Blondeau K, Hu N, Quartino A, Clayton D, Dolton M, Dang Y, Ostaszewski B, Sanabria-Bohórquez SM, Rabbia M, Toth B, Eichenlaub U, Smith J, Honigberg LA, Doody RS. Evaluating the Safety and Efficacy of Crenezumab vs Placebo in Adults With Early Alzheimer Disease: Two Phase 3 Randomized Placebo-Controlled Trials. JAMA Neurol. 2022 Nov 1;79(11):1113-1121. doi: 10.1001/jamaneurol.2022.2909. PMID: 36121669; PMCID: PMC9486635.
- Ouyang Q, Liu K, Zhu Q, Deng H, Le Y, Ouyang W, Yan X, Zhou W, Tong J. Brain-Penetration and Neuron-Targeting DNA Nanoflowers Co-Delivering miR-124 and Rutin for Synergistic Therapy of Alzheimer's Disease. Small. 2022 Apr;18(14):e2107534. doi: 10.1002/smll.202107534. Epub 2022 Feb 19. PMID: 35182016.
- Pádua MS, Guil-Guerrero JL, Lopes PA. Behaviour Hallmarks in Alzheimer's Disease 5xFAD Mouse Model. Int J Mol Sci. 2024; 20;25(12):6766.
- Palko SI, Benoit MR, Yao AY, Mohan R, Yan R. ER-stress response in retinal Müller glia occurs significantly earlier than amyloid pathology in the Alzheimer's mouse brain and retina. Glia. 2024 Jun;72(6):1067-1081. doi: 10.1002/glia.24514. Epub 2024 Mar 18. PMID: 38497356; PMCID: PMC11006574.
- Palmer JC, Barker R, Kehoe PG, Love S. Endothelin-1 is elevated in Alzheimer's disease and upregulated by amyloid-β. J Alzheimers Dis. 2012;29(4):853-61. doi: 10.3233/JAD-2012-111760. PMID: 22330820.
- Panza F, Lozupone M, Logroscino G, Imbimbo BP. A critical appraisal of amyloid-β-targeting therapies for Alzheimer disease. Nat Rev Neurol. 2019 Feb;15(2):73-88. doi: 10.1038/s41582-018-0116-6. PMID: 30610216.
- Park JH, Hong JH, Lee SW, Ji HD, Jung JA, Yoon KW, Lee JI, Won KS, Song BI, Kim HW. The effect of chronic cerebral hypoperfusion on the pathology of Alzheimer's disease: A positron emission tomography study in rats. Sci Rep. 2019 Oct 1;9(1):14102. doi: 10.1038/s41598-019-50681-4. PMID: 31575996; PMCID: PMC6773854.

- Patel S, Bansoad AV, Singh R, Khatik GL. BACE1: A Key Regulator in Alzheimer's Disease Progression and Current Development of its Inhibitors. Curr Neuropharmacol. 2022;20(6):1174-1193. doi: 10.2174/1570159X19666211201094031. PMID: 34852746; PMCID: PMC9886827.
- Peng Y, Jin H, Xue YH, Chen Q, Yao SY, Du MQ, Liu S. Current and future therapeutic strategies for Alzheimer's disease: an overview of drug development bottlenecks. Front Aging Neurosci. 2023 Aug 3;15:1206572. doi: 10.3389/fnagi.2023.1206572. PMID: 37600514; PMCID: PMC10438465.
- Peng Y, Jin H, Xue YH, Chen Q, Yao SY, Du MQ, Liu S. Current and future therapeutic strategies for Alzheimer's disease: an overview of drug development bottlenecks. Front Aging Neurosci. 2023 Aug 3;15:1206572. doi: 10.3389/fnagi.2023.1206572. PMID: 37600514; PMCID: PMC10438465.
- Peng Y, Jin H, Xue YH, Chen Q, Yao SY, Du MQ, Liu S. Current and future therapeutic strategies for Alzheimer's disease: an overview of drug development bottlenecks. Front Aging Neurosci. 2023 Aug 3;15:1206572. doi: 10.3389/fnagi.2023.1206572. PMID: 37600514; PMCID: PMC10438465.
- Penke B, Szűcs M, Bogár F. Oligomerization and Conformational Change Turn Monomeric β-Amyloid and Tau Proteins Toxic: Their Role in Alzheimer's Pathogenesis. Molecules. 2020 Apr 3;25(7):1659. doi: 10.3390/molecules25071659. PMID: 32260279; PMCID: PMC7180792.
- Pistritto G, Trisciuoglio D, Ceci C, Garufi A, D'Orazi G. Apoptosis as anticancer mechanism: function and dysfunction of its modulators and targeted therapeutic strategies. Aging (Albany NY). 2016 Apr;8(4):603-19. doi: 10.18632/aging.100934. PMID: 27019364; PMCID: PMC4925817.
- Pradeepkiran JA, Baig J, Seman A, Reddy PH. Mitochondria in Aging and Alzheimer's Disease: Focus on Mitophagy. Neuroscientist. 2024 Aug;30(4):440-457. doi: 10.1177/10738584221139761. Epub 2023 Jan 3. PMID: 36597577.
- Prusky GT, West PW, Douglas RM. Behavioral assessment of visual acuity in mice and rats. Vision Res. 2000;40(16):2201-9. doi: 10.1016/s0042-6989(00)00081-x. PMID: 10878281.
- Ptito M, Bleau M, Bouskila J. The Retina: A Window into the Brain. Cells. 2021 Nov 23;10(12):3269. doi: 10.3390/cells10123269. PMID: 34943777; PMCID: PMC8699497.
- Qosa H, Mohamed LA, Batarseh YS, Alqahtani S, Ibrahim B, LeVine H 3rd, Keller JN, Kaddoumi A. Extra-virgin olive oil attenuates amyloid-β and tau pathologies in the brains of TgSwDI mice. J Nutr Biochem. 2015 Dec;26(12):1479-90. doi: 10.1016/j.jnutbio.2015.07.022. Epub 2015 Aug 13. PMID: 26344778; PMCID: PMC4679638.
- Rabinovici GD. Late-onset Alzheimer Disease. Continuum (Minneap Minn). 2019 Feb;25(1):14-33. doi: 10.1212/CON.0000000000000700. PMID: 30707185; PMCID: PMC6548536.
- Rahman S, Ikram AR, Azeem F, Tahir Ul Qamar M, Shaheen T, Mehboob-Ur-Rahman. Precision Genome Editing with CRISPR-Cas9. Methods Mol Biol. 2024;2788:355-372. doi: 10.1007/978-1-0716-3782-1_21. PMID: 38656525.
- Rathnasamy G, Foulds WS, Ling EA, Kaur C. Retinal microglia - A key player in healthy and diseased retina. Prog Neurobiol. 2019 Feb;173:18-40. doi: 10.1016/j.pneurobio.2018.05.006. Epub 2018 Jun 1. PMID: 29864456.

- Rehman A, Al Khalili Y. Neuroanatomy, Occipital Lobe. 2023 Jul 24. In: StatPearls [Internet]. Treasure Island (FL): StatPearls Publishing; 2025 Jan–. PMID: 31335040.
- Richard N, Arnold S, Hoeller U, Kilpert C, Wertz K, Schwager J. Hydroxytyrosol is the major anti-inflammatory compound in aqueous olive extracts and impairs cytokine and chemokine production in macrophages. Planta Med. 2011 Nov;77(17):1890-7. doi: 10.1055/s-0031-1280022. Epub 2011 Aug 9. PMID: 21830187.
- Rigacci S. Olive Oil Phenols as Promising Multi-targeting Agents Against Alzheimer's Disease. Adv Exp Med Biol. 2015;863:1-20. doi: 10.1007/978-3-319-18365-7_1. PMID: 26092624.
- Rodriguez BN, Huang H, Chia JJ, Hoffmann A. The noncanonical NFκB pathway: Regulatory mechanisms in health and disease. WIREs Mech Dis. 2024 Nov-Dec;16(6):e1646. doi: 10.1002/wsbm.1646. Epub 2024 Apr 18. PMID: 38634218; PMCID: PMC11486840.
- Ru Y, Kechris KJ, Tabakoff B, Hoffman P, Radcliffe RA, Bowler R, Mahaffey S, Rossi S, Calin GA, Bemis L, Theodorescu D. The multiMiR R package and database: integration of microRNA-target interactions along with their disease and drug associations. Nucleic Acids Res. 2014;42(17):e133. doi: 10.1093/nar/gku631. Epub 2014 Jul 24. PMID: 25063298; PMCID: PMC4176155.
- Rudolph S, Badura A, Lutzu S, Pathak SS, Thieme A, Verpeut JL, Wagner MJ, Yang YM, Fioravante D. Cognitive-Affective Functions of the Cerebellum. J Neurosci. 2023 Nov 8;43(45):7554-7564. doi: 10.1523/JNEUROSCI.1451-23.2023. PMID: 37940582; PMCID: PMC10634583.
- Rumble SM, Lacroute P, Dalca AV, Fiume M, Sidow A, Brudno M. SHRiMP: accurate mapping of short color-space reads. PLoS Comput Biol. 2009 May;5(5):e1000386. doi: 10.1371/journal.pcbi.1000386. Epub 2009 May 22. PMID: 19461883; PMCID: PMC2678294.
- Safadi AO, Tadi P. Anatomy, Head and Neck: Cerebral Venous System. 2023 Jul 24. In: StatPearls [Internet]. Treasure Island (FL): StatPearls Publishing; 2025 Jan–. PMID: 32809331.
- Saido T, Leissring MA. Proteolytic degradation of amyloid β-protein. Cold Spring Harb Perspect Med. 2012 Jun;2(6):a006379. doi: 10.1101/cshperspect.a006379. PMID: 22675659; PMCID: PMC3367539.
- Salloway S, Honigberg LA, Cho W, Ward M, Friesenhahn M, Brunstein F, Quartino A, Clayton D, Mortensen D, Bittner T, Ho C, Rabe C, Schauer SP, Wildsmith KR, Fuji RN, Suliman S, Reiman EM, Chen K, Paul R. Amyloid positron emission tomography and cerebrospinal fluid results from a crenezumab anti-amyloid-beta antibody double-blind, placebo-controlled, randomized phase II study in mild-to-moderate Alzheimer's disease (BLAZE). Alzheimers Res Ther. 2018 Sep 19;10(1):96. doi: 10.1186/s13195-018-0424-5. PMID: 30231896; PMCID: PMC6146627.
- Salminen A, Kauppinen A, Kaarniranta K. Hypoxia/ischemia activate processing of Amyloid Precursor Protein: impact of vascular dysfunction in the pathogenesis of Alzheimer's disease. J Neurochem. 2017 Feb;140(4):536-549. doi: 10.1111/jnc.13932. Epub 2017 Jan 9. PMID: 27987381.
- Sánchez CQ, Schmitt FW, Curdt N, Westhoff AC, Bänfer IWH, Bayer TA, Bouter Y. Search Strategy Analysis of 5xFAD Alzheimer Mice in the Morris Water Maze Reveals Sex- and Age-Specific Spatial

Navigation Deficits. Biomedicines. 2023 Feb 17;11(2):599. doi: 10.3390/biomedicines11020599. PMID: 36831135; PMCID: PMC9953202.

- Sanchez-Varo R, Mejias-Ortega M, Fernandez-Valenzuela JJ, Nuñez-Diaz C, Caceres-Palomo L, Vegas-Gomez L, Sanchez-Mejias E, Trujillo-Estrada L, Garcia-Leon JA, Moreno-Gonzalez I, Vizuete M, Vitorica J, Baglietto-Vargas D, Gutierrez A. Transgenic Mouse Models of Alzheimer's Disease: An Integrative Analysis. Int J Mol Sci. 2022 May 12;23(10):5404. doi: 10.3390/ijms23105404. PMID: 35628216; PMCID: PMC9142061.
- Santana-Garrido Á, Reyes-Goya C, André H, Vázquez CM, Mate A. Exploring the Potential of Wild Olive (Acebuche) Oil as a Pharm-Food to Prevent Ocular Hypertension and Fibrotic Events in the Retina of Hypertensive Mice. Mol Nutr Food Res. 2024 Feb;68(3):e2200623. doi: 10.1002/mnfr.202200623. Epub 2023 Dec 3. PMID: 38044285.
- Santana-Garrido Á, Reyes-Goya C, Milla-Navarro S, de la Villa P, André H, Vázquez CM, Mate A. Anti-Inflammatory Action of Dietary Wild Olive (Acebuche) Oil in the Retina of Hypertensive Mice. Foods. 2021 Aug 25;10(9):1993. doi: 10.3390/foods10091993. PMID: 34574102; PMCID: PMC8466332.
- Santana-Garrido Á, Reyes-Goya C, Pérez-Camino MC, André H, Mate A, Vázquez CM. Retinoprotective Effect of Wild Olive (Acebuche) Oil-Enriched Diet against Ocular Oxidative Stress Induced by Arterial Hypertension. Antioxidants (Basel). 2020 Sep 18;9(9):885. doi: 10.3390/antiox9090885. PMID: 32961933; PMCID: PMC7555058.
- Sasaguri H, Takamura R, Watamura N, Kakiya N, Ohshima T, Fujioka R, Yamazaki N, Sekiguchi M, Iwata K, Matsuba Y, Hashimoto S, Tsubuki S, Saito T, Iwata N, Saido TC. Neprilysin-sensitive amyloidogenic Aβ versus IDE-sensitive soluble Aβ: a probable mechanistic cause for sporadic Alzheimer's disease. bioRxiv 2021.08.22.457281; doi: https://doi.org/10.1101/2021.08.22.457281.
- Schafer ZT, Kornbluth S. The apoptosome: physiological, developmental, and pathological modes of regulation. Dev Cell. 2006 May;10(5):549-61. doi: 10.1016/j.devcel.2006.04.008. PMID: 16678772.
- Schiavone S, Trabace L. Small Molecules: Therapeutic Application in Neuropsychiatric and Neurodegenerative Disorders. Molecules. 2018 Feb 13;23(2):411. doi: 10.3390/molecules23020411. PMID: 29438357; PMCID: PMC6017408.
- Schilling S, Pradhan A, Heesch A, Helbig A, Blennow K, Koch C, Bertgen L, Koo EH, Brinkmalm G, Zetterberg H, Kins S, Eggert S. Differential effects of familial Alzheimer's disease-causing mutations on amyloid precursor protein (APP) trafficking, proteolytic conversion, and synaptogenic activity. Acta Neuropathol Commun. 2023 Jun 1;11(1):87. doi: 10.1186/s40478-023-01577-y. PMID: 37259128; PMCID: PMC10234039.
- Shevtsova EF, Maltsev AV, Vinogradova DV, Shevtsov PN, Bachurin SO. Mitochondria as a promising target for developing novel agents for treating Alzheimer's disease. Med Res Rev. 2021 Mar;41(2):803-827. doi: 10.1002/med.21715. Epub 2020 Jul 20. PMID: 32687230.
- Shi L, Winchester LM, Westwood S, Baird AL, Anand SN, Buckley NJ, Hye A, Ashton NJ, Bos I, Vos SJB, Kate MT, Scheltens P, Teunissen CE, Vandenberghe R, Gabel S, Meersmans K, Engelborghs S, De

Roeck EE, Sleegers K, Frisoni GB, Blin O, Richardson JC, Bordet R, Molinuevo JL, Rami L, Wallin A, Kettunen P, Tsolaki M, Verhey F, Lléo A, Sala I, Popp J, Peyratout G, Martinez-Lage P, Tainta M, Johannsen P, Freund-Levi Y, Frölich L, Dobricic V, Legido-Quigley C, Barkhof F, Andreasson U, Blennow K, Zetterberg H, Streffer J, Lill CM, Bertram L, Visser PJ, Kolb HC, Narayan VA, Lovestone S, Nevado-Holgado AJ. Replication study of plasma proteins relating to Alzheimer's pathology. Alzheimers Dement. 2021 Sep;17(9):1452-1464. doi: 10.1002/alz.12322. Epub 2021 Mar 31. PMID: 33792144.

- Shibly AZ, Sheikh AM, Michikawa M, Tabassum S, Azad AK, Zhou X, Zhang Y, Yano S, Nagai A. Analysis of Cerebral Small Vessel Changes in AD Model Mice. Biomedicines. 2022 Dec 25;11(1):50. doi: 10.3390/biomedicines11010050. Erratum in: Biomedicines. 2024 Jan 04;12(1):104. doi: 10.3390/biomedicines12010104. PMID: 36672558; PMCID: PMC9855388.
- Shin HJ, Kim IS, Choi SG, Lee K, Park H, Shin J, Kim D, Beom J, Yi YY, Gupta DP, Song GJ, Chung WS, Lee CJ, Kim DW. Rejuvenating aged microglia by p16ink4a-siRNA-loaded nanoparticles increases amyloid-β clearance in animal models of Alzheimer's disease. Mol Neurodegener. 2024 Mar 16;19(1):25. doi: 10.1186/s13024-024-00715-x. PMID: 38493185; PMCID: PMC10943801.
- Silva-Llanes I, Madruga E, Martínez A, Lastres-Becker I. RIPK1 expression and inhibition in tauopathies: implications for neuroinflammation and neuroprotection. Front Neurosci. 2025 Jan 27;18:1530809. doi: 10.3389/fnins.2024.1530809. PMID: 39931431; PMCID: PMC11808139.
- Sivamaruthi BS, Raghani N, Chorawala M, Bhattacharya S, Prajapati BG, Elossaily GM, Chaiyasut C. NF-κB Pathway and Its Inhibitors: A Promising Frontier in the Management of Alzheimer's Disease. Biomedicines. 2023 Sep 21;11(9):2587. doi: 10.3390/biomedicines11092587. PMID: 37761028; PMCID: PMC10526355.
- Solis E Jr, Hascup KN, Hascup ER. Alzheimer's Disease: The Link Between Amyloid-β and Neurovascular Dysfunction. J Alzheimers Dis. 2020;76(4):1179-1198. doi: 10.3233/JAD-200473. PMID: 32597813; PMCID: PMC7483596.
- Song D, Li Y, Yang LL, Luo YX, Yao XQ. Bridging systemic metabolic dysfunction and Alzheimer's disease: the liver interface. Mol Neurodegener. 2025 May 28;20(1):61. doi: 10.1186/s13024-025-00849-6. PMID: 40437610; PMCID: PMC12121119.
- Stefaniak O, Dobrzyńska M, Drzymała-Czyż S, Przysławski J. Diet in the Prevention of Alzheimer's Disease: Current Knowledge and Future Research Requirements. Nutrients. 2022 Oct 30;14(21):4564. doi: 10.3390/nu14214564. PMID: 36364826; PMCID: PMC9656789.
- Stiles J, Jernigan TL. The basics of brain development. Neuropsychol Rev. 2010 Dec;20(4):327-48. doi: 10.1007/s11065-010-9148-4. Epub 2010 Nov 3. PMID: 21042938; PMCID: PMC2989000.
- Sugiyama S, Sasaki T, Tanaka H, Yan H, Ikegami T, Kanki H, Nishiyama K, Beck G, Gon Y, Okazaki S, Todo K, Tamura A, Tsukita S, Mochizuki H. The tight junction protein occludin modulates blood-brain barrier integrity and neurological function after ischemic stroke in mice. Sci Rep. 2023 Feb 18;13(1):2892. doi: 10.1038/s41598-023-29894-1. PMID: 36806348; PMCID: PMC9938878.

- Sun E, Motolani A, Campos L, Lu T. The Pivotal Role of NF-kB in the Pathogenesis and Therapeutics of Alzheimer's Disease. Int J Mol Sci. 2022 Aug 11;23(16):8972. doi: 10.3390/ijms23168972. PMID: 36012242; PMCID: PMC9408758.
- Sun E, Motolani A, Campos L, Lu T. The Pivotal Role of NF-kB in the Pathogenesis and Therapeutics of Alzheimer's Disease. Int J Mol Sci. 2022 Aug 11;23(16):8972. doi: 10.3390/ijms23168972. PMID: 36012242; PMCID: PMC9408758.
- Sun SC. Non-canonical NF-κB signaling pathway. Cell Res. 2011 Jan;21(1):71-85. doi: 10.1038/cr.2010.177. Epub 2010 Dec 21. PMID: 21173796; PMCID: PMC3193406.
- Sun X, He G, Qing H, Zhou W, Dobie F, Cai F, Staufenbiel M, Huang LE, Song W. Hypoxia facilitates Alzheimer's disease pathogenesis by up-regulating BACE1 gene expression. Proc Natl Acad Sci U S A. 2006 Dec 5;103(49):18727-32. doi: 10.1073/pnas.0606298103. Epub 2006 Nov 22. PMID: 17121991; PMCID: PMC1693730.
- Sun Z, Zhang X, So KF, Jiang W, Chiu K. Targeting Microglia in Alzheimer's Disease: Pathogenesis and Potential Therapeutic Strategies. Biomolecules. 2024 Jul 11;14(7):833. doi: 10.3390/biom14070833. PMID: 39062547; PMCID: PMC11274940.
- Sweeney MD, Ayyadurai S, Zlokovic BV. Pericytes of the neurovascular unit: key functions and signaling pathways. Nat Neurosci. 2016 May 26;19(6):771-83. doi: 10.1038/nn.4288. PMID: 27227366; PMCID: PMC5745011.
- Sweeney MD, Kisler K, Montagne A, Toga AW, Zlokovic BV. The role of brain vasculature in neurodegenerative disorders. Nat Neurosci. 2018 Oct;21(10):1318-1331. doi: 10.1038/s41593-018-0234-x. Epub 2018 Sep 24. PMID: 30250261; PMCID: PMC6198802.
- Sweeney MD, Sagare AP, Zlokovic BV. Blood-brain barrier breakdown in Alzheimer disease and other neurodegenerative disorders. Nat Rev Neurol. 2018 Mar;14(3):133-150. doi: 10.1038/nrneurol.2017.188. Epub 2018 Jan 29. PMID: 29377008; PMCID: PMC5829048.
- Sylvie Claeysen, Patrizia Giannoni, Caroline Ismeurt. The 5×FAD mouse model of Alzheimer's disease. The Neuroscience of Dementia, 1 (Chapter 13), Academic Press, pp.207-221, 2020, Diagnosis and Management in Dementia, 9780128158548. ⟨10.1016/B978-0-12-815854-8.00013-6⟩.
- Szu JI, Obenaus A. Cerebrovascular phenotypes in mouse models of Alzheimer's disease. J Cereb Blood Flow Metab. 2021 Aug;41(8):1821-1841. doi: 10.1177/0271678X21992462. Epub 2021 Feb 8. PMID: 33557692; PMCID: PMC8327123.
- Tan JZA, Gleeson PA. The role of membrane trafficking in the processing of amyloid precursor protein and production of amyloid peptides in Alzheimer's disease. Biochim Biophys Acta Biomembr. 2019 Apr 1;1861(4):697-712. doi: 10.1016/j.bbamem.2018.11.013. Epub 2019 Jan 11. PMID: 30639513.
- Tao B, Gong W, Xu C, Ma Z, Mei J, Chen M. The relationship between hypoxia and Alzheimer's disease: an updated review. Front Aging Neurosci. 2024 Jul 17;16:1402774. doi: 10.3389/fnagi.2024.1402774. PMID: 39086755; PMCID: PMC11288848.

- Tarawneh R. Microvascular Contributions to Alzheimer Disease Pathogenesis: Is Alzheimer Disease Primarily an Endotheliopathy? Biomolecules. 2023 May 13;13(5):830. doi: 10.3390/biom13050830. PMID: 37238700; PMCID: PMC10216678.
- Tartaglia MC, Ingelsson M. Molecular Therapeutics in Development to Treat Alzheimer's Disease. Mol Diagn Ther. 2025 Jan;29(1):9-24. doi: 10.1007/s40291-024-00738-6. Epub 2024 Sep 24. Erratum in: Mol Diagn Ther. 2025 Jan;29(1):143. doi: 10.1007/s40291-024-00752-8. PMID: 39316339; PMCID: PMC11748464.
- Tartaglia MC, Ingelsson M. Molecular Therapeutics in Development to Treat Alzheimer's Disease. Mol Diagn Ther. 2025 Jan;29(1):9-24. doi: 10.1007/s40291-024-00738-6. Epub 2024 Sep 24. Erratum in: Mol Diagn Ther. 2025 Jan;29(1):143. doi: 10.1007/s40291-024-00752-8. PMID: 39316339; PMCID: PMC11748464.
- Thordardottir S, Kinhult Ståhlbom A, Almkvist O, Thonberg H, Eriksdotter M, Zetterberg H, Blennow K, Graff C. The effects of different familial Alzheimer's disease mutations on APP processing in vivo. Alzheimers Res Ther. 2017 Feb 16;9(1):9. doi: 10.1186/s13195-017-0234-1. PMID: 28209190; PMCID: PMC5312523.
- Trares K, Ackermann J, Koch I. The canonical and non-canonical NF-κB pathways and their crosstalk: A comparative study based on Petri nets. Biosystems. 2022 Jan;211:104564. doi: 10.1016/j.biosystems.2021.104564. Epub 2021 Oct 22. PMID: 34688841.
- Uddin MS, Lim LW. Glial cells in Alzheimer's disease: From neuropathological changes to therapeutic implications. Ageing Res Rev. 2022 Jun;78:101622. doi: 10.1016/j.arr.2022.101622. Epub 2022 Apr 12. PMID: 35427810.
- Urbanc B, Cruz L, Le R, Sanders J, Ashe KH, Duff K, Stanley HE, Irizarry MC, Hyman BT. Neurotoxic effects of thioflavin S-positive amyloid deposits in transgenic mice and Alzheimer's disease. Proc Natl Acad Sci U S A. 2002 Oct 29;99(22):13990-5. doi: 10.1073/pnas.222433299. Epub 2002 Oct 9. PMID: 12374847; PMCID: PMC137824.
- van Dyck CH, Swanson CJ, Aisen P, Bateman RJ, Chen C, Gee M, Kanekiyo M, Li D, Reyderman L, Cohen S, Froelich L, Katayama S, Sabbagh M, Vellas B, Watson D, Dhadda S, Irizarry M, Kramer LD, Iwatsubo T. Lecanemab in Early Alzheimer's Disease. N Engl J Med. 2023 Jan 5;388(1):9-21. doi: 10.1056/NEJMoa2212948. Epub 2022 Nov 29. PMID: 36449413.
- van Dyck CH, Swanson CJ, Aisen P, Bateman RJ, Chen C, Gee M, Kanekiyo M, Li D, Reyderman L, Cohen S, Froelich L, Katayama S, Sabbagh M, Vellas B, Watson D, Dhadda S, Irizarry M, Kramer LD, Iwatsubo T. Lecanemab in Early Alzheimer's Disease. N Engl J Med. 2023 Jan 5;388(1):9-21. doi: 10.1056/NEJMoa2212948. Epub 2022 Nov 29. PMID: 36449413.
- Vázquez-Liébanas E, Mocci G, Li W, Laviña B, Reddy A, O'Connor C, Hudson N, Elbeck Z, Nikoloudis I, Gaengel K, Vanlandewijck M, Campbell M, Betsholtz C, Mäe MA. Mosaic deletion of claudin-5 reveals rapid non-cell-autonomous consequences of blood-brain barrier leakage. Cell Rep. 2024 Mar 26;43(3):113911. doi: 10.1016/j.celrep.2024.113911. Epub 2024 Mar 5. PMID: 38446668.

- Villarreal AE, Grajales S, O'Bryant SE, Edwards M, López L, Montalván A, Britton GB; Panama Aging Research Initiative (PARI). Characterization of Alzheimer's Disease and Mild Cognitive Impairment in Older Adults in Panama. J Alzheimers Dis. 2016 Oct 4;54(3):897-901. doi: 10.3233/JAD-160402. PMID: 27567849.
- Villavicencio Tejo F, Quintanilla RA. Contribution of the Nrf2 Pathway on Oxidative Damage and Mitochondrial Failure in Parkinson and Alzheimer's Disease. Antioxidants (Basel). 2021 Jul 2;10(7):1069. doi: 10.3390/antiox10071069. PMID: 34356302; PMCID: PMC8301100.
- Wang C, Zong S, Cui X, Wang X, Wu S, Wang L, Liu Y, Lu Z. The effects of microglia-associated neuroinflammation on Alzheimer's disease. Front Immunol. 2023 Feb 22;14:1117172. doi: 10.3389/fimmu.2023.1117172. PMID: 36911732; PMCID: PMC9992739.
- Wang M, Qin L, Tang B. MicroRNAs in Alzheimer's Disease. Front Genet. 2019 Mar 1;10:153. doi: 10.3389/fgene.2019.00153. PMID: 30881384; PMCID: PMC6405631.
- Wang Q, Huang X, Su Y, Yin G, Wang S, Yu B, Li H, Qi J, Chen H, Zeng W, Zhang K, Verkhratsky A, Niu J, Yi C. Activation of Wnt/β-catenin pathway mitigates blood-brain barrier dysfunction in Alzheimer's disease. Brain. 2022 Dec 19;145(12):4474-4488. doi: 10.1093/brain/awac236. PMID: 35788280; PMCID: PMC9762951.
- Wang, M., Jo, J. & Song, J. Adiponectin improves long-term potentiation in the 5XFAD mouse brain. Sci Rep 9, 8918 (2019). https://doi.org/10.1038/s41598-019-45509-0.
- Wang, X., Xie, J., Tan, L. et al. N6-methyladenosine-modified circRIMS2 mediates synaptic and memory impairments by activating GluN2B ubiquitination in Alzheimer's disease. Transl Neurodegener 12, 53 (2023). doi:org/10.1186/s40035-023-00386-6.
- Weller RO, Subash M, Preston SD, Mazanti I, Carare RO. Perivascular drainage of amyloid-beta peptides from the brain and its failure in cerebral amyloid angiopathy and Alzheimer's disease. Brain Pathol. 2008 Apr;18(2):253-66. doi: 10.1111/j.1750-3639.2008.00133.x. PMID: 18363936; PMCID: PMC8095597.
- Wilkinson D, Windfeld K, Colding-Jørgensen E. Safety and efficacy of idalopirdine, a 5-HT6 receptor antagonist, in patients with moderate Alzheimer's disease (LADDER): a randomised, double-blind, placebo-controlled phase 2 trial. Lancet Neurol. 2014 Nov;13(11):1092-1099. doi: 10.1016/S1474-4422(14)70198-X. Epub 2014 Oct 5. PMID: 25297016.
- Willem M, Tahirovic S, Busche MA, Ovsepian SV, Chafai M, Kootar S, Hornburg D, Evans LD, Moore S, Daria A, Hampel H, Müller V, Giudici C, Nuscher B, Wenninger-Weinzierl A, Kremmer E, Heneka MT, Thal DR, Giedraitis V, Lannfelt L, Müller U, Livesey FJ, Meissner F, Herms J, Konnerth A, Marie H, Haass C. η-Secretase processing of APP inhibits neuronal activity in the hippocampus. Nature. 2015 Oct 15;526(7573):443-7. doi: 10.1038/nature14864. Epub 2015 Aug 31. PMID: 26322584; PMCID: PMC6570618.
- Williams JB, Cao Q, Yan Z. Transcriptomic analysis of human brains with Alzheimer's disease reveals the altered expression of synaptic genes linked to cognitive deficits. Brain Commun. 2021 Jun 3;3(3):fcab123. doi: 10.1093/braincomms/fcab123. PMID: 34423299; PMCID: PMC8374979.

- Willis BA, Zhang W, Ayan-Oshodi M, Lowe SL, Annes WF, Sirois PJ, Friedrich S, de la Peña A. Semagacestat pharmacokinetics are not significantly affected by formulation, food, or time of dosing in healthy participants. J Clin Pharmacol. 2012 Jun;52(6):904-13. doi: 10.1177/0091270011407195. Epub 2011 Jul 1. PMID: 21724950.
- Wilson DF, Matschinsky FM. Cerebrovascular Blood Flow Design and Regulation; Vulnerability in Aging Brain. Front Physiol. 2020 Oct 16;11:584891. doi: 10.3389/fphys.2020.584891. PMID: 33178048; PMCID: PMC7596697.
- Wischik CM, Staff RT, Wischik DJ, Bentham P, Murray AD, Storey JM, Kook KA, Harrington CR. Tau aggregation inhibitor therapy: an exploratory phase 2 study in mild or moderate Alzheimer's disease. J Alzheimers Dis. 2015;44(2):705-20. doi: 10.3233/JAD-142874. PMID: 25550228.
- Wolfe MS. Structure and Function of the γ-Secretase Complex. Biochemistry. 2019 Jul 9;58(27):2953-2966. doi: 10.1021/acs.biochem.9b00401. Epub 2019 Jun 25. PMID: 31198028; PMCID: PMC6618299.
- Wu B, Liu Y, Li H, Zhu L, Zeng L, Zhang Z, Peng W. Liver as a new target organ in Alzheimer's disease: insight from cholesterol metabolism and its role in amyloid-beta clearance. Neural Regen Res. 2025 Mar 1;20(3):695-714. doi: 10.4103/1673-5374.391305. Epub 2023 Dec 21. PMID: 38886936; PMCID: PMC11433892.
- Xu QA, Boerkoel P, Hirsch-Reinshagen V, Mackenzie IR, Hsiung GR, Charm G, To EF, Liu AQ, Schwab K, Jiang K, Sarunic M, Beg MF, Pham W, Cui J, To E, Lee S, Matsubara JA. Müller cell degeneration and microglial dysfunction in the Alzheimer's retina. Acta Neuropathol Commun. 2022 Oct 5;10(1):145. doi: 10.1186/s40478-022-01448-y. PMID: 36199154; PMCID: PMC9533552.
- Xu Z, Zhang K, Wang Q, Zheng Y. MicroRNA-124 improves functional recovery and suppresses Bax-dependent apoptosis in rats following spinal cord injury. Mol Med Rep. 2019 Apr;19(4):2551-2560. doi: 10.3892/mmr.2019.9904. Epub 2019 Jan 28. PMID: 30720072; PMCID: PMC6423616.
- Yamazaki Y, Shinohara M, Shinohara M, Yamazaki A, Murray ME, Liesinger AM, Heckman MG, Lesser ER, Parisi JE, Petersen RC, Dickson DW, Kanekiyo T, Bu G. Selective loss of cortical endothelial tight junction proteins during Alzheimer's disease progression. Brain. 2019 Apr 1;142(4):1077-1092. doi: 10.1093/brain/awz011. PMID: 30770921; PMCID: PMC6439325.
- Yang S, Zhou J, Li D. Functions and Diseases of the Retinal Pigment Epithelium. Front Pharmacol. 2021 Jul 28;12:727870. doi: 10.3389/fphar.2021.727870. PMID: 34393803; PMCID: PMC8355697.
- Yang TH, Kang EY, Lin PH, Yu BB, Wang JH, Chen V, Wang NK. Mitochondria in Retinal Ganglion Cells: Unraveling the Metabolic Nexus and Oxidative Stress. Int J Mol Sci. 2024 Aug 7;25(16):8626. doi: 10.3390/ijms25168626. PMID: 39201313; PMCID: PMC11354650.
- Yanumula A, Cusick JK. Biochemistry, Extrinsic Pathway of Apoptosis. 2023 Jul 31. In: StatPearls [Internet]. Treasure Island (FL): StatPearls Publishing; 2025 Jan–. PMID: 32809646.
- Yao M, Nguyen TV, Pike CJ. Beta-amyloid-induced neuronal apoptosis involves c-Jun N-terminal kinase-dependent downregulation of Bcl-w. J Neurosci. 2005 Feb 2;25(5):1149-58. doi: 10.1523/JNEUROSCI.4736-04.2005. PMID: 15689551; PMCID: PMC6725978.

- Yu G, Wang LG, Han Y, He QY. clusterProfiler: an R package for comparing biological themes among gene clusters. OMICS. 2012 May;16(5):284-7. doi: 10.1089/omi.2011.0118. Epub 2012 Mar 28. PMID: 22455463; PMCID: PMC3339379.
- Yu X, Ji C, Shao A. Neurovascular Unit Dysfunction and Neurodegenerative Disorders. Front Neurosci. 2020 Apr 29;14:334. doi: 10.3389/fnins.2020.00334. PMID: 32410936; PMCID: PMC7201055.
- Yu Y, Chen R, Mao K, Deng M, Li Z. The Role of Glial Cells in Synaptic Dysfunction: Insights into Alzheimer's Disease Mechanisms. Aging Dis. 2024 Apr 1;15(2):459-479. doi: 10.14336/AD.2023.0718. PMID: 37548934; PMCID: PMC10917533.
- Zamecnik PC, Stephenson ML. Inhibition of Rous sarcoma virus replication and cell transformation by a specific oligodeoxynucleotide. Proc Natl Acad Sci U S A. 1978 Jan;75(1):280-4. doi: 10.1073/pnas.75.1.280. PMID: 75545; PMCID: PMC411230.
- Zhang H, Liu D, Wang Y, Huang H, Zhao Y, Zhou H. Meta-analysis of expression and function of neprilysin in Alzheimer's disease. Neurosci Lett. 2017 Sep 14;657:69-76. doi: 10.1016/j.neulet.2017.07.060. Epub 2017 Aug 2. PMID: 28778804.
- Zhang J, Gao F, Ma Y, Xue T, Shen Y. Identification of early-onset photoreceptor degeneration in transgenic mouse models of Alzheimer's disease. iScience. 2021 Oct 21;24(11):103327. doi: 10.1016/j.isci.2021.103327. PMID: 34805789; PMCID: PMC8581578.
- Zhang J, Gao F, Ma Y, Xue T, Shen Y. Identification of early-onset photoreceptor degeneration in transgenic mouse models of Alzheimer's disease. iScience. 2021 Oct 21;24(11):103327. doi: 10.1016/j.isci.2021.103327. PMID: 34805789; PMCID: PMC8581578.
- Zhang M, Zhong L, Han X, Xiong G, Xu D, Zhang S, Cheng H, Chiu K, Xu Y. Brain and Retinal Abnormalities in the 5xFAD Mouse Model of Alzheimer's Disease at Early Stages. Front Neurosci. 2021 Jul 23;15:681831. doi: 10.3389/fnins.2021.681831. PMID: 34366774; PMCID: PMC8343228.
- Zhang M, Zhong L, Han X, Xiong G, Xu D, Zhang S, Cheng H, Chiu K, Xu Y. Brain and Retinal Abnormalities in the 5xFAD Mouse Model of Alzheimer's Disease at Early Stages. Front Neurosci. 2021 Jul 23;15:681831. doi: 10.3389/fnins.2021.681831. PMID: 34366774; PMCID: PMC8343228.
- Zhang X, Le W. Pathological role of hypoxia in Alzheimer's disease. Exp Neurol. 2010 Jun;223(2):299-303. doi: 10.1016/j.expneurol.2009.07.033. Epub 2009 Aug 11. PMID: 19679125.
- Zhang X, Zhou K, Wang R, Cui J, Lipton SA, Liao FF, Xu H, Zhang YW. Hypoxia-inducible factor 1alpha (HIF-1alpha)-mediated hypoxia increases BACE1 expression and beta-amyloid generation. J Biol Chem. 2007 Apr 13;282(15):10873-80. doi: 10.1074/jbc.M608856200. Epub 2007 Feb 15. PMID: 17303576.
- Zhao X, Sun J, Xiong L, She L, Li L, Tang H, Zeng Y, Chen F, Han X, Ye S, Wang W, Wang X, Liang G. β-amyloid binds to microglia Dectin-1 to induce inflammatory response in the pathogenesis of Alzheimer's disease. Int J Biol Sci. 2023 Jun 19;19(10):3249-3265. doi: 10.7150/ijbs.81900. PMID: 37416769; PMCID: PMC10321287.

- Zhong MZ, Peng T, Duarte ML, Wang M, Cai D. Updates on mouse models of Alzheimer's disease. Mol Neurodegener. 2024 Mar 11;19(1):23. doi: 10.1186/s13024-024-00712-0. PMID: 38462606; PMCID: PMC10926682.
- Zhu N, Wei M, Yuan L, He X, Chen C, Ji A, Zhang G. Claudin-5 relieves cognitive decline in Alzheimer's disease mice through suppression of inhibitory GABAergic neurotransmission. Aging (Albany NY). 2022 Apr 26;14(8):3554-3568. doi: 10.18632/aging.204029. Epub 2022 Apr 26. PMID: 35471411; PMCID: PMC9085235.
- Zlokovic BV. Neurovascular pathways to neurodegeneration in Alzheimer's disease and other disorders. Nat Rev Neurosci. 2011 Nov 3;12(12):723-38. doi: 10.1038/nrn3114. PMID: 22048062; PMCID: PMC4036520.

Disclosure statement on the use of generative AI in this PhD thesis

This disclaimer is not intended to discourage the use of generative Artificial Intelligence (AI), but rather to promote its critical, informed, and transparent use, in line with the principles of academic integrity. The purpose of this disclosure is to provide transparency regarding the role of AI in shaping the content and methodology of my research to align with the **fundamental principles of research integrity** reported by The European Code of Conduct for Research Integrity by European Federation of Academies of Sciences and Humanities (ALLEA) in 2023 (Revised Edition. Berlin. DOI 10.26356/ECOC) as reported below:

- **Reliability** in ensuring the quality of research, reflected in the design, methodology, analysis, and use of resources.
- **Honesty** in developing, undertaking, reviewing, reporting, and communicating research in a transparent, fair, full, and unbiased way.
- **Respect** for colleagues, research participants, research subjects, society, ecosystems, cultural heritage, and the environment.
- **Accountability** for the research from idea to publication, for its management and organisation, for training, supervision, and mentoring, and its wider societal impacts.

I, Lorenzo Guidotti, hereby acknowledge and disclose that NO generative AI technology was used in the development of my graduate thesis titled “New insights into retinal physiology and cerebral microcirculation in the 5xFAD murine model of Alzheimer’s disease”.

Acknowledgements

Prof. Massimo Dal Monte, PhD
Prof. Giovanni Casini, PhD
Prof. Maurizio Cammalleri, PhD
Prof.ssa Dominga Lapi, PhD
Prof.ssa Mercedes Garcia Gil, PhD
Prof.ssa Maria Claudia Gargini, PhD
Prof. Ugo Borello, PhD
Prof. Andrea Vornoli, PhD
Prof.ssa Ilaria Piano, PhD
Prof.ssa Veronica Marchetti, PhD
Dr.ssa Silvia Marracci, PhD
Dr. Rosario Amato, PhD
Dr.ssa Martina Lucchesi, PhD
Dr.ssa Lucia Giambastiani, PhD
Dr.ssa Francesca Corsi, PhD
Dr. Alberto Melecchi, PhD
Dr. Manuela Cosentino, PhD
Dr. Irene Ferraris, PhD
Dr.ssa Silvia Valori
Dr. Giuseppe Neri
Dr.ssa Alessia Galante
Dr.ssa Luisa Pozzo

Prof. Robert Gabriel, PhD
Prof. Völgyi Béla, PhD
Dr. Tamas Kovacs-Öller, PhD
Dr. Gergely Szarka, PhD
Dr.ssa Andrea Kovács-Valasek, PhD
Dr.ssa Boglàrka Mèszàrosnè Kiss
Mária Faragóné Papp

Appendix

Presented below are all articles published during the PhD period, encompassing both thesis-related and non-thesis-related publications:

- Encapsulation of Alpha-Lipoic Acid in Functional Hybrid Liposomes: Promising Tool for the Reduction of Cisplatin-Induced Ototoxicity. Manuela Curcio; Giuseppe Cirillo; Rosario Amato; **Lorenzo Guidotti**; Diana Amantea; Michele De Luca; Fiore Pasquale Nicoletta; Francesca Iemma; Mercedes Garcia-Gil. DOI: 10.3390/ph15040394.
- Effects of Nutraceuticals on Cisplatin-Induced Cytotoxicity in HEI-OC1 Cells. **Lorenzo Guidotti**; Elena Tomassi; Silvia Marracci; Michele Lai; Dominga Lapi; Rossana Pesi; Laura Pucci; Ettore Novellino; Elisabetta Albi; Mercedes Garcia-Gil. DOI: 10.3390/ijms242417416.
- Characterization and Otoprotective Effects of Polysaccharides from Arthrospira platensis. Matteo Banti; Mercedes Garcia-Gil; **Lorenzo Guidotti**; Graziano Di Giuseppe; Simona Rapposelli; Daniela Monti; Silvia Tampucci; Marinella De Leo; Francesca Gado; Paola Nieri; Clementina Manera. DOI: 10.3390/molecules30020224.
- Hypoxia-Dependent Upregulation of VEGF Relies on β3-Adrenoceptor Signaling in Human Retinal Endothelial and Müller Cells. Martina Lucchesi; Lorenza Di Marsico; **Lorenzo Guidotti**; Matteo Lulli; Luca Filippi; Silvia Marracci; Massimo Dal Monte. DOI: 10.3390/ijms26094043.
- An Acebuche Oil-Enriched Diet Prevents Early-Stage Cerebrovascular Alterations in the 5xFAD Mouse Model of Alzheimer's Disease. **Lorenzo Guidotti**; Dominga Lapi; Martina Lucchesi; Silvia Valori; Francesca Corsi; Lucia Giambastiani; Andrea Vornoli; Claudia Gargini; Maurizio Cammalleri; Massimo Dal Monte. DOI: 10.3390/nu18010172.
- Morpho-Functional Characterization and miRNA Profiling of the Retina in the 5xFAD Murine Model of Alzheimer's Disease. **Lorenzo Guidotti**; Martina Lucchesi; Eleonora Daghini; Rosario Amato; Giuseppe Neri; Francesca Corsi; Silvia Marracci; Claudia Gargini; Ugo Borello; Maurizio Cammalleri; Massimo Dal Monte; Giovanni Casini. (Accepted for publication; IOVS).

Lorenzo Guidotti
11.02.2026
18:13:47
UTC